NUMERICAL ANALYSIS OF POROUS PIEZOELECTRIC MATERIALS

by

Jaspreet Singh

A thesis submitted in partial fulfilment

of the requirements for the degree of

Master of Applied Science (MASc) in Natural Resources Engineering

The Faculty of Graduate Studies

Laurentian University

Sudbury, Ontario, Canada

THESIS DEFENCE COMMITTEE/COMITÉ DE SOUTENANCE DE THÈSE
Laurentian Université/Université Laurentienne
Faculty of Graduate Studies/Faculté des études supérieures

Title of Thesis Titre de la thèse	NUMERICAL ANALYSIS OF POROUS PIEZOELECTRIC MATERIALS
Name of Candidate Nom du candidat	Singh, Jaspreet
Degree Diplôme	Master of Applied Science
Department/Program Département/Programme	Natural Resources Engineering
Date of Defence Date de la soutenance	December 04, 2014

APPROVED/APPROUVÉ

Thesis Examiners/Examinateurs de thèse:

Dr. Krishna Challagulla
(Supervisor/Directeur de thèse)

Dr. Shailendra Sharan
(Committee member/Membre du comité)

Dr. Brent Lievers
(Committee member/Membre du comité)

Dr. Reinaldo Rodriguez Ramos
(External Examiner/Examinateur externe)

Approved for the Faculty of Graduate Studies
Approuvé pour la Faculté des études supérieures
Dr. David Lesbarrères
M. David Lesbarrères
Acting Dean, Faculty of Graduate Studies
Doyen intérimaire, Faculté des études supérieures

ACCESSIBILITY CLAUSE AND PERMISSION TO USE

Abstract

Three-dimensional finite element models based on unit-cell approach are developed to characterize the complete electromechanical properties of: (i) zero-dimensional (3-0), one-dimensional (3-1) and three-dimensional (3-3) type porous piezoelectric structures made of lead zirconium titanate (PZT-7A) and relaxor (PMN-PT based) ferroelectrics (RL); and (ii) 3-3 type porous piezoelectric foam structures made of several classes of piezoelectric materials such as barium sodium niobate (BNN), barium titanate ($BaTiO_3$) and relaxor (PMN-PT based) ferroelectrics (RL).

In this thesis, finite element software named ABAQUS is used to characterize the electromechanical response of 3-0, 3-1 and 3-3 type porous piezoelectric structures. Appropriate boundary conditions are invoked for various porous piezoelectric structures (i.e. 3-0, 3-1 and 3-3 type) to ensure that the electromechanical deformation response of the unit-cell, under conditions of electrical and mechanical loading, is representative of the entire porous piezoelectric structures.

Overall, this thesis demonstrates that the microstructural features such as porosity connectivity, porosity aspect ratio, porosity volume fraction, foam shape, and material selection play significant roles on the electromechanical properties and the figures of merit of porous piezoelectric structures.

Keywords: porous piezoelectric structures, Barium Sodium Niobate (BNN), Barium Titanate ($BaTiO_3$), Relaxor Ferroelectrics (RL), Polyvinylidene Fluoride (PVDF), Lead Zirconium Titanate (PZT-7A), Piezoelectric composites/piezocomposites, Piezoelectric properties.

Dedication

This work is dedicated to my mother Smt. Kulwant Kaur, father S. Karnail Singh and my wife Kamljeet Kaur. Without their prayers and blessings, reaching this milestone with such satisfying results would have been impossible. I love you always.

Acknowledgements

There are so many people that I want to thank for their help and support during my research. I would like to thank my supervisor Dr. Krishna Sri Challagulla for his support, and guidance throughout my research, as well as Dr. Shailendra Sharan and Dr. W. Brent Lievers for serving on the advisory committee.

Firstly, I would like to acknowledge my friend Benjamin Nguyen for guiding me in my research. I would like to thank him for his friendship, assistance and the beloved discussions we had.

Further I would like to thank all my friends and well-wishers who have given me wonderful advice, support and friendship over the years. Without their help and guidance, I would not have been able to achieve this milestone.

Lastly, I would like to thank my dad (S. Karnail Singh), mom (Smt. Kulwant Kaur), my wife (Kamljeet Kaur) and sister (Rupinder Kaur) for their support. I am blessed to have you in my life.

Table of Contents

List of Figures

List of Tables

Nomenclature

A_f	temperature at which transition from martensite to austenite finishes
A_s	temperature at which transition from martensite to austenite starts
$BaTiO_3$	barium titanate
BNN	barium sodium niobate
CNT	carbon nano-tube
CuZnAl	copper/zinc/aluminium alloy
CuAlNi	copper/aluminium/nickel alloy
C3D8E	eight-node, linear piezoelectric brick elements
C^E	fourth-order elasticity tensor
C_{22}^D	elastic constants being measured electric displacement
C_{22}^E	elastic constants being measured at zero/constant electric field
D	electric displacement vector
d_{22}	charge per unit force applied parallel to the poling direction (2-direction)
d_{21}	charge per unit force applied perpendicular (1-direction) to the poling direction
d_{23}	charge per unit force applied perpendicular (3-direction) to the poling direction
d_{22}	charge per unit force applied parallel to the poling direction (2-direction)
d_h	hydrostatic strain coefficient
$d_h g_h$	hydrostatic figure of merit
E	electric field vector
ER	electrorheological fluids
e	third-order coupling tensor
FOM	figures of merit

g_h	hydrostatic voltage coefficient
K_{ij}	dielectric permittivity of the magnetostrictive materials
$K^2{}_{me}$	magnetoelectric figure of merit of the magnetostrictive materials
K_t	piezoelectric coupling constant
M	receiving sensitivity
MR	magnetorheological fluids
M_s	temperature at which transition from austenite to martensite starts
M_f	temperature at which transition from austenite to martensite finishes
NiTi	nickel-titanium alloy
PZT-7A	lead zirconium titanate
RL	relaxor (PMN-PT based) ferroelectrics
SMA	shape memory alloys
t	thickness of piezoelectric structure along poling direction
Z	acoustic impedance
ρ	density of piezoelectric material
λ_{ij}	magnetoelectric permeability of the magnetostrictive materials
μ_{ij}	magnetic permeability of the magnetostrictive materials
ξ	martensite fraction
3-0	porosity is enclosed in all three directions
3-1	porosity exhibits connectivity in one direction
3-3	porosity exhibits connectivity in all three directions
σ	second-order stress tensor
ε	second-order strain tensors

κ^{ε} second-order permittivity tensor

CHAPTER 1

1 Introduction

1.1 What are composites?

Several conventional materials such as graphite, steel, aluminum etc. have proven to be the biggest innovation in the entire human history. These materials provide applications in basically every field starting from as small as pencils and big as aerospace applications such as missiles, tanks, and aircrafts.

However, due to advancement in the past couple of decades, several new structural materials have been developed to improve the performance as compared to conventional materials. Composites are one of the major fields in these structural materials. A composite material consists of two or more different materials with different physical and chemical properties. Advanced composites are one of the biggest growing fields, which became very important part in numerous engineering applications in various fields including aerospace, civil, transportation, sports, medicine etc. Additionally, composite materials can also be found in our day-to-day lives, from the cars we drive, to the boats, railway coach interiors, and sporting goods.

The most common approach used to create composites is by mixing reinforcing fibers in polymeric resin matrix. Due to resin cohesive and adhesive properties, it binds reinforced-fibers in place providing load-carrying characteristics of the composites. The fiber orientation as maintained by the matrix determines the properties of the composites.

Unlike traditional materials such as steel, composite materials can have different mechanical properties in different directions, and can be custom designed to the required strength in a specific direction. Composite materials have many other advantages than conventional materials such as light-weight, high specific-strength, corrosion resistance, high impact-strength, high thermal-resistance, ability to fabricate complex profiles, inherent durability etc. However there are some disadvantages of composite materials as well such as high maintenance cost, limited service-life condition, inability to transform into certain shapes when necessary, self-repair capability etc. To overcome these limitations, smart materials come into attention.

Also, significant development of new and highly developed sensors and actuators along with the development of various advanced composites gave birth to smart composite materials as explained in the next section.

1.2 Smart materials

1.2.1 Introduction

With the development of materials and technology (micro-electromechanical systems (MEMS), telecommunications, and other fields, significantly facilitates the development of new and highly effective sensors and actuators), many new materials find their applications in various fields such as civil engineering, aerospace, transportation industry, oil and gas in order to deal with the deteriorating infrastructures. Smart materials are promising example that deserves a wide focus, from research to application.

According to *Canadian Militiary Journal* [1], “Smart or intelligent materials are materials that have the intrinsic and extrinsic capabilities, first, to respond to stimuli and environmental changes and, second, to activate their functions according to these changes”. “Smart material

systems refer to the integration of actuators, sensors in structural components, and the usage of some kind of control unit or enhanced signal processing with a material or structural component" [2].

Smart materials possess characteristics such as; a) adaptive, makes modification according to required output using sensors and actuators; b) metamorphic and active, smart materials have self-adjustment or self-repair capability as change in conditions; and c) smart materials and systems reproducing biological functions in load bearing structural systems. Classifications and applications of various smart materials are explained in the next section.

1.2.2 Classification of smart materials

Depending upon the functionalities of smart materials, Figure 1.1 shows common smart materials systems used for actuators and sensors.

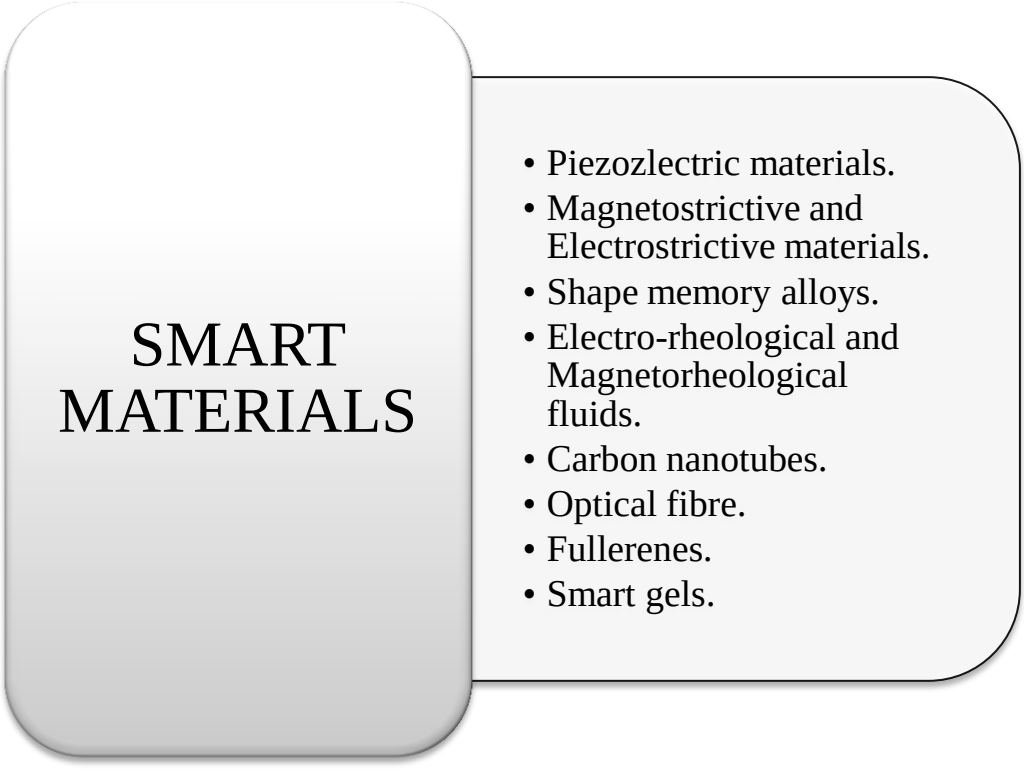

Figure 1.1: Classification of smart materials

In the following sections an overview of these smart materials is presented including definitions, applications etc. as reported in the literature.

1.2.2.1 Piezoelectric materials

Piezoelectric materials are materials which show the appearance of an electrical potential across some faces of a crystal when it is under pressure, and of distortion when an electrical field is applied. Piezoelectric materials are being more and more studied as they turn out to be very useful materials with specific and interesting properties. Some common piezoelectric materials are given in Table 1.1.

Table 1-1: Common piezoelectric materials [3]

Natural crystals	Quartz, Rochelle salt, ammonium phosphate etc.
Noncrystalline materials	Glass rubber, paraffin, etc.
Textures	Bone, wood etc.
Synthetic piezoelectric materials	a) Piezoceramics: Lead zirconate titanate (PZT), barium titanate, lead niobate, lead lanthanium zirconate titanate (PLZT), etc. b) Crystallines: ammonium dihydrogen phosphate, lithium sulfate, etc. c) Piezoelectric polymer: polyvinylidene fluoride (PVDF), etc.

1.2.2.1.1 History of piezoelectric materials

Piezoelectricity is derived from the Greek word *Piezo*, which means pressure. In 1880, Jacques and Pierre Curie found certain materials which exhibit unusual characteristics: materials develop electric charge when subjected to pressure [4,5]. This effect later on named as "piezoelectricity" by Wilhelm-Gottlieb Hankel [4,5]. "The piezoelectric formulation was carried out more completely by Pierre. Duhem and Friedrich Pockels and most fully and rigorously by Woldemar Voigt in 1894" [4,5]. Principle of crystal symmetry describing the behaviour of

piezoelectric materials was explained by F. Neumann [4,5]. The major breakthrough in this field came with the discovery of barium titanate and lead zirconium titanate (PZT) in the 1940's and 1950's [4,5].

1.2.2.1.2 Poling

Ceramic materials in the basic state are composed of randomly orientated domains and hence the effect from individual domains cancels each other (Figure 1.2). Consequently, they exhibit no piezoelectric behaviour and are isotropic. Poling is the common process used to orient the domains. Strong direct electric field is then applied (Figure 1.2), usually at a temperature slightly below the Curie point, to rotate and orient the domains in the direction of electric field [6]. When the electric field is removed most of the dipoles are locked into a configuration of near alignment [6] and the ceramic exhibits the piezoelectric behaviour (Figure 1.2). Through the polarization process the element lengthens along the poling axis and contracts in both directions perpendicular to it, as a direct consequence of the piezoelectric effect.

1.2.2.1.3 Piezoelectric effect

Piezoelectric materials consist of two effects, direct effect and converse effect [4,5]. When piezoelectric crystals get stressed, they develop certain amount of electric field whose magnitude is proportional to the applied stress, is known as direct piezoelectric effect [4, 5]. On the other hand, when an electric field is applied in a piezoelectric crystal, the shape of the crystal changes slightly, which is known as converse piezoelectric effect [4, 5]. Figure 1.3 [6] illustrates the piezoelectric effect.

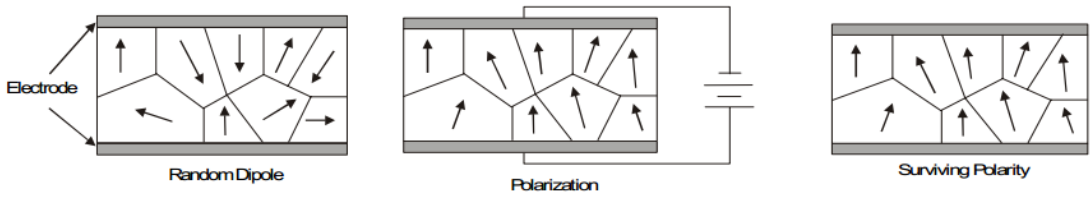

Figure 1.2: Polarization of ceramic material to generate piezoelectric effect [6]

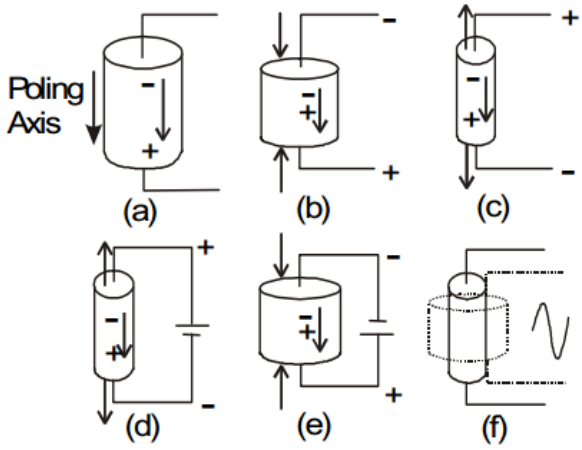

Figure 1.3: Piezoelectric effect [6]; (a) Shows that the piezoelectric material is poled in the poling direction, (b) Voltage generated between the electrodes when material is compressed, (c) Voltage generated between the electrodes when material is stretched, (d) Conversely, voltage applied with opposite polarity will stretch the material, (e) Voltage applied with the same polarity will compress the material, and (f) Shows that material vibrates (with the same frequency) if AC signal is applied.

1.2.2.1.4 Constitutive relations for piezoelectric materials

The complete electromechanical response of piezoelectric material in the linear elastic domain is captured by the coupled constitutive relationships represented as:

$$\sigma_{ij} = C^{E}_{ijkl}\varepsilon_{kl} - e_{ijk}E_{k}$$
$$D_{i} = e_{ikl}\varepsilon_{kl} + \kappa^{\varepsilon}_{ij}E_{j} \qquad [1\text{-}1]$$

where σ is the second-order stress tensor, ε is the second-order strain tensors, C^E is the fourth-order elasticity tensor with the superscript "E" indicating that the elasticity tensor corresponds to measurement of C at constant/zero electric field, e is the third-order coupling tensor, E is the electric field vector, D is the electric displacement vector, and κ^ε is the second-order permittivity tensor measured at constant/zero strain. Equation 1-1 can be represented by a matrix using the following mapping of adjacent indices: $11 \to 1,\ 22 \to 2,\ 33 \to 3,\ 23 \to 4,\ 13 \to 5,\ 12 \to 6$, as:

$$\begin{pmatrix} \sigma_{11} \\ \sigma_{22} \\ \sigma_{33} \\ \sigma_{23} \\ \sigma_{13} \\ \sigma_{12} \\ D_1 \\ D_2 \\ D_3 \end{pmatrix} = \begin{pmatrix} C_{11}^E & C_{12}^E & C_{13}^E & C_{14}^E & C_{15}^E & C_{16}^E & -e_{11} & -e_{21} & -e_{31} \\ . & C_{22}^E & C_{23}^E & C_{24}^E & C_{25}^E & C_{26}^E & -e_{12} & -e_{22} & -e_{32} \\ . & . & C_{33}^E & C_{34}^E & C_{35}^E & C_{36}^E & -e_{13} & -e_{23} & -e_{33} \\ . & . & . & C_{44}^E & C_{45}^E & C_{46}^E & -e_{14} & -e_{24} & -e_{34} \\ . & . & . & . & C_{55}^E & C_{56}^E & -e_{15} & -e_{25} & -e_{35} \\ . & . & . & . & . & C_{66}^E & -e_{16} & -e_{26} & -e_{36} \\ e_{11} & e_{12} & e_{13} & e_{14} & e_{15} & e_{16} & \kappa_{11}^\varepsilon & \kappa_{12}^\varepsilon & \kappa_{13}^\varepsilon \\ e_{21} & e_{22} & e_{23} & e_{24} & e_{25} & e_{26} & . & \kappa_{22}^\varepsilon & \kappa_{23}^\varepsilon \\ e_{31} & e_{32} & e_{33} & e_{34} & e_{35} & e_{36} & . & . & \kappa_{33}^\varepsilon \end{pmatrix} \begin{pmatrix} \varepsilon_{11} \\ \varepsilon_{22} \\ \varepsilon_{33} \\ 2\varepsilon_{23} \\ 2\varepsilon_{13} \\ 2\varepsilon_{12} \\ E_1 \\ E_2 \\ E_3 \end{pmatrix} \quad [1\text{-}2]$$

The (.) in equation 1-2 represents the elastic, piezoelectric and dielectric coefficients are symmetric about the diagonal. Equation 1-2 is the most general representation of the constitutive behavior of piezoelectric materials with 45 independent constants (21 elastic, 18 piezoelectric and 6 permittivity constants). Thus, a complete characterization of a piezoelectric foam structure in the linear elastic domain requires an identification of all the 45 material constants.

1.2.2.1.5 Figures of merit

In order to assess the utility of porous piezoelectric materials for practical applications such as hydrophone devices, several combinations of figures of merit such as piezoelectric coupling constant (K_t), acoustic impedance (Z), hydrostatic strain coefficient (d_h), hydrostatic

voltage coefficient (g_h), hydrostatic figure of merit ($d_h g_h$) and receiving sensitivity (M) are derived from the fundamental material constants and are typically invoked [7, 8] (Table 1.2).

1.2.2.1.5.1 Piezoelectric coupling constant

The piezoelectric coupling constant (K_t) is given as: $K_t = \sqrt{1 - C_{22}^E/C_{22}^D}$, where $C_{22}^D = C_{22}^E + \frac{e_{22}^2}{k_{22}^E}$ (C_{22}^E and C_{22}^D are, respectively, the elastic constants being measured at zero/constant electric field and electric displacement, and e_{22}^2 and k_{22}^E are, respectively, the piezoelectric and dielectric constants being measured at zero/constant electric field). The piezoelectric coupling constant represents the efficiency of energy conversion from electric to mechanical domains and vice versa [7]. The ratio of the stored converted energy of one kind (mechanical or electrical) to the input energy of the second kind (electrical or mechanical) is defined as the square of the coupling coefficient [7]. Materials with high piezoelectric coupling coefficients (ideally~1) are desired.

1.2.2.1.5.2 Acoustic impedance

Acoustic impedance *Z*, modulates the extent of signal transmission or reflection at the interface between a device and the environment and is given as: $Z = \sqrt{\rho C_{22}^D}$, where ρ is density of piezoelectric material [7]. Good impendence matching between hydrophones and surrounding medium (e.g. water) is desired for better performance. Generally, porous piezoelectric materials with low densities exhibits lower acoustic impedance and match well with acoustic impedance of surrounding aqueous environment and, hence are desirable for use in hydrophones.

Table 1.2: Common piezoelectric figures of merit used to assess the utility of porous piezoelectric materials for practical applications [7].

Figures of merit	Description	Formulation	Desired Value
Piezoelectric coupling constant (K_t)	Represents the efficiency of energy conversion between electric to mechanical domains.	$K_t = \sqrt{1 - C_{22}^E/C_{22}^D}$	~1
Acoustic impedance (*Z*)	Reflects the extent of signal transmission or reflection at the hydrophone/environment interface.	$Z=\sqrt{\rho C_{22}^D}$	Close to substrate
Hydrostatic strain coefficient (d_h)	Captures the effective strength of electromechanical coupling in a piezoelectric material under hydrostatic loading conditions.	$d_h = d_{22}+d_{21}+d_{23}$	High
Hydrostatic voltage coefficient (g_h)	Relates the electric field generated across a transducer in response to an applied hydrostatic stress.	$g_h = d_h/k_{22}$	High
Hydrostatic figure of merit ($d_h g_h$)	Relates signal-to-noise ratio in a hydrophone device.	$d_h g_h$	High
Receiving sensitivity (*M*)	Represents the sensitivity of a device.	$g_h * t$	High

1.2.2.1.5.3 Hydrostatic strain coefficient

The hydrostatic strain coefficient captures the effective strength of electromechanical coupling in a piezoelectric material under hydrostatic loading conditions [7] and is given as: $d_h = d_{22}+d_{21}+d_{23,}$ where d_{22} is the charge per unit force applied parallel to the poling direction (2-direction), d_{21} and d_{23} are the charge per unit force applied perpendicular (1 and 3-direction) to the poling direction. In applications such as hydrophones, large values of the hydrostatic strain coefficient are desirable in order to achieve enhanced sensitivity to the detection of sound waves.

1.2.2.1.5.4 Hydrostatic voltage coefficient

The hydrostatic voltage coefficient, g_h, relates the electric field developed across a transducer in response to an applied hydrostatic stress [7]. The hydrostatic voltage coefficient, g_h, is given as: $g_h = d_h/k_{22}$. Higher values for hydrostatic voltage coefficient are desirable.

1.2.2.1.5.5 Hydrostatic figure of merit

The hydrostatic figure of merit, $d_h g_h$, provides a measure of the ability of a hydrophone device to identify a signal and distinguish it from ambient background noise [7]. Higher values of hydrostatic figure of merit imply that the device exhibits higher signal-to-noise ratio.

1.2.2.1.5.6 Receiving Sensitivity

The receiving sensitivity, *M*, represents the sensitivity of piezoelectric device. The receiving sensitivity of a device operating under hydrostatic conditions is related to g_h (hydrostatic voltage coefficient) and the thickness (t) of piezocomposite element as: $M = g_h \times t$ [8].

1.2.2.1.6 Applications of piezoelectric materials

The one of the main application of piezoelectric materials is to acts as transducers in hydrophones i.e. sound detecting devices [4, 5]. Hydrophone based on piezoelectric transducers detects sound (pressure waves) in underwater and converts it into electric signal [4, 5]. Thus, various electric signals can be recorded using hydrophones. Hydrophones can also be used to detect sound in air, but they are more suitable for underwater applications; due to the better acoustic impedance (Z) match [4, 5]. Since, porous piezoelectric materials with high porosity have low acoustic impedance (Z) which is closer to the acoustic impedance of water [4, 5].

Figure 1.4 shows the stricture of single crystal cymbal hydrophone made of PMN-0.33 PT (relaxor ferroelectrics) [9]. It consists of piezoelectric (PMN-0.33 PT) disc sandwiched between two metal cymbal-shaped endcaps [9].

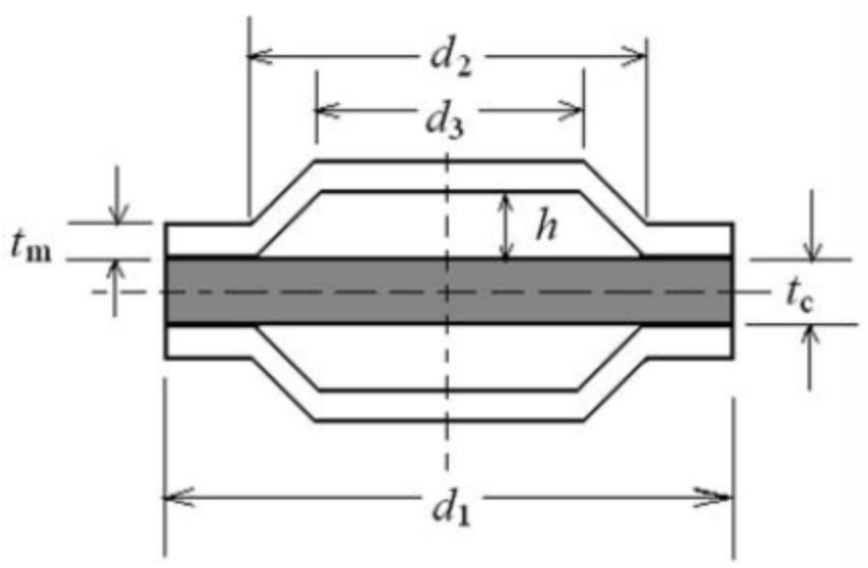

t_c (mm)	t_m (mm)	h (mm)	d_1 (mm)	d_2 (mm)	d_3 (mm)
1.0	0.5	0.8	20.0	16.0	7.5

Figure 1.4: Illustration of single crystal cymbal hydrophone and its structural parameters [9]

In this thesis, unit-cell approach has been utilized in order to capture full electromechanical response of porous piezoelectric materials. So, unit-cells which are modelled in this thesis can be assumed to be of any size as it represents the entire porous piezoelectric structure. Also, as hydrophones consists of piezoelectric disc so the effect of different piezoelectric foam shapes have also been considered, while analyzing porous piezoelectric foam structures.

Piezoelectric materials can be used as sensors as well as actuators. Hence, piezoelectric material can be used as a transduction element in accelerometers [10]. They can be used as high-

frequency ultrasonic transducers [11]. Piezoelectric materials act as sensors to detect damage in structures in which they are imbedded [11]. In ink-jet printing heads, piezoelectric element acts like a fast piston on which applying pressure results into ejection of ink through a suitable placed orifice [12]. They are well suitable for energy harvesting devices [13]. Lead zirconium titanate is a well-known piezoelectric material to be used as power harvesting devices [13]. Other useful applications of piezoelectric materials are such as valve actuators or active control systems and vibration absorbers [14].

Piezoelectric materials found their applications in transportation industry as shown in Table 1.3. The availability of piezoelectric materials in many forms such as bulk material, multilayer, thin films, rods and their light weight made them the strong candidate for smart composite applications [15]. Table 1.3 shows the use of direct and indirect piezoelectric effect in making different devices such as accelerometers, high voltage spark igniters, vibration reducer devices etc.

Table 1.3: Summary of the different effects and the designs of piezoelectric materials, which are candidates for application in transportation industry [15]

Design/ effect direction	**Direct piezoeffect**		**Indirect piezoeffect**	**Both effects**
	Sensor	**Generator**	**Actuator**	**transducer**
Bulk material (d_{33} – effect)	Accelerometers Knock sensors Pressure/Force sensor	High voltage spark igniters	-	Ultrasonic sonar devices Distance meters Ultrasonic materials charac-terisation
Multilayer (d_{33} – effect)	-	Energy harvesting	Active Vibration Reduction Nano – Positioning High–force–actuation	-
Patch (monolithic) (d_{31} – effect)	Dynamic strain sensor	Energy harvesting	Active Vibration Reduction	-
Patch (fibre composites) (d_{31} and d_{33} – effect)	Dynamic Strain sensors	Energy harvesting	Active Vibration Reduction	-
Bi-/trimorph d_{31} + bimorp effect	-	-	Textile machines Fans	-
Special designs	-	Cymbal trans-ducers for Energy harvesting	Ultrasonic Motors	Transformers

Other applications of piezoelectric materials are in the areas of: military (depth sounders, targets, telephony and adaptive optics); commercial (ultrasonic cleaners, welders, thickness gauging, flaw detection, fans, relays, ink jet printers and strain gauges); medical (ultrasonic cataract removal, ultrasonic therapy, insulin pumps, flow meters, ultrasonic imaging); automotive (knock sensors, wheel balancers, seat belt buzzers, air flow, fuel atomization, tire pressure indication, and audible alarms); and consumer goods (humidifiers, gas grill igniters, telephones, smoke detectors, microwave ovens, sneakers, cigarette lighters, lighting security, and ultrasonic sewing) [15].

1.2.2.2 Magnetostrictive and electrostrictive materials

Materials in which strains are produced due to applied magnetic field and vice-versa i.e. when material is strained (with applied mechanical force) it induces magnetic field, are known as Magnetostrictive materials [16]. The strength of magnetic field is proportional to the material's rate of strain [17]. Early magnetostrictive materials were studied extensively but few practical applications existed because the force and the strain that they generate were much less than piezoelectric and electrostrictive materials.

The magnetostrictive behaviour was noticed in 1840's and since 1860's, the various devices utilizing magnetostrictive properties came into existence [18]. However, the revolution came into the field of magnetostrictive behaviour was in 1978, when A.E. Clark and his coworkers developed "giant" magnetostrictive alloy named as Terfenol-D because of its ability to produce massive strains with change in magnetic field [19].

Figure 1.5 illustrates the cross-section of a prototypical Terfenol-D magnetostrictive transducer [19]. Marcelo et al. [20] discussed the modelling of strains generated using

magnetostrictive transducers in response to an applied magnetic field. Magnetostrictive materials like Terfenol-D can be incorporated in multifunctional composites for the controlling of mechanical deformations as well as for the sensing of deformation and forces. Terfenol-D can potentially replace conventional aircraft parts and reduce weight resulting in a lower annual fuel consumption rate [21]

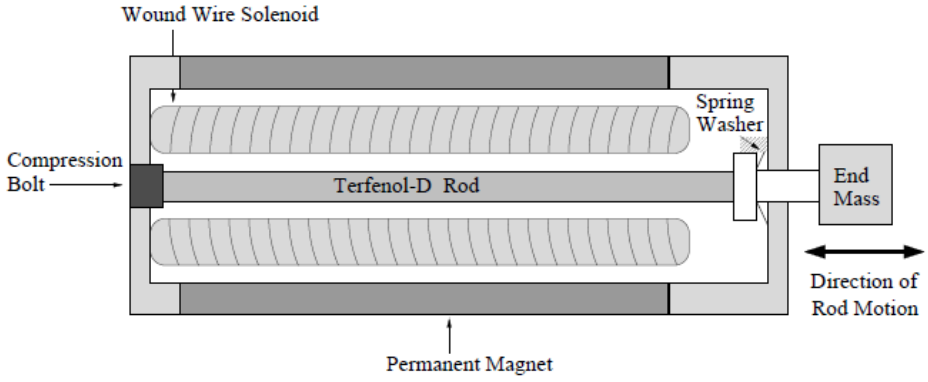

Figure 1.5: Cross section of prototypical terfenol-D magnetostrictive transducer [20]

Likewise piezoelectric materials, magnetostrictive material's performance can be recognised using magnetostrictive figure of merit [22] K_{me}, which characterizes the energy conversion along the longitudinal direction and is defined in equation 1-3;

$$K^2{}_{me} = \frac{\lambda_{ij}}{K_{ij}\mu_{ij}} \qquad [1\text{-}3]$$

Where K_{ij}, λ_{ij}, μ_{ij} represent, respectively, the dielectric permittivity, the magnetoelectric, and the magnetic permeability tensors. i, j varies as 11, 22, 33, 23, 13, or 12 and depends upon the axis of symmetry of magnetostrictive materials [22].

Electrostrictives are another class of materials that are similar in function to piezoelectric materials but generate more strain and have a nonlinear strain to field dependence [23]. Both electrostrictors and piezoelectrics belong to the ferroelectric family. Piezoelectricity is a first-

order effect; however, electrostriction is a second-order effect, that is, the induced strain is proportional to the square of the applied electric field [3]. Thus, the induced strain is independent of the direction of the applied field and the same deformation (direction and magnitude) occurs when the field is reversed [3].

Electrostriction is usually present in all dielectric materials but is very weak due to the dominating stronger first-order piezoelectric effect. Thus, during the development of piezoelectric applications, the smaller, second-order electrostrictive effect is ignored for most practical purposes. However, materials that have high dielectric constants (high polarizations), such as relaxor ferroelectrics, can exhibit very large electrostrictive strains [3].

1.2.2.3 Shape memory alloys (SMA'S)

Shape memory alloys (SMA's) are also one of the important members of the family of smart materials. It exhibits two unique properties such as shape memory effect and pseudo-elasticity [21].These materials are referred to as adaptive materials which can convert thermal energy directly to mechanical work. The most popular and effectively used alloys include NiTi (Nickel-Titanium), CuZnAl (Copper/Zinc/Aluminium alloy), and CuAlNi (Copper/Aluminium/Nickel alloy).

In most shape memory alloys, a temperature change of only 10°C is necessary to initiate this phase change. This phase change occurs between certain temperature range named as martensite (low temperature range) and austenite (high temperature range [24].

The nature of shape memory can be understood by considering the phase diagram as shown in Figure 1.6. In this figure, M_s and M_f respectively are, the temperatures where phase transition from austenite to martensite starts and finishes, and A_s and A_f respectively are, the temperatures where phase transition from martensite to austenite starts and finishes. ξ represents

the martensite fraction [24]. SMA's returns to its original shape by cooling as shown in Figure 1.6. With decrease in temperature i.e. M_s to M_f, phase change of NiTi from austenite to martensite occurs. Also vice-versa, with increase in temperature i.e A_s to A_f, phase change of NiTi from martensite to austenite occurs [24].

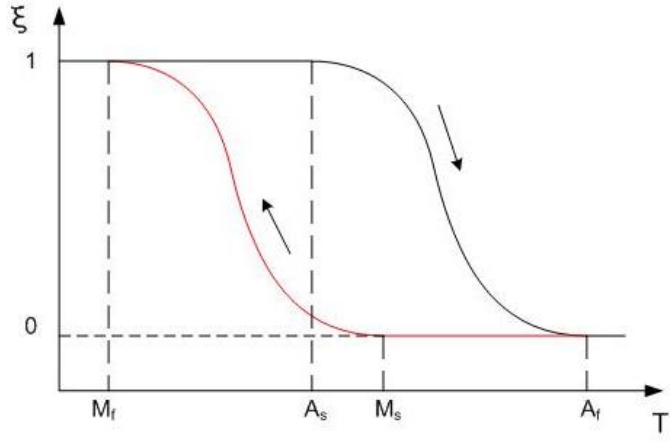

Figure1.6: Transformation at various temperatures of shape memory alloys (SMA's) [24]

In the actuation field, shape memory alloys are used for the actuation of flaps, as shock mounts, for external store vibration control, as antennae or helicopter rotor blades [16]. One of the most popular areas of application of SMA actuators is noise and vibration control. Some examples can be found in Adachi et al. [25], Saadat et al. [26], and Humbeeck and Kustov [27].

1.2.2.4 Electrorheological (ER) and magnetorheological (MR) fluids

Electrorheological fluids (ER) consist of extremely fine non-conducting particles dispersed in electrically insulating fluid and are capable of varying viscosity or even solidification in response to an applied electric field [28]. The response time can be as short as few milliseconds [28].

Figure 1.7 shows ER effect [28]. When electric field of 400 V/mm is applied (interelectrode gap of 5mm) to ER fluid with the disperse phase (30%) on the basis of a TiO_2-

hydroxypropyl cellulose hybrid nano composite [27], ER fluid tends to be more viscous as shown in Figure 1.7 (a) and when electric field is removed, ER fluid's viscosity decreases in a few milliseconds as shown in Figure 1.7 (b).

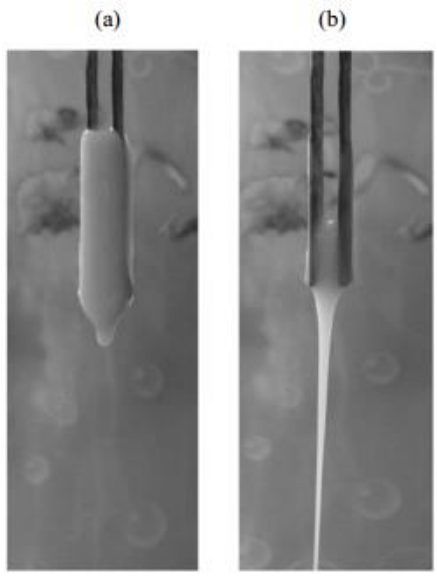

Figure 1.7: Demonstration of the electrorheological effect [28]

ER fluids find various applications in various fields. For example, Bohon and Krause [29] presented application in medical field as an artificial muscle actuator based on ER fluid and silioxane gel. Ribakov and Gluck [30] explained the application of ER fluid as ER dampers in designing control system for multistory structures. Sheng and Wen [31] explained the mechanism and dynamics behind ER fluids, and explained that ER fluids can be used as pumps, actuators, individual droplet sensing and routing and logic gates.

Magnetorheological fluids (MR) change viscosity and other properties as an external magnetic field is applied similar to electrorheological fluids. When magnetic field is removed they transform back to liquid. MR fluids are considerably less studied than ER fluids. Both fluids are non-colloidal suspension of a polarizable particle having a size on the order of few microns. Magnetorheological fluids consist of three major components: ferromagnetic dispersed

particles, a carrying fluid, and a stabilizer [32]. Applications of magnetorheological fluids can be found in automotive shocks, mounts and bushings, vibration dampers for vehicular seats and home appliances, precision lens grinding processes, pneumatic motion control systems, and seismic dampers for buildings and bridges.

1.2.2.5 Carbon nano-tubes (CNT's)

Carbon nano-tubes (CNT's) are one of the most important members of smart material family (Figure 1.8). The term nano-tube is normally used to refer carbon nano-tube, which has received enormous attention from researchers over the last few years. "CNT's were 'discovered' in 1991 by Sumio Iijima of NEC (*Nippon Electric Company Ltd.*) and are effectively long, thin cylinders of graphite" [33].

CNT's are allotropes of carbon and it consists of cylinder-shaped macro-molecules, radius of which is very small as few nanometers and length can be varied up to 20cm [34]. The wall of CNT's consists of hexagonal lattice of carbon atoms similar to graphite [34]. Basically CNT's are classified as Single wall and multi-wall tubes (Figure 1.9).

A single wall carbon nano-tube is technically defined as a cylinder made up of rolled up sheet of graphene as described artistically in Figure 1.9 [35]. Tubes with single shell are called single wall carbon nano-tubes while those with more than one shell are multiwall carbon nano-tubes [35] (Figure 1.9).

Few other types of CNT's are as follows [36]

(i) Torus (carbon nano-tube bent into a doughnut shape);

(ii) Nanobud (combination of carbon nano-tubes and fullerenes);

(iii) graphenated carbon nano-tubes (graphitic foliates grown along the side walls of multiwalled or bamboo style CNT's);

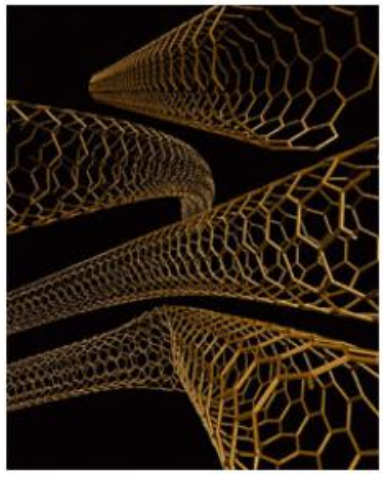

Figure1.8: Bent Carbon Nano-Tubes (CNT's) [A. Rochefort, Nano-CERCA, Univeristy of Montreal Canada, [33]]

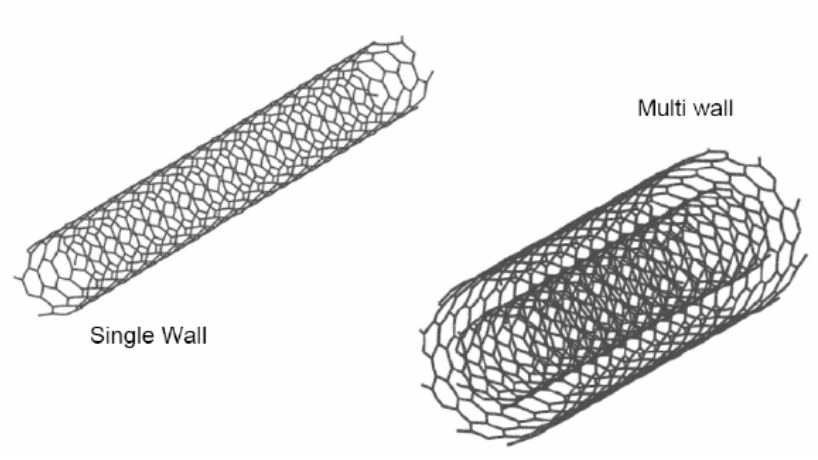

Figure 1.9: Single-Wall and Multi-Wall CNT's [35]

(iv) Nitrogen-doped carbon nano-tubes, peapod, cup-stacked carbon nano-tubes and extreme carbon nano-tubes.

Recently, a new type of carbon nano-tube film is prepared by the filtration of carbon nano-tubes on porous membrane such as polycarbonate, which is known as bucky paper. Bucky paper is found to have unique properties such as good electrical conductivity, field emission

properties, and unique mechanical properties due to distinctive structure of carbon nanotubes [37-39].

Sometimes, CNT's are composed of coaxial cylinders of graphene sheets [34, 35]. Graphene sheet is pure carbon in the form of thin, strong, stiff, very light and nearly transparent sheet [40]. Graphene sheets used in sectors such as automobiles, trains and also in biomedical sector [40].

In general, CNT's found its applications in fuel cells, LCD screen displays as conducting films, low resistance metal interconnects, optically transparent conducting films for display applications, high surface area catalytic support etc.

1.3 Thesis Objective and outline

Overall, smart materials are promising materials to meet the demands of this globalising world. Of the various available smart materials, piezoelectric materials have been chosen to study in this thesis, considering their importance in various sectors especially underwater sonars and transducers.

To utilize piezoelectric materials in applications such as transducers and hydrophones, the two main approaches that are typically invoked to enhance the properties of monolithic piezoelectric materials and fabricating components made of piezoelectric materials are: (i) The additive approach, wherein two or more constituents are added to create several types of piezoelectric composites, thereby enhancing the overall electromechanical response of piezoelectric composites; and, (ii) The subtractive approach, wherein controlled porosity is introduced in the monolithic materials to create porous piezoelectric materials, thereby enhancing the signal to noise ratios, impedance matching, and figures of merit such as

hydrostatic strain coefficients (d_h) and the hydrostatic figure of merit ($d_h g_h$), receiving sensitivity (M) and thus making them useful for applications such as hydrophone devices.

However, the main objective of this thesis is to analyse porous piezoelectric structures to capture the full electromechanical response of piezoelectric materials in order to study their suitability for various underwater applications. The thesis has been organised as follows:

Literature review related to piezoelectric materials (porous and composite piezoelectric materials) has been presented in Chapter 2. Finite element modelling using unit-cell approach to characterize electromechanical response of porous piezoelectric materials has been explained in Chapter 3. Considering the importance of porous piezoelectric materials, various porous piezoelectric structures made up of lead zirconium titanate (PZT-7A) and relaxor ferroelectrics (RL) have been analyzed using 3-D finite element modelling, and are presented in Chapter 4. Chapter 5 analysed 3-3 type porous piezoelectric structures made up of several classes of piezoelectric materials such as barium sodium niobate (BNN), barium titanate ($BaTiO_3$) and relaxor (PMN-PT based) ferroelectrics (RL) using 3-D finite element modelling and characterize their electromechanical response as a function of foam shape, porosity aspect ratio, porosity volume fraction and simultaneously material properties. Various conclusions and future work have been presented in Chapter 6.

CHAPTER 2

2 Literature review

2.1 Introduction

Piezoelectric materials with their unique electromechanical coupling characteristics have been widely recognized for their potential utility in a large number of sensor and actuator applications [4,5] Furthermore, it has also been demonstrated that the microstructure of a piezoelectric material can be modified by the addition of a second phase (as in piezoelectric composites) or by introducing porosity (as in piezoelectric foams), in order to optimize the properties of the piezoelectric material for specific applications [42-44]. For example, by introducing porosity in a piezoelectric material, its signal-to-noise ratio, impedance matching, and sensitivity characteristics can be improved, and thus the piezoelectric material can be made more suitable for hydrophone applications [45-47].

2.2 Porous piezoelectric materials

Within the context of porous piezoelectric materials, depending on the nature of the connectivity of the porosity in the matrix material, three classes of foams are generally identified—3-0 type (where porosity is enclosed in all three dimensions), 3-1 type (where porosity exhibits connectivity in one direction and the matrix phase is connected in all three directions), and 3-3 type (where porosity exists in an open interconnecting network with both the porosity and matrix phase exhibiting connectivity in all the three dimensions).Several analytical [48-56], numerical [7, 57-62] and experimental [45-47, 63-67] studies have focused on understanding and characterizing the effect of porosity on the electromechanical response of (zero-dimensional (3-0), one-dimensional (3-1) and three-dimensional (3-3)) porous piezoelectric materials. Mikata [48] and Dunn and Taya [49] developed analytical models to

assess the piezoelectric properties of zero-dimensional (3-0) and one-dimensional (3-1) porous piezoelectric materials. Bowen and Topolov [50] presented a simplified model based on the Banno unit-cell approach [50] to assess the sensitivity of piezoelectric composites with zero-dimensional (3-0) and three-dimensional (3-3) connectivity. Della and Shu [52] developed micromechanics based method to assess the performance of 1-3 type piezoelectric composites with a porous non-piezoelectric matrix. Bowen and Kara [56] derived an analytical model to characterize the effect of pore anisotropy on the hydrostatic properties of 3-3 type piezoelectric composites and concluded that the pores aligned in the poling direction results in increased permittivity, hydrostatic strain coefficients (d_h) and the hydrostatic figure of merit ($d_h g_h$) as shown in Figure 2.1.

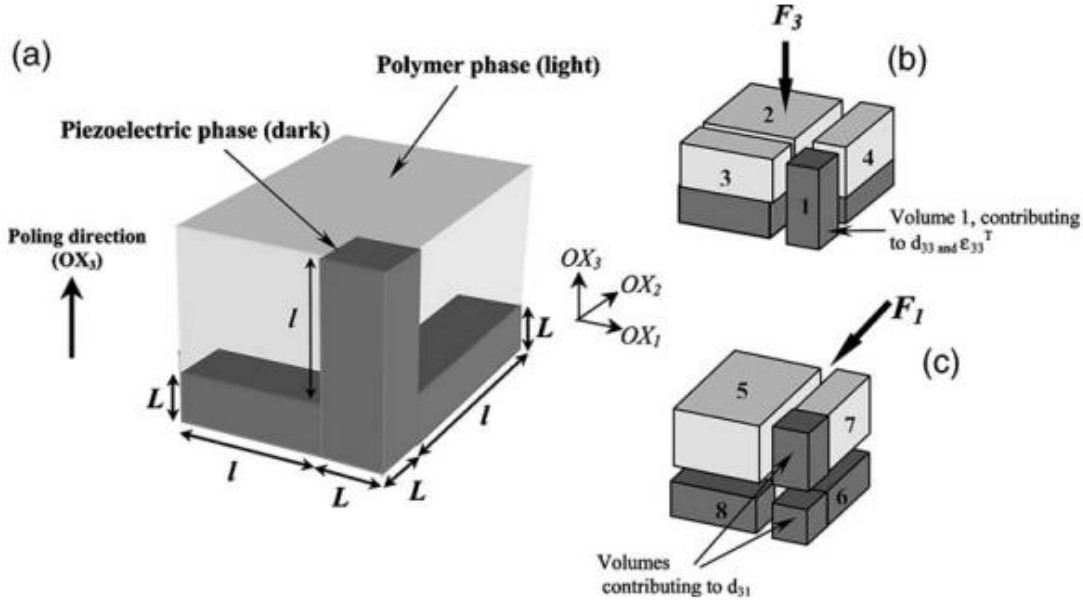

Figure 2.1: (a) Model representing an interpenetrating 3–3 piezocomposite structure. (b) The force (F3) is distributed through the volumes shown. (c) The force (F1) is distributed through the volumes [56]

Several numerical models have been developed to study the behaviour of porous piezoelectric materials. For example, Iyer and Venkatesh (Figure 2.2) [57-58] and Kar-Gupta and Venkatesh [7, 59] used commercially available software ABAQUS to develop finite element

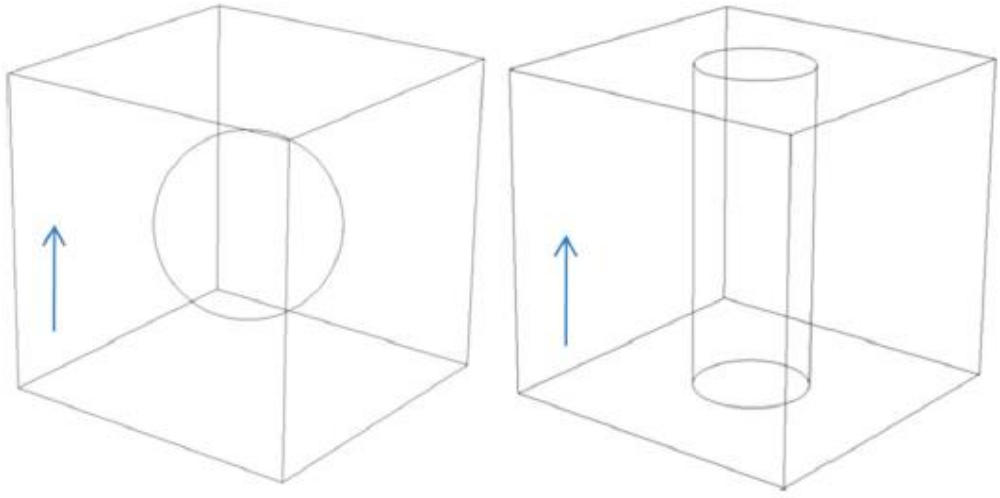

Figure 2.2: Schematic illustrating zero-dimensional (3–0) and one-dimensional (3–1) connectivity, respectively, in piezoelectric materials with spherical and cylindrical porosity [57]

models of various porous piezoelectric materials (zero-dimensional (3-0) and one-dimensional (3-1) porous piezoelectric materials) and assessed the performance of these piezoelectric materials for application such as hydrophones. Challagulla and Venkatesh [60] studied the effect of porosity volume fraction, interconnect geometry and architecture of the piezoelectric foam structures on the electromechanical response of 3-3 type piezoelectric foam structures as shown in Figure 2.3. Bosse et al. [61] developed a unit-cell based finite element model to study the electromechanical response of 3-3 type piezoelectric foam structures and demonstrated that the foam shape and porosity aspect ratio can significantly influence the performance characteristics of 3-3 type piezoelectric foam structures.

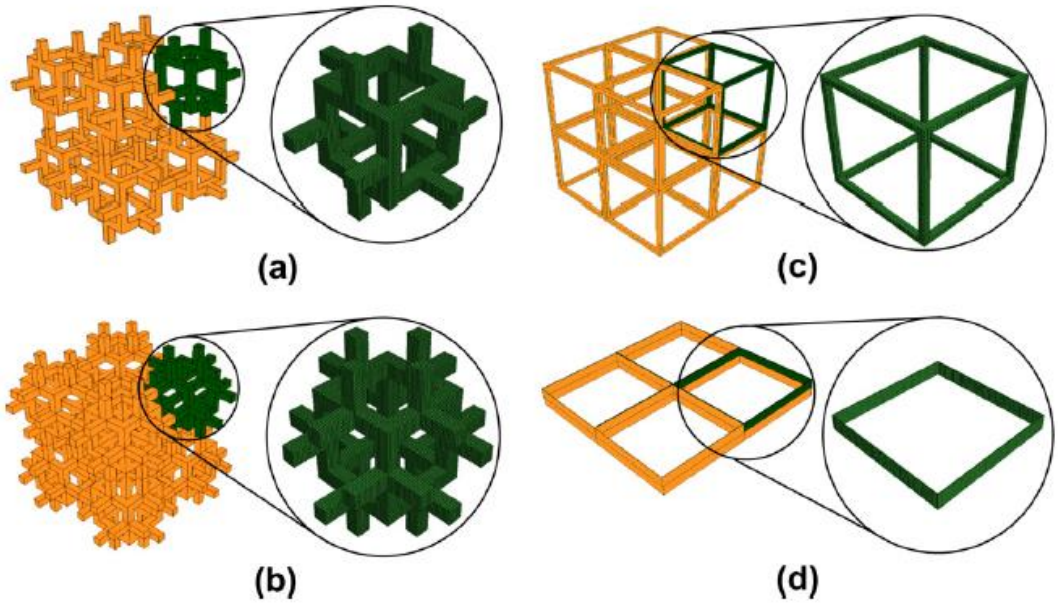

Figure 2.3: Schematic illustrating three kinds of 3-3 type piezoelectric foam structures: (a) with asymmetric interconnects; (b) with symmetric interconnects; (c) without any interconnects; and (d) the 3-1 type long porous structures [60]

Guo et al. [63] synthesized 3-1 type porous piezoelectric using freeze-casting process and demonstrated that the pore size and orientation influence the dielectric and piezoelectric properties of 3-1 type porous PZT ceramics as shown in Figure 2.4. Boumchedda et al. [64] fabricated porous 3-3 type PZT piezoelectric transducer and concluded that figures of merit (i.e. d_h, g_h *and* $d_h g_h$) improved by inducing porosity in piezoelectric materials and therefore suitable for hydrophone applications. Bowen et al. [65] fabricated range of porous structure using PZT-5H piezoelectric ceramic and concluded that increase in porosity results in increase in figures of merit such as g_h and $d_h g_h$. Bowen and co-workers [66] have demonstrated experimentally that introducing porosity in traditional piezoelectric materials results in improving their hydrostatic figure of merit.

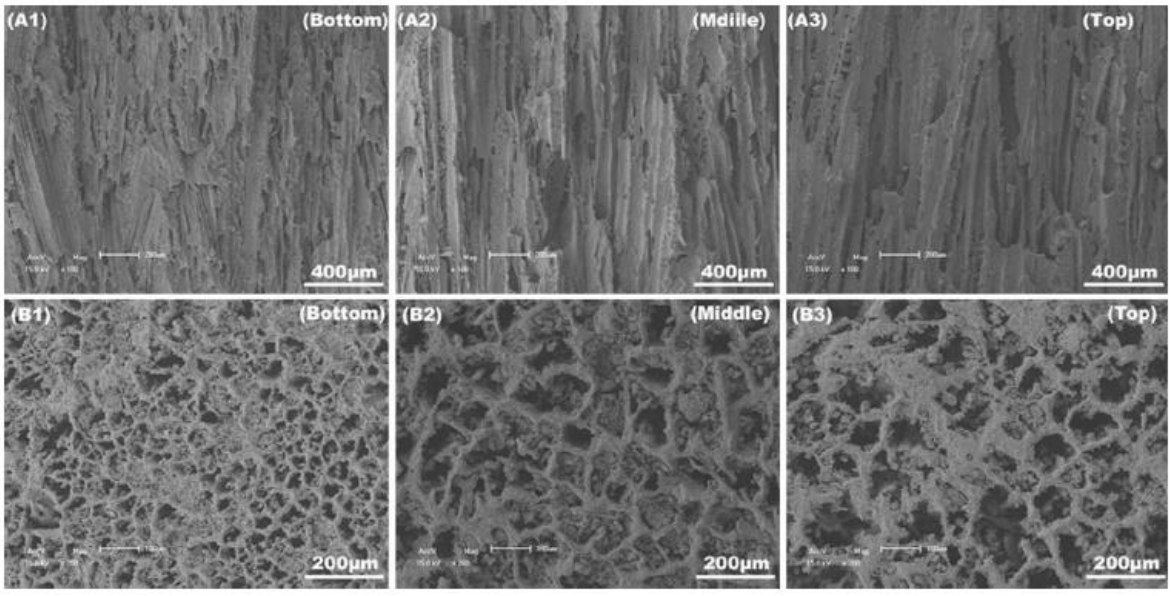

Figure 2.4: Fracture surfaces of 1–3 type porous PZT ceramics with different locations (A1–A3) and (B1–B3) are vertical sections (parallel to the freezing direction) and transverse sections (perpendicular to the freezing direction) for bottom, middle and top section, respectively [63]

2.3 Piezo-composites

The determination of effective properties for piezoelectric composite consisting of inclusion and matrix phases has received considerable attention during the past decades. A number of methods have been developed such as experimental methods [66-76], analytical methods [77-92] and numerical methods [42, 93-102] to predict and simulate the linear coupled piezoelectric and mechanical behavior of composites. For example, Zhang and Wu [93] used ABAQUS to characterize eight different unit cell representing 3-0, 3-1, 3-2 and 3-3 type connectivity for PZT-polymer and polymer-PZT composites and study the influence of connectivity and fiber volume fraction on effective material coefficients. Kar-Gupta and Venkatesh [42] presented unit-cell based finite element modelling to capture elecromechanical response of piezocomposites having 0-3, 1-3, 2-2 and 3-3 connectivity made up of ceramic-

polymer ($BaTiO_3$-PVDF) system using ABAQUS, and also demonstrated that geometric connectivity of active phase in piezoelectric composites has significant influence on effective properties of piezoelectric composites. More recently, Kar Gupta and Venkatesh [94] developed finite element (using ABAQUS) and analytical model (based on asymptotic homogenisation technique) to predict elecromechanical response of 2-2 piezoelectric composites and finite element results were found to be in good agreement with analytical calculations.

Earlier, Kar Gupta and Venkatesh [95] developed unit-cell based models using ABAQUS to characterize the coupled behaviour of 1-3 active matrix/active fiber systems and also considered the effects of poling characteristics of the constituent phases. Pettermann and Suresh [96] developed unit-cell model for 1-3 type piezoelectric composite using ABAQUS and invoked various boundary conditions to predict complete electromechanical response for the piezoelectric composite. Berger et al. [97] developed 1-3 type piezoelectric composite (unidirectional cylindrical fibers embedded in a soft piezoelectric matrix) models using the finite element software ANSYS and predicted effective piezoelectric coefficient using numerical homogenisation technique. Li et al. [99] developed 3 types of unit-cell model for 1-3 piezoelectric composites using ABAQUS and also elastic, piezoelectric and dielectric coefficients were calculated using asymptotic homogenisation technique. Lewis et al. [101] captured elecromechanical response of 3-3 type piezocomposite structure (consisting of ceramic as PZT-5H with air (representing porous piezoelectric system) and ceramic PZT-5H with polymer such as polyethylene and epoxy (representing ceramic-polymer system)) by calculating hydrostatic figures of merit (d_h, g_h *and* $d_h g_h$) and used ANSYS.

2.4 Classification of piezoelectric materials

In conjunction with studies that have been focused on optimizing the properties of existing piezoelectric matrix materials by the additive or subtractive approaches to create composite or porous piezoelectric materials, several studies have focused on analysing different piezoelectric materials (barium sodium niobate (BNN) [103], barium titanate ($BaTiO_3$) [104] and relaxor ferroelectrics (RL) [105-119]). For example, Bao et al. [103] synthesized barium sodium niobate using $BaCO_3$ and Nb_2O_5 in molten NaCl via templated grain growth procedure. Kumar et al. [104] demonstrated enhanced dielectric properties with increase in zirconium contents in barium titanate. Reznitchenko et al. [105] developed materials based on relaxor ferroelectrics and demonstrated correlations between crystal structure and piezoelectric properties. Park et al. [108] demonstrated that piezoelectric and dielectric properties for PMN-PT based relaxor ferroelectric system with MnO_2 additions are highly dependent on temperature. More recently, Singh et al. [111] studied the electromechanical response of relaxor ferroelectric foams. Furthermore, a few studies have also recently illustrated that relaxor ferroelectric-based foams (with 3-0 type connectivity) could provide enhanced piezoelectric figures of merit as well [109,110, 112-119].

In addition to analytical, numerical, and experimental studies on piezoelectric composites, several studies have focused on analysing piezoelectric composites made up of different piezoelectric materials [120-138] (such as barium titanate ($BaTiO_3$)/polyvinylidene fluoride (PVDF) [120-129] and relaxor ferroelectrics (RL) [130-138]). For example, Kar-Gupta and Venkatesh [120] used 2 combination of fiber/matrix (PZT-7A as fiber and $BaTiO_3$ as matrix, and PZT-7A as fiber/PVDF as matrix) to develop finite element model of 1-3 piezoelectric composite using ABAQUS. Della and Shu [121] studied 1-3 piezoelectric composite with active ceramic (PZT-7A, $BaTiO_3$) and passive polymer matrix (Araldite D, P(VDF-TrFE)), and found

out that hydrostatic response (i.e. d_h, g_h *and* $d_h g_h$) is better when P(VDF-TrFE) passive polymer is used in combination with PZT-7A. Li et al. [138] explained importance of relaxor ferroelectrics (PMN-PT based) piezocomposites over traditional PZT 1-3 type piezocomposites by fabricating PIN-PMN-PT single crystal based 1-3 type piezocomposites using dice and fill method.

A summary of various relevant literatures based on piezoelectric porous as well as composite materials, studied in section 2.1-2.4 has been presented in Table 2.1.

Table 2-1: Summary of the various literatures studied for porous as well as composite piezoelectric materials

Methods	Porous piezoelectric materials			Piezo-composite materials	
	3-0 type	3-1 type	3-3 type	3-1 type	3-3 type
Analytical	Dunn and Taya [49] Bowen and Topolov [50]	Della and Shu [52] Bravo-Castillero et al. [55]	Bowen and Topolov [50] Bowen and Kara [56]	Kar-Gupta and Venkatesh [78] Guinovart-Diaz et al. [79] Della and Shu [80] Ren and Fan [81] Rodrigues-Ramos et al. [91] Berger et al. [97] Lopez-Lopez et al. [98]	Newnhamm et al. [43] Bowen et al. [83]
Numerical	Kar-Gupta and Venkatesh [7] Iyer and Venkatesh[57-58]	Iyer and Venkatesh[57] Kar-Gupta and Venkatesh [7, 59]	Bosse et al. [61] Challagulla and Venkatesh [62]	Zhang and Wu [93] Kar-Gupta and Venkatesh [94, 95] Pettermann and Suresh [96] Berger et al. [97] Li et al. [99]	Zhang and Wu [93] Kar-Gupta and Venkatesh [95] Lewis et al. [101]
Experimental		Guo et al. [63]	Boumchedda et al. [64]	Yoon et al. [68] Schwarzer and Roosen [70] Steinhausen et al. [71]	Rittenmyer et al. [73] Chen and Wu [74]

Table 2-2: Summary of the various literatures which are based on classification of porous piezoelectric materials

Classification of Porous Piezoelectric materials			
Lead Zirconium Titanate (PZT-7A)	Barium Sodium Niobate (BNN)	Barium Titanate ($BaTiO_3$)	Relaxor Ferroelectrics (RL)
Bosse et al. [55] Challagulla and Venkatesh [56]	Bao et al. [103] Warner et al. [140]	Kar-Gupta and Venkatesh [7] Kumar et al. [104]	Reznitchenko et al. [105] Lee et al. [107] Park et al. [108] Topolov et al. [109, 110] Singh et al. [111] Zhou et al. [117] Cao et al. [118] Zhang et al. [139]

Overall, a broad research has been done in the field of porous piezoelectric ceramics (section 2.2) by various authors, in order to increase their performance to make them suitable for various applications. Some authors briefly compared piezoelectric structures consisting of different type of porosity; for example, Iyer and Venkatesh [57] compared the electromechanical response of 3-0 and 3-1type porous piezoelectric materials, and Challagulla and Venkatesh [62] compared the electromechanical response of 3-1 and 3-3 type porous piezoelectric materials. However, a brief comparison using 3-D finite element modelling of all three types of porous piezoelectric structure (i.e. 3-0, 3-1 and 3-3 type), made up of different type of piezoelectric materials has not been studied in detail. Other effects such as foam shape, porosity aspect ratio and porosity volume fraction on various available porous piezoelectric materials (section 2.4) consisting of 3-3 type porosity has yet to be considered in detail as well.

Furthermore, poling could be an extremely challenge due to the typical ceramic behaviour (i.e. brittle behaviour) of piezoelectric porous ceramics, that's why piezoelectric composite materials (combination of piezoelectric ceramics and passive polymers) are getting importance as they eliminates some of the limitations of monolithic piezoelectric ceramics (section 2.3).

However, this thesis only limits the research on numerical modelling of the porous piezoelectric materials consisting of different types of porosity such as 3-0, 3-1 and 3-3 type. Also, this thesis considers the importance of 3-3 type porous piezoelectric materials; therefore study the effects of foam shape, porosity aspect ratio and porosity volume fraction on 3-3 type porous piezoelectric materials as well.

CHAPTER 3

3 Finite element modelling of porous piezoelectric foam structures

3.1 Unit-cell method

The finite element method (FEM) is a widespread and powerful tool for numerical analysis of complex structures. Commercially available finite element software ABAQUS has been used to develop unit-cell based finite element models to determine all the 45 independent material constants and the figures of merit of porous piezoelectric structures (i.e. 3-0, 3-1 and 3-3 type porous piezoelectric structures).

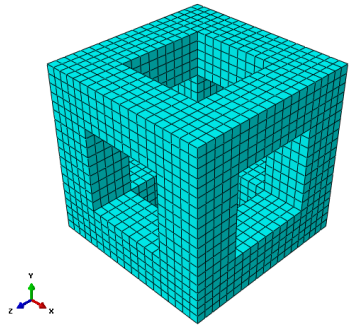

Figure 3.1: Representation of the meshed unit-cell utilizing piezoelectric family (Eight-node, linear piezoelectric brick elements (C3D8E)) as an element type for 3-3 type piezoelectric foam structure

Standard element library, Linear geometric order and piezoelectric family (Eight-node, linear piezoelectric brick elements (C3D8E)) are utilized for the piezoelectric foam structures where each node is allowed four degrees of freedom as shown in Figure 3.1 (three translational and one electric potential). As the unit cell is expected to capture the electromechanical response of composite system, particular care has been taken in invoking boundary conditions to ensure that the electromechanical deformation characteristics of the microscopic unit cells under

conditions of electric and mechanical loading are representative of the deformation of the macroscopic piezoelectric structures.

It is assumed that the piezoelectric material is poled in the 2-direction in all studies. The applied electric field is assumed to be high enough that can polarize the entire material in the poling direction but small enough to prevent dielectric breakdown of the material. To ensure that the deformation and electric potential across the boundaries of the representative unit cell is compatible with the deformation of the adjacent unit cells, the constraint equations for 3-1, 3-2 and 3-3 type porous structures are identified (Figure 3.2), where the nodes A (AA), B (BB), C (CC), D (DD) are designated as master nodes and *u* refers to all four degrees of freedom (i.e., *u* = 1, 2, 3 (mechanical) and 9 (electrical, notation "9" is according to the ABAQUS standard)):

(i) For periodicity in 1-direction: $u^{R} - u^{A} = u^{S} - u^{B}$; $u^{V} - u^{A} = u^{W} - u^{B}$; $u^{VV} - u^{DD} = u^{WW} - u^{CC}$; and $u^{XM} - u^{A} = u^{XP} - u^{B}$; $u^{RR} - u^{AA} = u^{SS} - u^{BB}$ [3-1]

(ii) For periodicity in 2-direction: $u^{U} - u^{A} = u^{UU} - u^{AA}$; $u^{S} - u^{\mathbf{B}} = u^{SS} - u^{BB}$; $u^{YM} - u^{A} = u^{YP} - u^{AA}$ [3-2]

(iii) For periodicity in 3-direction: $u^{T} - u^{D} = u^{U} - u^{A}$, $u^{TT} - u^{DD} = u^{UU} - u^{AA}$, $u^{W} - u^{B} = u^{WW} - u^{C}$; $u^{ZM} - u^{B} = u^{ZP} - u^{C}$ [3-3]

By observing the electromechanical response of a particular unit cell to a series of controlled mechanical and electrical loading conditions, all the 45 material constants that corresponds to particular composite can be identified. Figures of merit (Chapter 1) can then be evaluated from these identified material constants to assess the performance of piezoelectric materials. A key feature of this type of finite element modelling is that all types of unit cells

analyzed are subjected to one general set of periodic boundary conditions for all loading conditions.

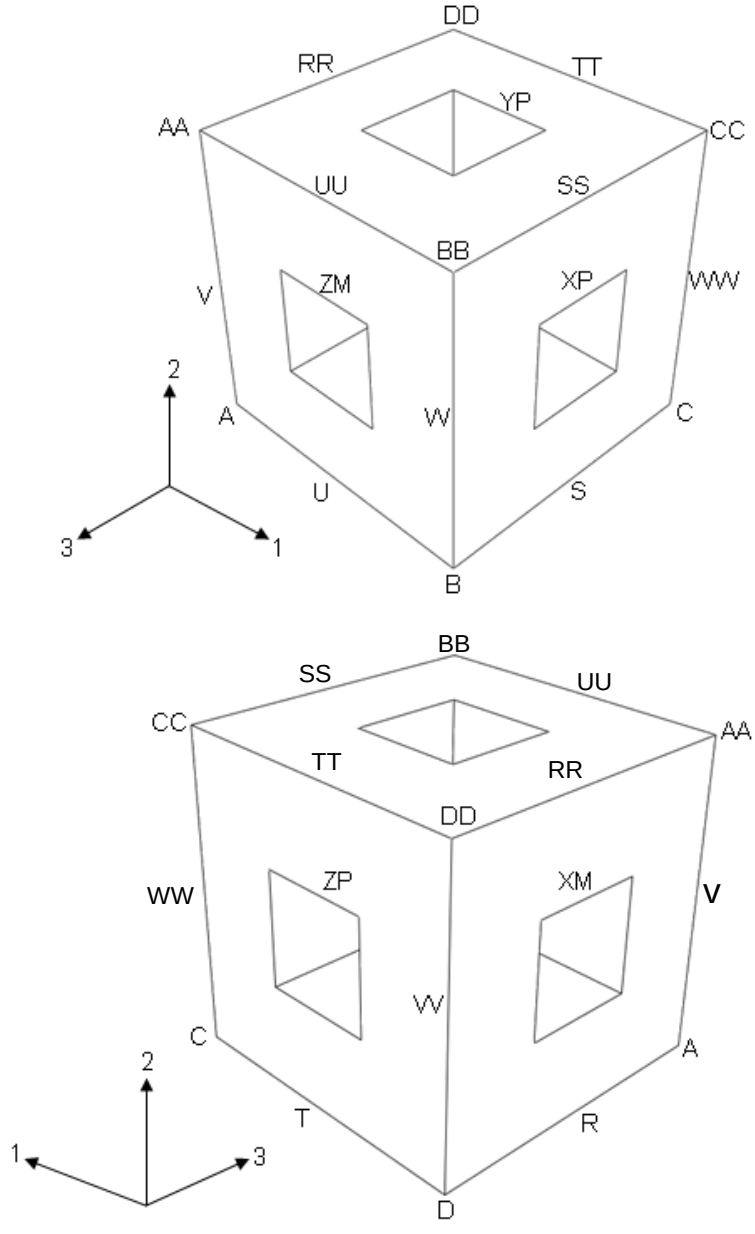

Figure 3.2: Schematic representing various node sets identified for the finite element modeling of the 3-3 type piezoelectric foam structures (Chapter 3 and 4)

3.2 Calculations of various effective properties of porous piezoelectric structures

As explained in section 1.2.2.1.4, there are 81 elastic, piezoelectric and dielectric constants need to be calculated to fully characterize the electromechanical response of piezoelectric materials, of which 45 (21 elastic, 15 piezoelectric and 6 dielectric) constants are generally identified as being truly independent constants. The basic procedure invoked to calculate first column of constitutive relation matrix (equation 1-2) (i.e. C_{11}, C_{12}, C_{13}, C_{14}, C_{15}, C_{16}, e_{11}, e_{21}, e_{31}) and also dielectric constants (i.e. κ_{11}, κ_{22}, and κ_{33}) are obtained as below and the same procedure will be used for the rest of the columns of constitutive relation matrix (equation 1-2) in order to calculate other constants.

(i) By applying a known displacement (δ) on master nodes B-BB-CC-C, strain ϵ_{11} is applied on face B-BB-CC-C (Figure 3.2) in the 1-direction by keeping face A-AA-DD-D mechanically fixed (equations 3-4, 3-5 and 3-6). All other strain components are set to zero (i.e. $\epsilon_{22}= \epsilon_{33}= \epsilon_{13}= \epsilon_{12}=0$) as well as electric potentials are assumed to be electrically grounded (i.e. E1=E2=E3=0).

$$u^{B} = u^{BB} = u^{C} = u^{CC} = \delta, \text{ for u=1} \quad [3\text{-}4]$$

$$u^{B} = u^{BB} = u^{C} = u^{CC} = 0, \text{ for u=2, 3 and 9} \quad [3\text{-}5]$$

$$u^{B} = u^{BB} = u^{C} = u^{CC} = 0, \text{ for u=1, 2, 3 and 9.} \quad [3\text{-}6]$$

So, strain in the 1-direction (i.e. ϵ_{11}) is given as equation 3-7:

$$\epsilon_{11} = \frac{\text{Displacement } (\delta)}{\text{Orginal length along } 1-\text{direction}} \quad [3\text{-}7]$$

Similarly, other strain components (i.e. ϵ_{22}, ϵ_{33}, ϵ_{23}, ϵ_{13}, ϵ_{12}) can be computed as well.

(ii) Stress components (i.e. σ_{11}, σ_{22}, σ_{33}, σ_{23}, σ_{13}, σ_{12}) can be then calculated. For example, σ_{11} is calculated by summing the reaction forces in the 1-direction acting on master nodes B-BB-CC-C (equation 3-8), dividing by area of unit-cell normal to the 1-direction.

$$\text{Stress } (\sigma_{11}) = \frac{\text{Sum of reaction forces on B}-\text{BB}-\text{CC}-\text{C}}{\text{Normal area}} \quad [3\text{-}8]$$

Similarly, other stress components (i.e. σ_{22}, σ_{33}, σ_{23}, σ_{13}, σ_{12}) can be computed as well.

(iii) Depending upon the continuity, the unit-cell can be divided into various sections (named as Fiber and Matrix in this thesis). Fiber and matrix distribution based on the continuity in the 1-direction is shown in Figure 3.3 (named as Fiber1 and Matrix1). Similarly, Fiber2, Matrix2 and Fiber3, Matrix 3 in 2 and 3-direction respectively, can be determined as well.

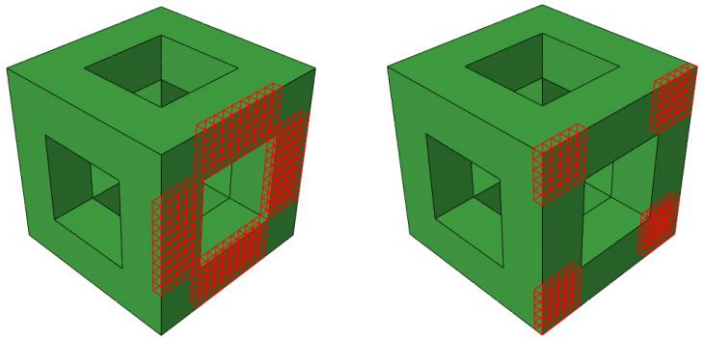

(a) (b)

Figure 3.3: Distribution of (a) Fiber1 and (b) Matrix1 section in the 1-direction on the unit-cell depending upon continuity of the unit-cell representing 3-3 type piezoelectric foam structure

Three electric displacement component vectors (i.e. D_1, D_2, and D3) as shown in equation 1-2 are then determined by considering the total effective electric flux on the Fibers and Matrixes in various directions over the total area of face of the unit-cell.

For example, electric displacement component along 1-direction (i.e. $D_{1)}$ can be calculated (equation 3-9) using electric flux of face B-BB-C-CC as:

$$D_1 = \frac{\text{Total electric flux(Fiber1)} * \text{Area of Fiber1}}{\text{Total Area of face B}-\text{BB}-\text{C}-\text{CC}} + \frac{\text{Total electric flux(Matrix)} * \text{Area of Matrix}}{\text{Total Area of face B}-\text{BB}-\text{C}-\text{CC}} \quad [3\text{-}9]$$

Similarly, electric displacement component along 2 and 3-direction (i.e. D_2 and D_3) can be computed as well.

(iv) So after calculating 6 stress components (i.e. σ_{11}, σ_{22}, σ_{33}, σ_{23}, σ_{13}, σ_{12}) and 3 electric displacement components (i.e. D_1, D_2, and D_3) and using constitutive relation matrix (equation 1-2), C_{11}, C_{12}, C_{13}, C_{14}, C_{15}, C_{16}, e_{11}, e_{21}, e_{31} are obtained.

For an instance, elastic, piezoelectric constants in the 1-direction (i.e. C_{11} and e_{11}) can be calculated as (equations 3-10 and 3-11):

$$C_{11} = \frac{\sigma 11}{\epsilon 11} \text{ (GPa);} \quad [3\text{-}10]$$

$$e_{11} = \frac{D1}{\epsilon 11} \text{ (C/m}^2\text{).} \quad [3\text{-}11]$$

Similarly, other constants (i.e. C_{12}, C_{13}, C_{14}, C_{15}, C_{16}, e_{21}, e_{31}) can be computed as well.

(v) Also, after calculating electric displacement components (i.e. D_1, D_2, and D_3), and electric field vector (i.e. E_1, E_2, and E_3), dielectric constants (i.e. κ_{11}, κ_{22}, and κ_{33}) can be computed as follows:

For example, dielectric constant in the 1-direction i.e. κ_{11} can be calculated as (equation 3-12);

$$\kappa_{11} = \frac{D1}{\text{Electric field vector E1}} \quad [3\text{-}12]$$

Where electric field vector (E_1) is given as (equation 3-13);

$$E_1 = \frac{\text{Applied Electric potential in 1-direction}}{\text{Lenth of unit-cell along 1-direction}} \quad [3\text{-}13]$$

Similarly, other dielectric constants in 2 and 3-directions (i.e. κ_{22} and κ_{33}) can be determined as well.

Using this general approach and eight other boundary conditions, other constants can be easily evaluated as well. Figures of merit which determines the capability of piezoelectric materials can be determined using elastic, dielectric and piezoelectric constants as explained in section 1.2.2.1.5.

3.3. Assumptions

Following is the list of the assumptions for analyzing various porous structures:

(i) The porous piezoelectric structures have been assumed to be perfectly poled in 2-direction.

(ii) The porous piezoelectric structures are assumed to be periodic and poled in 2-direction.

(iii) All porous piezoelectric structures have been assumed to have only cubic porosity.

(iv) It is assumed that no micro-porosity exists within the struts

(v) All porous piezoelectric structures are assumed to be not having multiple porosities.

3.4 Mesh Sensitivity Analysis

To check the accuracy of the results, mesh analysis have been performed for the 3-3 type porous piezoelectric material (to be decribed in next chapter) made of lead zirconium titanate PZT 7-A [62]. The unit cell model for 3-3 type porous piezoelectric material subjected to four different global seed sizes i.e. 0.25, 0.35, 0.55 and 5, while meshing unit-cell as shown in Figure 3.4.

With the interpretation of the results obtained by fine (0.25, 0.35 and 0.55 global seed size) and coarse (5 global seed size) mesh, the accuracy can be anticipated. The complete electromechanical response for the 3-3 type porous piezoelectric foam structure has been obtained as explained in the section 3.2, however, only the elastic (C_{22}) constant, dielectric (κ_{22}) constant and piezoelectric coefficient (e_{22}) is presented in Figure 3.5.

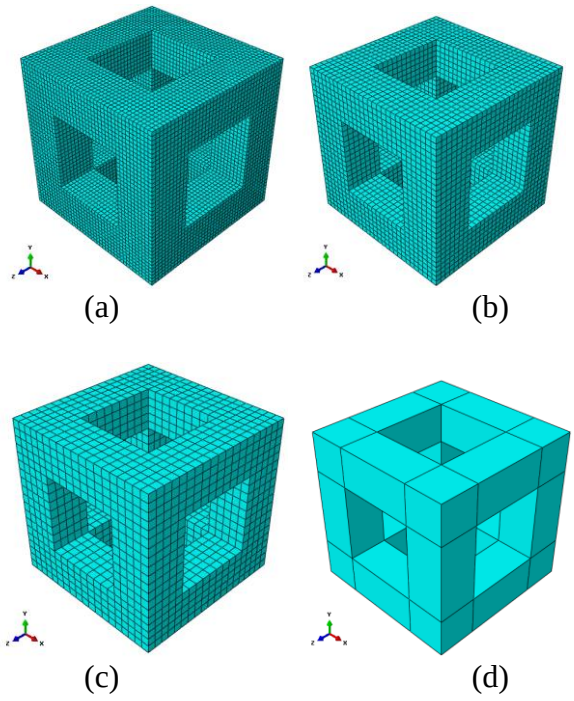

Figure 3.4: Illustration of the unit-cell for 3-3 type porous piezoelectric structure by subjecting to various global seed size's; (a) 3-3 type porous piezoelectric structure with global seed size of 0.25 (b) 3-3 type porous piezoelectric structure with global seed size of 0.35 (c) 3-3 type porous piezoelectric structure with global seed size of 0.55 and (d) 3-3 type porous piezoelectric structure with global seed size of 5

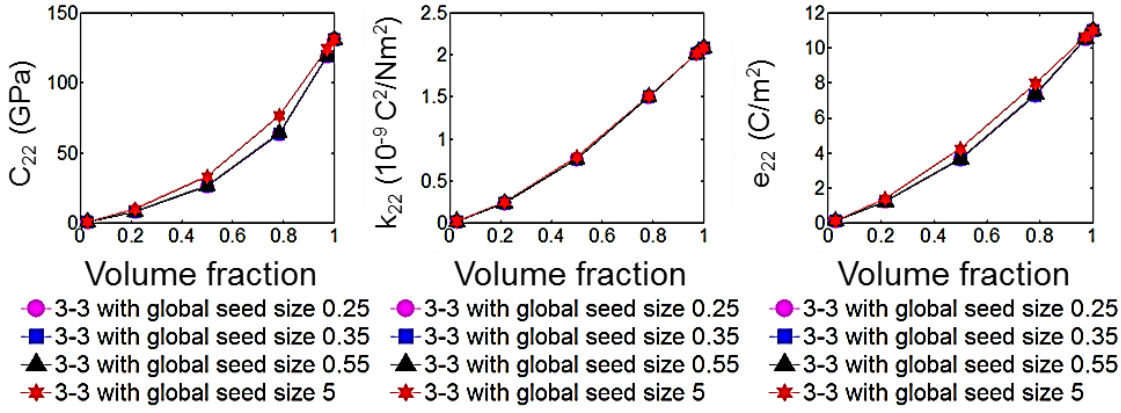

Figure 3.5: Mesh analysis results obtained by implementing various global seed size's (0.25, 0.35, 0.55 and 5) for 3-3 type porous piezoelectric material made up of lead zirconium titanate (PZT-7A)

Results found in the mesh analysis have shown convergence at the selected global seed sizes (i.e. 0.25, 0.35 and 0.55) and divergence at the global seed size of 5 as shown in Figure 3.5. From this analysis, it is evident that any seed size between 0.25-0.55 can be used for characterizing the electromechanical response of porous piezoelectric structures. However, all models in this thesis have been modelled and analysed using very fine mesh with the selected global seed size between 0.25-0.55.

3.5 Element Analysis

To further investigate the accuracy of results, element analysis has been performed for the 3-3 type porous piezoelectric material (to be decribed in next chapter) made up of lead zirconium titanate PZT-7A [62]. The unit cell model for 3-3 type porous piezoelectric material has been developed, using ABAQUS as explained in section 3.1. By taking into consideration, the convergence of various results obtained with the implementation of different global seed size's to the unit-cell as explained in the section 3.3, seed size of 0.35 has been selected in order to perform the element type analysis on 3-3 type porous piezoelectric structure. The unit-cell has been subjected to the three meshing element types i.e. eight-node linear piezoelectric brick elements (C3D8E), twenty-node quadratic piezoelectric brick elements (C3D20E) and twenty-node quadratic piezoelectric brick, reduced integration elements (C3D20RE), while meshing the unit-cell. The complete elecromechanical response for the 3-3 type porous piezoelectric foam structure has been obtained as explained in the section 3.2, however, only the elastic (C_{22}) constant, dielectric (κ_{22}) constant and piezoelectric coefficients (e_{22}) are presented in Figure 3.6.

The convergence of results as shown in Figure 3.6 proves that various element type options available in ABAQUS could be utilized while performing finite element analysis of porous piezoelectric structures. However, the total time consumed for performing simulations

(workstation processor was Intel (R) Xeon (R) CPU W3540 @2.93GHz with RAM of 16.0GB) was maximum for C3D20E, followed by C3D20RE and lowest for C3D8E. For example, total CPU time consumption for 3-3 type porous piezoelectric foam structure (porosity volume fraction of 78.4%) with global seed size of 0.55 and element types such as C3D20E, C3D20RE and C3D8E respectively, is 812.8 secs (13.54 mins), 731.5 secs (12.19 mins) and 44.6 secs (0.74 mins). So in order to maintain the consistency and also due to lowest time consumption for performing various finite element analysis simulations, eight-node linear piezoelectric brick elements (C3D8E) has been used as an element type to obtain complete elecromechanical response for all of the porous piezoelectric structures analysed in this thesis.

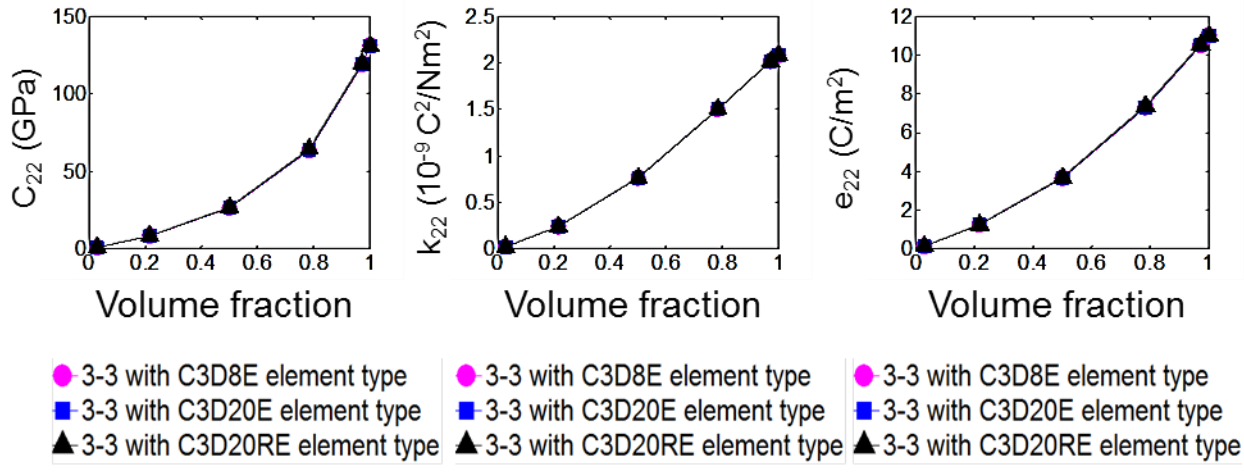

Figure 3.6: Element analysis results obtained by implementing various element types (C3D8E, C3D20E and C3D20RE) for 3-3 type porous piezoelectric material made up of lead zirconium titanate (PZT-7A)

3.6 Validation of results

The verification of results as shown in Figure 3.7 has been performed by comparing the current model (to be decribed in next chapter) results of various piezoelectric porous structures

(i.e. 3-0, 3-1 and 3-3 type) results with an analytical 3-0 model [49], analytical 3-1 model [55] and a numerical 3-3 finite element unit-cell model [61].

A PZT-5 (lead zirconium titanate) [49] based 3-0 porosity type unit-cell model (to be decribed in next chapter) developed in current study is used to compare the results with the analytical model based on effective medium approach developed by Dunn and Taya [49]. Also, a barium titanate ($BaTiO_3$) [7] based 3-1 porosity type unit-cell model (to be decribed in next chapter) develpoed in current study is used to compare the results with that of the analytical model based on asymptotic homogensation technique developed by Bravo-Castillero et. al. [55].

By comparing, the elastic constant, dielectric constant and piezoelectric coefficient along poling direction i.e. C_{22}, κ_{22}, and e_{22} respecively, for the three-dimensional finite element model of 3-0 and 3-1 porosity type piezoelectric material with those of the analytical models [49, 55], it is demonstrated that the finite element model is able to reliably and accurately capture the electromechanical response of a porous piezoelectric material with 3-0 and 3-1 type porosity. Furthermore, the finite element model is also extended to evaluate the complete electromechanical response of a 3-3 type porous piezoelectric material. 3-3 type porous piezoelectric material results have been compared using numerical results by unit-cell model method developed earlier by Bosse et. al. [61].

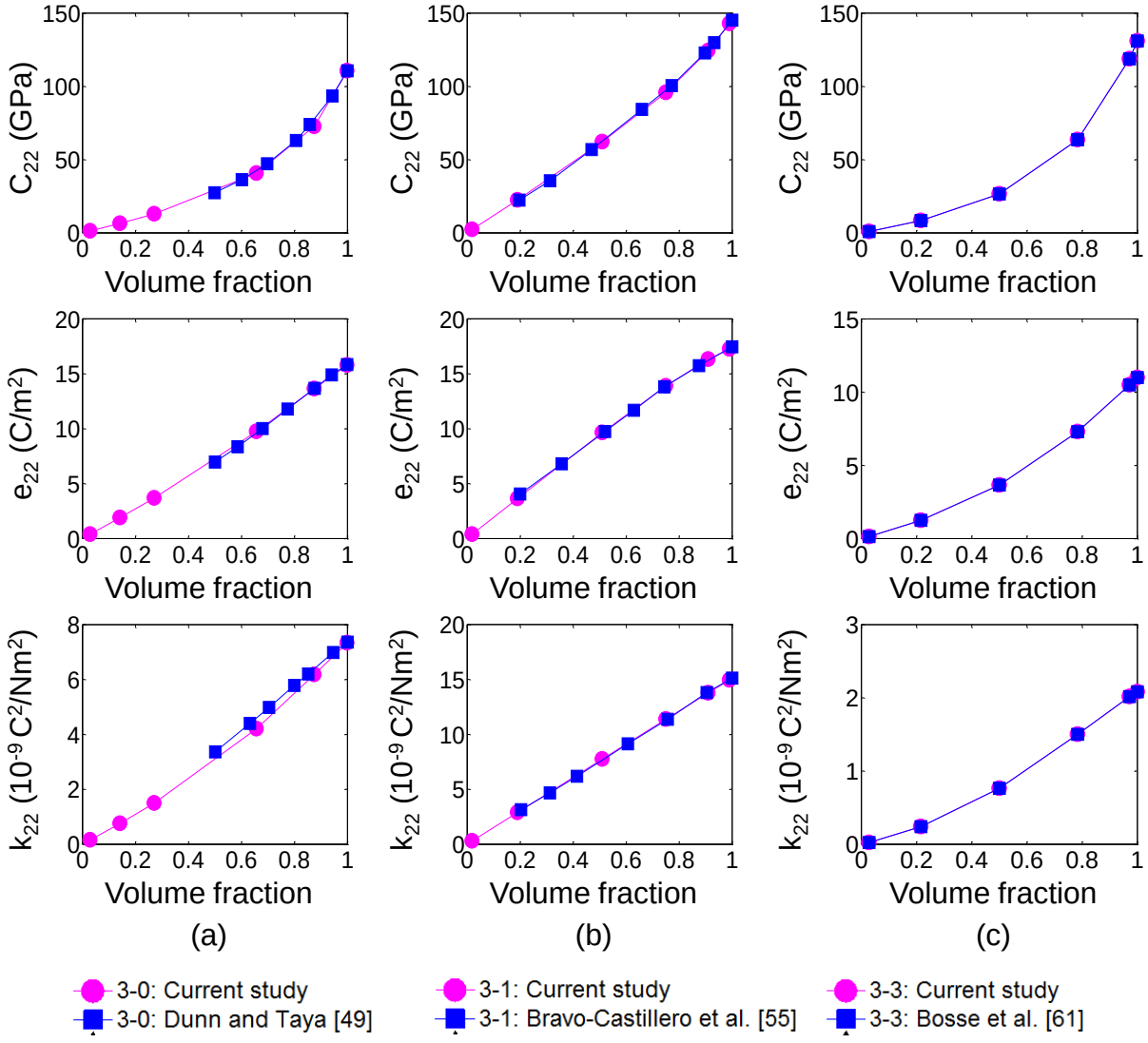

Figure 3.7: Comparisons of results of various unit-cell models (i.e. 3-0, 3-1 and 3-3 type) developed in the current study with that of; (a) analytical [49] model results for 3-0 type porosity; (b) analytical [55] model results for 3-1 type porosity; and (c) numerical model [61] results for 3-3 type porosity

As shown in Figure 3.7, various porous piezoelectric models (i.e. 3-0, 3-1 and 3-3 type) developed in this study shown good agreement with the other various analytical as well as numerical results for a wide range of porosity volume fractions.

CHAPTER 4

4 Electromechanical properties of relaxor ferroelectric foams

4.1. Introduction

Three-dimensional finite element models are developed to characterize the complete electromechanical properties of relaxor ferroelectric-based foams. In this chapter, it is demonstrated that microstructural features such as porosity volume fraction and connectivity play significant roles in determining the elastic, dielectric, and piezoelectric properties of relaxor foams.

4.2. Objectives

A comprehensive study of the effects of microstructural features such as porosity volume fraction and porosity connectivity on the overall electromechanical properties of relaxor ferroelectric-based piezoelectric foams is not yet available. Hence, the objectives of the present chapter are:

(i) To invoke a unit-cell based finite element model to predict the complete elastic, dielectric, and piezoelectric properties of relaxor ferroelectric-based piezoelectric foams;

(ii) To understand the connections between the microstructural features (such as porosity connectivity and porosity volume fraction) and their effective electromechanical response in the relaxor ferroelectric foams;

(iii) To assess the effects of microstructural features (i.e., porosity connectivity and porosity volume fraction) on the effective figures of merit in relaxor ferroelectric foams; and

(iv) To benchmark the improvement in properties and performance characteristics of relaxor ferroelectric foams in comparison to conventional piezoelectric foams such as those based on lead zirconate titanate (e.g., PZT-7A).

4.3. Classification of porous piezoelectric materials (3-0, 3-1, 3-3)

In the present chapter, three-dimensional finite element models are developed (Figure 4.1) to determine all the 45 independent material constants and the figures of merit of foam materials with zero-dimensional (3-0), one-dimensional (3-1), and three-dimensional (3-3) connectivity.

(i) [3-0] type, where the porosity is enclosed in all three dimensions by a matrix phase as shown in Figure 4.1a.

(ii) [3-1] type, where the porosity exhibits connectivity in the 1-direction as shown in Figure 4.1b.

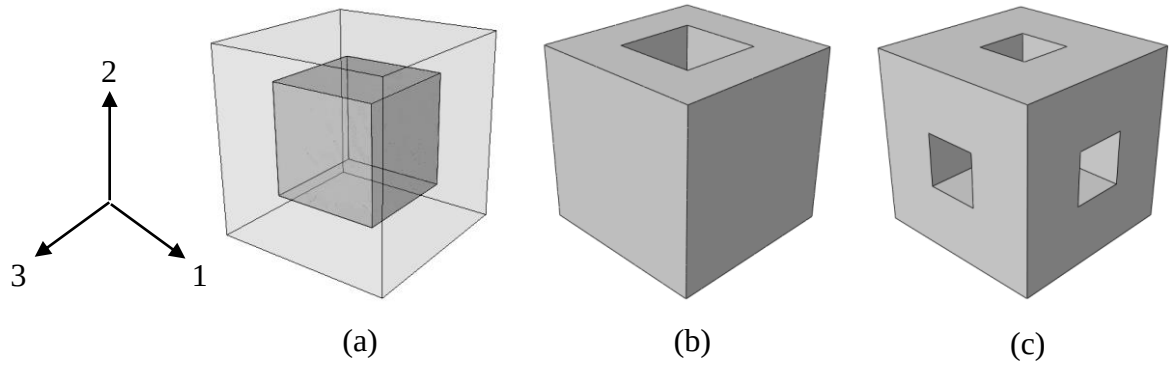

Figure 4.1: Schematic illustrating (a) zero-dimensional (3-0), (b) one-dimensional (3-1) and (c) three-dimensional (3-3) connectivity, respectively, in piezoelectric foam materials (The piezoelectric material is poled along the 2-direction)

(iii) [3-3] type, where the porosity exists in an open inter-connecting network where both the matrix phase and the porosity exhibit connectivity in all three directions as shown in Figure 4.1c.

From a knowledge of the fundamental properties of a piezoelectric material, several figures of merit, such as the coupling constant (K_t), the hydrostatic strain coefficient (d_h), the hydrostatic voltage coefficient (g_h), the hydrostatic figure of merit ($d_h g_h$), the acoustic impedance (Z), the receiving sensitivity (M), can be quantitatively determined to assess the utility of porous piezoelectric materials in practical applications. (Higher d_h, g_h , $d_h g_h$ and K_t, respectively, result in improved receiving sensitivity *(M)*, enhanced signal-to-noise ratio, and enhanced efficiency in devices such as hydrophones).

A representative relaxor ferroelectric (i.e., PMN-33%PT) [139] and a conventional piezoelectric (i.e., PZT-7A) [62] are selected for the present study (The fundamental properties of these materials are shown in Table 4.1). In the finite element model, appropriate geometric and boundary conditions are invoked to ensure that the electromechanical deformation response of the unit-cell, under conditions of electrical and mechanical loading, is representative of the entire porous piezoelectric system [42]. The piezoelectric materials are considered to be poled in the 2- direction.

4.4. Results and discussions

The principal results (Figures 4.2, 4.3 and Table 4.2) obtained from the present study on characterizing the electromechanical properties of the relaxor ferroelectric-based foam materials are described below.

(i) In general, all the elastic, dielectric, and piezoelectric properties of relaxor foams vary non-linearly with changes in the porosity volume fraction.

(ii) For all the piezoelectric porosity structures (i.e. 3-0, 3-1 and 3-3 type) are analyzed, relaxor foams exhibits higher dielectric constant (κ_{22}) and piezoelectric coefficient (e_{22}) in longitudinal direction (parallel to poling direction) as compared to lead zirconium titanate. Whereas, lead zirconium titanate has higher elastic constant in longitudinal direction as compared to relaxor foams. For example, at porosity volume fraction of 21.6%, the dielectric constant (κ_{22}) and piezoelectric coefficient (e_{22}) respectively, for foams made up of relaxor and exhibits 3-0 type porosity connectivity are, 14.98 C/m^2 and $4.56*10^{-9}$ C^2/Nm^2. Whereas, the dielectric constant (κ_{22}) and piezoelectric coefficient (e_{22}) for foams made up of lead zirconium titanate and exhibits 3-0 type porosity connectivity respectively are, 7.84 C/m^2 and $1.53\times e^{-9}$ C^2/Nm^2.

(iii) Amongst the relaxor foams with a particular porosity volume fraction, the porosity connectivity plays a significant role in determining their electro-elastic properties. The principal material constants along the poling direction such as C_{22}, κ_{22}, and e_{22} of the relaxor foams with 3-1 connectivity are typically higher than that of foams with 3-3 connectivity.

For example, at porosity volume fraction of 21.6% C_{22}, κ_{22}, and e_{22} respectively for foams made up of relaxor ferroelectrics are, 28.58GPa, 17.90 C /m2 and 4.79 C^2/Nm^2 for 3-1 type porous piezoelectric structures. Whereas C_{22}, κ_{22}, and e_{22} respectively for foams made up of relaxor ferroelectrics are, 25.43GPa, 14.07 C $/m^2$ and 4.72 C^2/Nm^2 for 3-3 type porous piezoelectric structures.

Table 4.1: Fundamental properties of novel materials analyzed (relaxor ferroelectric (i.e., PMN-33%PT) [138] and a conventional piezoelectric (i.e., PZT-7A) [61])

	Lead zirconium titanate (PZT-7A) (ρ=7700 kg/m^3)	Relaxor ferroelectric (PMN-33%PT) (ρ= 8060 Kg/m^3)
C_{11}^{E} (GPa)	148	115
C_{12}^{E} (GPa)	74.2	102
C_{13}^{E} (GPa)	76.2	103
C_{22}^{E} (GPa)	131	103
C_{23}^{E} (GPa)	74.2	102
C_{33}^{E} (GPa)	148	115
C_{44}^{E} (GPa)	25.3	69
C_{55}^{E} (GPa)	35.9	66
C_{66}^{E} (GPa)	25.3	69
e_{16} (C/m$^{2)}$	9.31	10.1
e_{21} (C/m$^{2)}$	-2.324	-3.9
e_{22} (C/m$^{2)}$	10.9	20.3
e_{23} (C/m$^{2)}$	-2.324	-3.9
e_{34} (C/m$^{2)}$	9.31	10.1
k_{11}^{ϵ} (10^{-9} C^2/Nm^2)	3.98	12.7
k_{22}^{ϵ} (10^{-9} C^2/Nm^2)	2.081	6.02
k_{33}^{ϵ} (10^{-9} C^2/Nm^2)	3.98	12.7

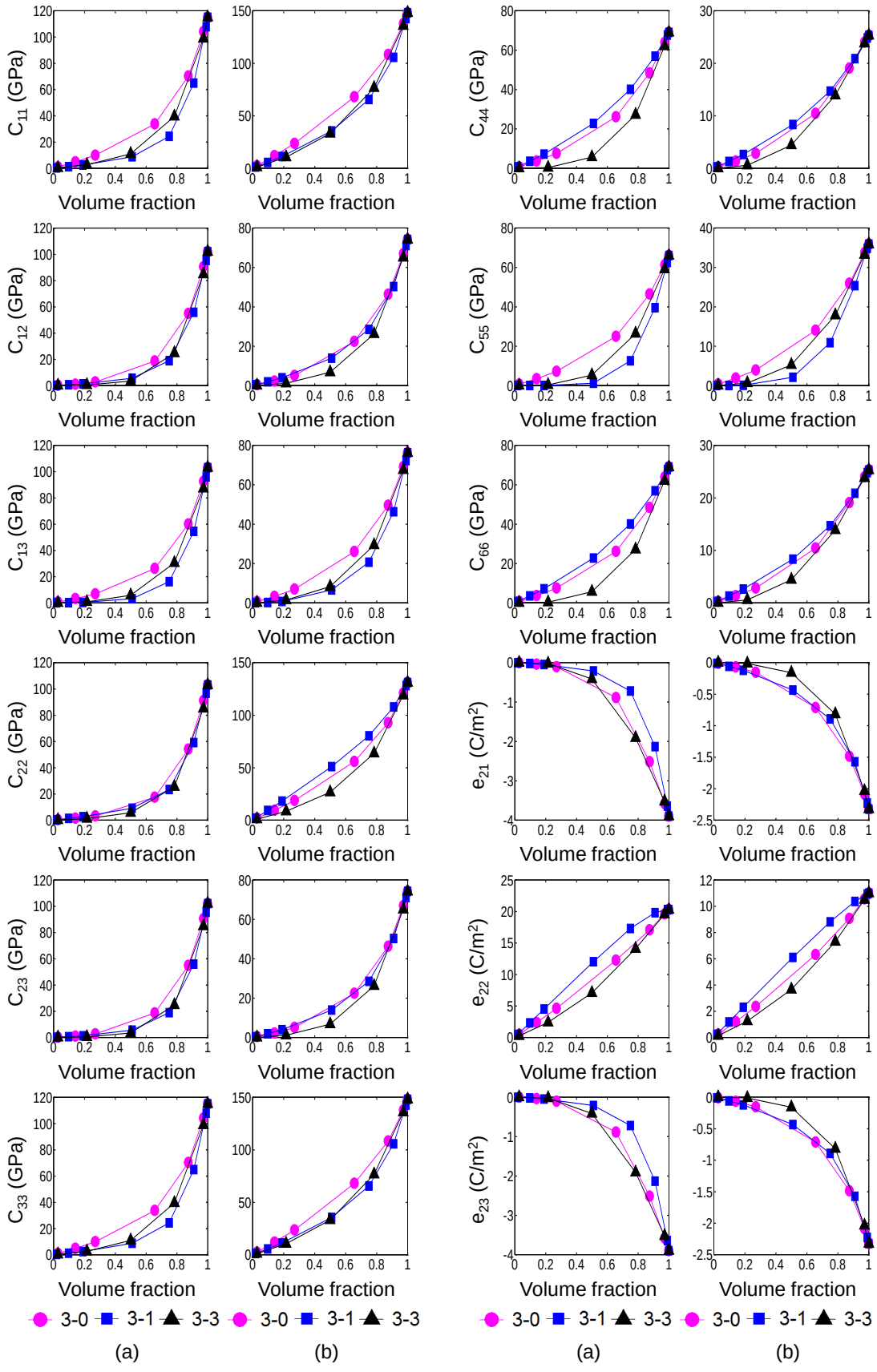
C11 (GPa)
C44 (GPa)
C12 (GPa)
C55 (GPa)
C13 (GPa)
C66 (GPa)
C22 (GPa)
e21 (C/m2)
C23 (GPa)
e22 (C/m2)
C33 (GPa)
e23 (C/m2)
Volume fraction
3-0 3-1 3-3
(a)
(b)

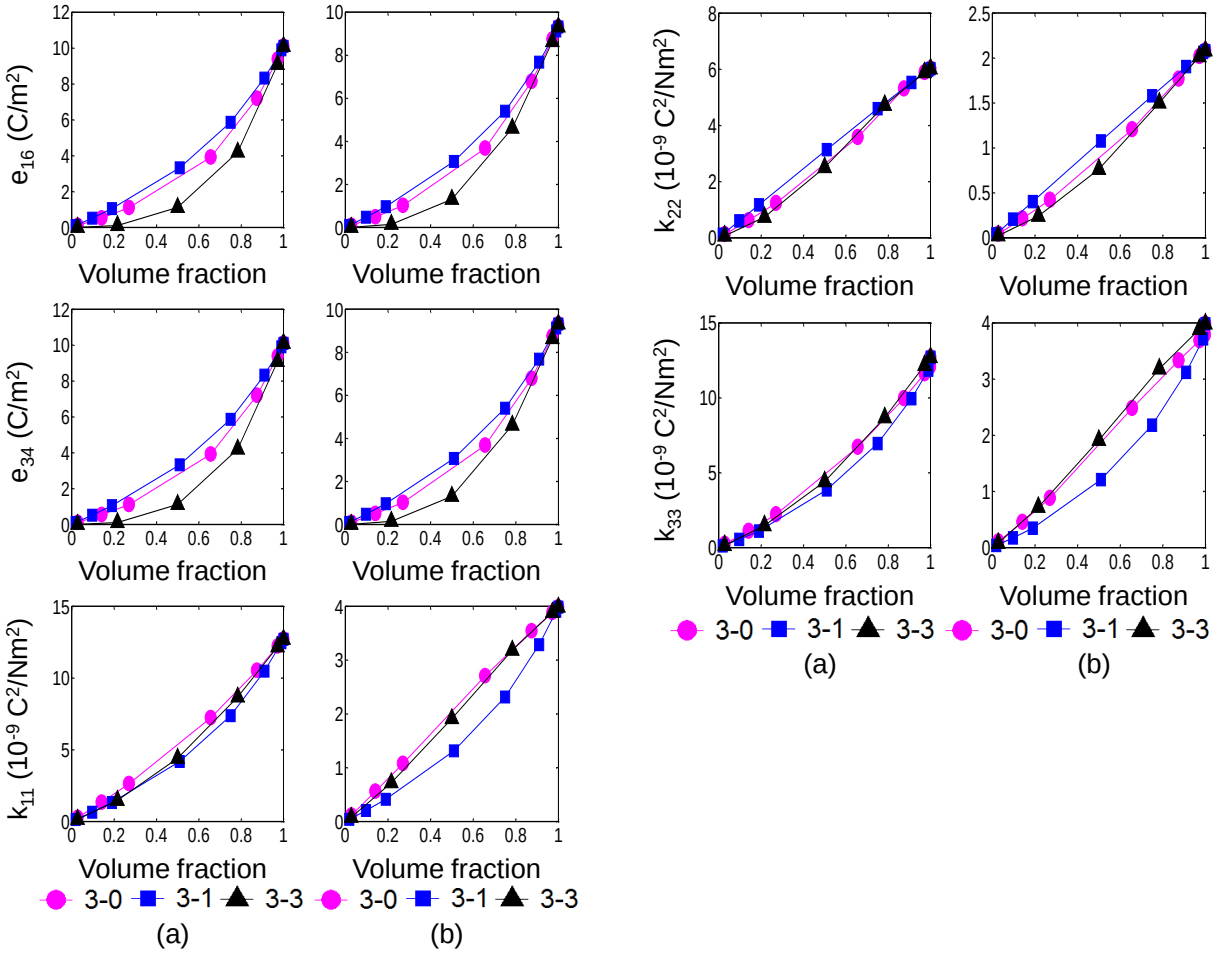

Figure 4.2: Variations of the fundamental elastic, piezoelectric and dielectric constants with material volume fraction in (a) novel relaxor ferroelectric (PMN-PT) - based and (b) traditional piezoelectric (PZT-7A) - based foam materials

On the other hand, the principal material constants in the transverse direction, such as C_{11} and κ_{11}, are higher for the foams with 3-0 type connectivity. Some of the shear constants, such as C_{12} and C_{13}, are higher for foams with 3-0 type connectivity while other shear constants, such as C_{44} and C_{66}, are higher for foams with 3-1 type of connectivity. The trends observed in relaxor foams are similar to that observed in PZT-7A foams as well.

(iv) The figures of merit such as the piezoelectric coupling constant (K_t), hydrostatic strain coefficient (d_h), hydrostatic voltage coefficient (g_h) and the hydrostatic figure of merit ($d_h g_h$) generally increase and the acoustic impedance (Z) decreases, as expected, with the introduction of porosity in the relaxor ferroelectric and PZT-7A foams (Figure 4.3). However, the potential performance characteristics of relaxor foams in applications, such as hydrophones, are significantly higher than that of PZT-7A foams. For example, at 50% porosity volume fraction of porosity, the K_t, d_h, *and* $d_h g_h$ figures of merit of relaxor foams with 3-3 type connectivity, are, respectively, 40%, 900%, and 3000%, higher than that of 3-3 type PZT-7A foams, while the acoustic impedance of the relaxor foams are almost the same as that of equivalent PZT-7A foams. Thus, the desirable combination of figures of merit, i.e., high coupling constant, strain coefficient, and hydrostatic figure of merit are obtained without increasing the acoustic impedance in the relaxor foams as compared to PZT-7A foams.

(v) It is interesting to note that if strut widths are increased (while the strut shape is unchanged), then, effectively, the porosity volume fraction decreases (Conversely, the material volume fraction in the foam increases). Correspondingly, the electromechanical constants increase with increasing strut thickness. However, the figures of merit such as the piezoelectric coupling constant (Kt), hydrostatic strain coefficient (d_h), and the hydrostatic figure of merit ($d_h g_h$) decrease and the acoustic impedance (Z) increases, with an increase in strut thickness.

(vi) As the figures of merit, such as $d_h g_h$, are influenced by almost all the electro-elastic constants of the piezoelectric (solid/foam) material, a numerical analysis of the sensitivity of the figures of merit to the variations in the fundamental electro-elastic properties was conducted to identify those material constants that have a major influence on the figures of merit. From this study, it was observed that the principal properties along the poling direction, i.e., C_{22}, κ_{22}, and e_{22}, are the most dominant factors that influence the hydrostatic figure of merit ($d_h g_h$), with $d_h g_h$

being maximized by a reduction in the elastic and dielectric constants—C_{22} and κ_{22} and an increase in the piezoelectric constant—e_{22}. In comparing the fundamental properties of relaxor (solid and foam) materials with that of PZT-7A (solid and foam) materials, it is evident that the C_{22} and e_{22} of relaxor ferroelectrics are, respectively, lower and higher than that of PZT-7A and thus their $d_h g_h$ are also higher as well. (The dielectric constant κ_{22} of relaxor is higher than that of PZT-7A which should cause $d_h g_h$ of the relaxor foams to be lower than that of PZT-7A foams. However, the combined effects of C_{22} and e_{22} in increasing the $d_h g_h$ of the relaxor foams are more dominant than that of κ_{22} in decreasing $d_h g_h$.)

(vii) In the finite element models developed in this chapter, it is assumed that the piezoelectric material is poled uniformly in one direction. From a practical point of view, such uniform poling can be readily realized in foams with 3-1 type connectivity. However, poling piezoelectric foams in a uniform manner could be challenging, in the 3-0 and 3-3 type foams.

(viii) From our simulations and analysis, it is postulated that, if the porous regions were to be filled by a low elastic modulus material such as a polymer with a lower dielectric constant, considerable improvements in the uniformity of the poling characteristics across a wide regions of the foams would be achieved while retaining the key advantages of the relaxor foams.

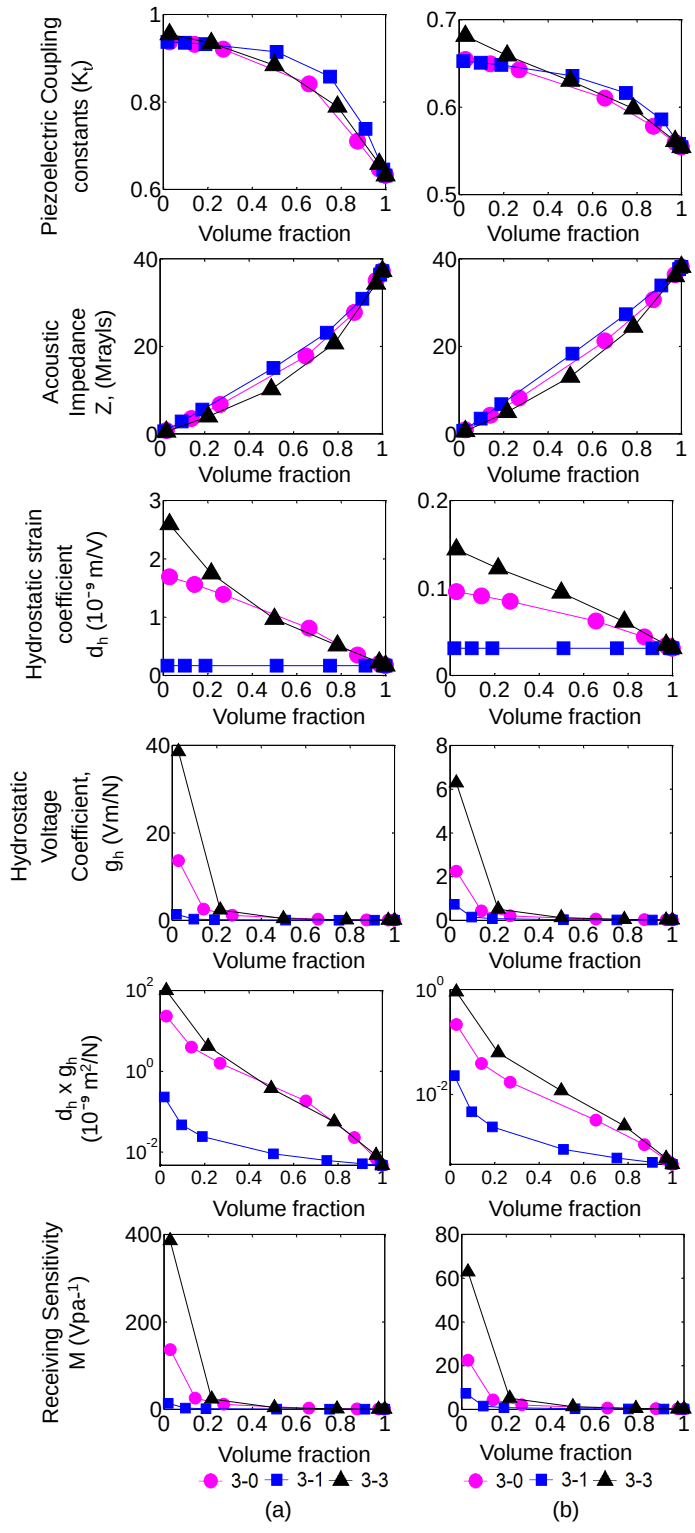

Figure 4.3: Variations of the various piezoelectric figures of merit with material volume fraction in (a) novel relaxor ferroelectric (PMN-PT) - based and (b) traditional piezoelectric (PZT-7A) - based foam materials

In this thesis, it is assumed that no micro-porosity exists within the struts. However, if the struts do contain some micro-porosity, the effective porosity volume fraction in the foam is increased. The electromechanical constants and the figures of merit of the foams with micro-porous struts are expected to be similar to those of foams with solid struts but with higher porosity. The influence of the shape and distribution of micro-porosity within the strut on the effective electromechanical properties of 3-3 type foams will be examined in detail in a future study.

(ix) Table 4.2 shows the variation of various fundamental electromechanical constants and selected figures of merit, with the introduction of various porosities i.e. 3-0, 3-1 and 3-3 (porosity volume fraction of 21.6%) for piezoelectric materials such as lead zirconium titanate (PZT-7A) and relaxor ferroelectric (PMN-PT), by normalising them with respect to their single cell properties. Various elastic, dielectric and piezoelectric constants varied differently for both materials with change in the structure from the single cell (no porosity) structure to the porous structures (3-0, 3-1 and 3-3 type). For example, when the single cell structure changed to the 3-0 type porous structure, elastic constant in the 2-direction i.e. C_{22} is 43% less for PZT-7A and 69% less for PMN-PT.

Significant variations have been noted in the selected figure of merits i.e. d_h, g_h, $d_h g_h$ *and* M. For example, $d_h g_h$ is increased by approximately 1300% and 1100% respectively, when single cell structure has changed to the 3-0 and 3-3 type porous structure for PMN-PT. Whereas, $d_h g_h$ is only increased by approximately 300% and 400% respectively, when single cell structure has changed to the 3-0 and 3-3 type porous structure for PZT-7A.

Table 4.2: Normalised values for the porous (3-0, 3-1 and 3-3 type) piezoelectric structures (with porosity volume fraction of 21.6% i.e. material volume fraction i.e. v.f= 0.78) for both materials i.e. lead zirconium titanate (PZT- 7A) and relaxor ferroelectric (PMN-PT), with respect to the bulk material properties

v.f= 0.78	Lead Zirconium Titanate, PZT-7A				Relaxor Ferroelectric, PMN-PT based		
	3-0	3-1	3-3		3-0	3-1	3-3
C_{11}	0.60	0.44	0.52		0.43	0.21	0.34
C_{12}	0.46	0.38	0.35		0.33	0.19	0.24
C_{13}	0.49	0.27	0.38		0.39	0.16	0.30
C_{22}	0.57	0.61	0.49		0.31	0.23	0.25
C_{23}	0.46	0.38	0.35		0.33	0.19	0.24
C_{33}	0.60	0.44	0.52		0.43	0.21	0.34
C_{44}	0.59	0.58	0.55		0.54	0.58	0.39
C_{55}	0.56	0.30	0.50		0.54	0.19	0.40
C_{66}	0.59	0.58	0.55		0.54	0.58	0.39
e_{16}	0.57	0.58	0.50		0.55	0.58	0.42
e_{21}	0.47	0.38	0.35		0.43	0.19	0.49
e_{22}	0.71	0.80	0.66		0.74	0.85	0.69
e_{23}	0.47	0.38	0.35		0.43	0.19	0.49
e_{34}	0.57	0.58	0.50		0.55	0.58	0.42
κ_{11}	0.81	0.58	0.80		0.71	0.58	0.68
κ_{22}	0.73	0.76	0.72		0.76	0.76	0.78
κ_{33}	0.75	0.55	0.80		0.67	0.55	0.68
K_t	1.07	1.11	1.08		1.23	1.36	1.25
Z	0.69	0.72	0.64		0.61	0.62	0.56
d_h	1.68	1.00	1.98		3.28	1.00	3.05
g_h	2.29	1.32	2.75		4.33	1.31	3.90
$d_h * g_h$	3.85	1.32	5.44		14.19	1.31	11.90
M	2.29	1.32	2.75		4.33	1.31	3.90

4.5 Conclusions

(i) Three-dimensional finite models have been developed to characterize the complete electromechanical properties of relaxor ferroelectric-based foams materials.

(ii) It is demonstrated that the microstructural features of foams, such as porosity volume fraction and porosity connectivity, play a significant role in determining the fundamental elastic, dielectric, and piezoelectric properties of relaxor foams.

(iii) Furthermore, ferroelectric-based foam materials exhibit piezoelectric figures of merit such as the piezoelectric coupling constant (Kt), hydrostatic strain coefficient (d_h), hydrostatic voltage coefficient (g_h), the hydrostatic figure of merit ($d_h g_h$), and the receiving sensitivity (M) which are significantly higher than those observed in traditional piezoelectric foams such as those based on PZT-7A which make them highly desirable for applications such as hydrophones.

CHAPTER 5

5 Electromechanical response of 3-3 piezoelectric foams: a comparative study of novel material systems

5.1 Introduction

3-3 type porous piezoelectric structures made up of several classes of piezoelectric materials such as barium sodium niobate (BNN), barium titanate ($BaTiO_3$) and relaxor (PMN-PT based) ferroelectrics (RL) have been analysed using 3-D finite element modelling (ABAQUS). 9 different types of foam structures are identified by varying microstructural features such as porosity aspect ratio and porosity volume fraction for 3-3 type porous piezoelectric structures made up of various piezoelectric materials.

5.2 Objectives

Several studies have demonstrated that porous piezoelectric materials with unique electromechanical properties are desirable in certain practical applications However, a detailed study of the effect of foam shape, porosity aspect ratio, porosity volume fraction and simultaneously piezoelectric material properties in a range of piezoelectric material systems such as barium sodium niobate (BNN), barium titanate ($BaTiO_3$) and relaxor ferroelectric (RL) material on the overall electromechanical response of 3-3 type piezoelectric foam structures have not been studied in the past. Hence the objectives of present chapter are:

(i) To develop unit-cell based finite element models to predict complete elastic, dielectric and piezoelectric properties of 3-3 type piezoelectric foam structures for a broad range of piezoelectric material systems;

(ii) To investigate the effects of various microstructural features such as foam shape, porosity aspect ratio, porosity volume fraction and simultaneously the fundamental piezoelectric material properties on the effective electromechanical response of 3-3 type piezoelectric foam structures;

(iii) To assess the effects of various microstructural features and simultaneously the fundamental piezoelectric material properties on the effective figures of merit of 3-3 type piezoelectric foam structures.

The rest of the chapter is organized as follows: A Classification of foam structures is presented in section 5.3. Classification of novel materials analysed in this present chapter is presented in section 5.4. The trends observed are presented in section 5.5 and principal conclusions are highlighted in section 5.6.

5.3 Classification of 3-3 type piezoelectric foam structures

Nine distinct foam structures are identified to study the effect of microstructural features such as structural aspect ratio and porosity aspect ratio on effective electromechanical properties of foam structures for broad range of piezoelectric materials systems (Figures 5.1 and 5.2) [61].

(i) Depending on the structural aspect ratio of the foam structure along with the poling direction (i.e., the 2-direction), this chapter identify "longitudinally short'' (L1=L3, L2= 0.25L1) structures (Class I) or "longitudinally tall'' (L1=L3, L2= 1.75 L1) structures (Class III).

(ii) The "equiaxed'' (L1=L2=L3) foam structure (Class II) with cuboidal porosity (porosity aspect ratio = 1).

(iii) Depending on the porosity aspect ratio of the foam structure, for each of above mentioned foam structures, this chapter identify structures with "flat" (i.e. $b= 0.25a$) or "elongated" porosity (i.e. $b=4a$).

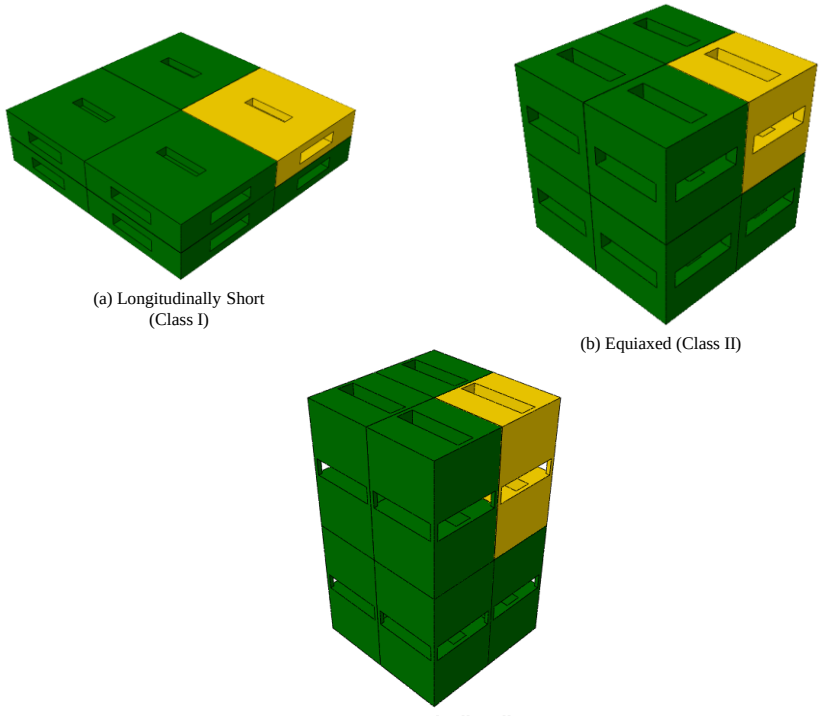

Figure 5.1: Schematic illustrating three classes of piezoelectric foam structures: (a) longitudinally short structure (Class I); (b) equiaxed structure (Class II); and (c) longitudinally tall structure (Class III)

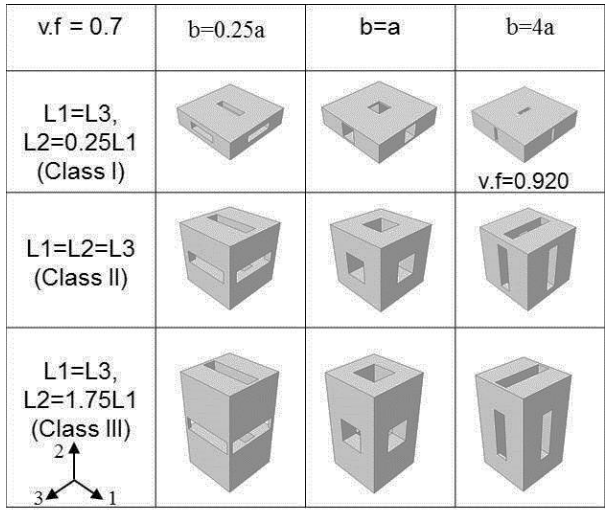

Figure 5.2: Schematic illustrating nine piezoelectric foam structures based on structural aspect ratio and porosity aspect ratio for three different classes (Class I, Class II and Class III)

5.4 Classification of piezoelectric materials used in this chapter

In order to study the effects of material properties on the effective properties of 3-3 type piezoelectric foam structures, 3 types of novel materials are analysed. Following is the basic description of the materials analyzed in the present chapter:

5.4.1. Barium sodium niobate (BNN)

Barium sodium niobate exhibits tungsten-bronze structure in which all 15 and 12-fold-coordinated sites are occupied by Ba and Na ions [103]. Single crystal barium sodium niobate exhibits the lowest crystal symmetry of mm2 (orthorhombic crystal class). Table 5.1 shows elastic, piezoelectric and dielectric properties of single crystal barium sodium niobate [140].

5.4.2. Barium titanate ($BaTiO_3$)

Barium titanate exhibit excellent piezoelectric properties and has been used in various applications such as multi-layer ceramic capacitors (MLCC), positive temperature coefficient of resistance thermistors, piezoelectric sensors, transducers, actuators and ferroelectric random access memories and electro optic devices [104]. Table 5.1 shows the properties of single crystal barium titanate [7]. Barium titanate has the highest elastic and dielectric properties along poling direction (i.e. 2-direction) compared to barium sodium niobate and relaxor ferroelectric material. Barium titanate exhibits 4mm (tetragonal crystal class) crystal symmetry.

5.4.3. Relaxor ferroelectrics (PMN-33%PT)

Due to exceptionally large dielectric permittivity, electrostrictive and piezoelectric parameters, relaxor ferroelectrics was found to have excellent piezoelectric properties [105-111]. Table 5.1 shows various elastic, piezoelectric and dielectric properties of single crystal relaxor

ferroelectrics [139] used in the present study. Single crystal relaxor ferroelectric exhibits 4mm (tetragonal crystal class) crystal symmetry.

Table 5.1: Fundamental properties of three novel materials analyzed (barium sodium niobate (BNN) [140], barium titanate ($BaTiO_3$) [7] and relaxor ferroelectrics (RL) [139])

	Barium sodium niobate (BNN) (ρ= 5300 Kg/m^3)	Barium titanate ($BaTiO_3$) (ρ= 5700 kg/m^3)	Relaxor ferroelectric (RL) (ρ= 8060 Kg/m^3)
C_{11}^E (GPa)	238.9	150.4	115
C_{12}^E (GPa)	50.06	65.94	102
C_{13}^E (GPa)	104.2	65.6	103
C_{22}^E (GPa)	135.1	145.5	103
C_{23}^E (GPa)	52.14	65.94	102
C_{33}^E (GPa)	247.4	150.4	115
C_{44}^E (GPa)	64.94	43.86	69
C_{55}^E (GPa)	75.76	42.37	66
C_{66}^E (GPa)	65.79	43.86	69
e_{16} (C/m$^{2)}$	2.763	11.40	10.1
e_{21} (C/m$^{2)}$	-0.445	-4.320	-3.9
e_{22} (C/m$^{2)}$	4.335	17.40	20.3
e_{23} (C/m$^{2)}$	-0.285	-4.320	-3.9
e_{34} (C/m$^{2)}$	3.377	11.40	10.1
κ_{11}^{ϵ} (nC^2/Nm^2)	2.081	12.80	12.7
κ_{22}^{ϵ} (nC^2/Nm^2)	2.656	15.10	6.02
κ_{33}^{ϵ} (nC^2/Nm^2)	2.187	12.80	12.7

5.5 Results and discussions

Figures 5.3 and 5.4 show the variation of fundamental elastic, dielectric and piezoelectric properties and figures of merit with increasing material volume fraction for three different classes (Class I, Class II and Class III), each with three porosity shapes (i.e. *b=0.25a*, *b=a* and *b=4a*) of piezoelectric foam structures for three novel materials; (a) barium sodium niobate (BNN), (b) barium titanate ($BaTiO_3$) and (c) relaxor ferroelectrics (RL). The effects of porosity aspect ratio, foam shape and simultaneously the fundamental piezoelectric material properties on

the fundamental electromechanical properties of piezoelectric foams are described in detail in the following Sections (Table 5.3- 5.5).

(i) In general, for all foam structures made of different piezoelectric materials, the fundamental elastic, dielectric and piezoelectric properties increase nonlinearly with increasing material volume fraction. For all the foam structures analyzed, barium titanate foams exhibits higher dielectric constant (κ_{22}) in longitudinal direction (parallel to poling direction) as compared to barium sodium niobate and relaxor ferroelectrics foams. For example, at 38% porosity volume fraction (i.e. 62% material volume fraction), the fundamental dielectric constant, κ_{22} for barium titanate foams is 9.218 nC^2/Nm^2 and for barium sodium niobate and relaxor ferroelectric foams are, 1.6036 nC^2/Nm^2 and 3.736 nC^2/Nm^2 respectively, for equiaxed structure (i.e. Class II with L1=L2=L3) with elongated porosity aspect ratio (i.e. *b=4a*). On the other hand, relaxor ferroelectrics foams exhibit higher piezoelectric coefficient (e_{22}) in longitudinal direction as compared to barium sodium niobate and barium titanate foams. For example, in the equiaxed structure (Class II) with elongated porosity aspect ratio (i.e. *b=4a*) with 38% porosity volume fraction, e_{22} for relaxor ferroelectrics is 14.39 C/m^2, whereas, e_{22} for barium sodium niobate and barium titanate foams are, respectively, 2.67 C/m^2 and 11.97 C/m^2.

In transverse direction (i.e. perpendicular to poling direction), barium sodium niobate foams exhibits higher elastic constant in the 1-direction (C_{11}) as compared to barium titanate and relaxor ferroelectrics foams whereas, barium titanate foams exhibits higher dielectric constant (κ_{11}) in transverse direction. For example, Class I foam structure with flat-cuboidal porosity (i.e. *b=0.25a*) with 41% porosity volume fraction (i.e. 59% material volume fraction), C_{11} for barium sodium niobate, barium titanate and relaxor ferroelectrics foams are, 108.25 GPa, 65.07 GPa and 25.40 GPa respectively. However, for the same structure and porosity volume fraction, barium titanate foams exhibit higher dielectric constant in the 1-direction (κ_{11}) of 8.276 nC^2/Nm^2,

whereas, κ_{11} for barium sodium niobate and relaxor ferroelectrics foams are, respectively, 1.17 nC^2/Nm^2 and 7.588 nC^2/Nm^2.

(ii) For foam structures with a particular shape and made of barium sodium niobate and barium titanate, the principal electromechanical properties in transverse direction (perpendicular to poling direction) such as C_{11} and κ_{11} are higher for piezoelectric foam structure with flat-cuboidal porosity (i.e. *b=0.25a*) as compared to foam structures with cuboidal and elongated-cuboidal porosity (i.e. *b=a* and *b=4a*) whereas, in longitudinal direction (parallel to poling direction) the electromechanical properties such as C_{22}, κ_{22} and e_{22} are equal or higher for piezoelectric foam structures with elongated porosity (i.e. *b=4a*) as compared to lower porosity aspect ratios i.e. b=0.25a (flat-cuboidal) and b=a (cuboidal). For example, for equiaxed foam structures (Class II) with 30% porosity volume fraction (i.e. 70% material volume fraction), C_{11} and κ_{11} for barium sodium niobate foams are, respectively, increased by 27.7% and 27.5% by changing the porosity shape from cuboidal (i.e. *b=a*) to flat-cuboidal (i.e. *b=0.25a*) whereas, for the same structure and porosity volume fraction, C_{22}, κ_{22} and e_{22} are, respectively, increased by 450.2%, 381% and 446%, by changing the porosity shape from flat-cuboidal porosity (i.e. *b=0.25a*) to elongated porosity structure (i.e. *b=4a*).

Furthermore, for relaxor ferroelectrics foams, elastic constant in transverse and longitudinal direction i.e. C_{11} and C_{22} respectively, are higher for foam structures with cuboidal porosity (i.e. *b=a*) than for foam structures with flat-cuboidal (i.e. *b=0.25a*) and elongated-cuboidal (i.e. *b=4a*) porosity aspect ratios for all classes except Class I, the elastic constant C_{11} are higher for foam structures with flat-cuboidal porosity aspect ratio (i.e. *b=0.25a*) as compared to higher porosity aspect ratios. The piezoelectric coefficient (e_{22}) and dielectric constant (κ_{22}) are higher for foam structures with elongated porosity aspect ratio (i.e. *b=4a*) as compared to lower porosity aspect ratios (i.e. *b=0.25a* or *b=a*) for the foam structures with a particular shape.

For example, at 30% porosity volume fraction, e_{22} and κ_{22} increased respectively, by 34.19% and 4.91% for equiaxed structure (Class II), by changing the shape of the porosity from cuboidal (i.e. $b=a$) to elongated-cuboidal (i.e. $b=4a$).

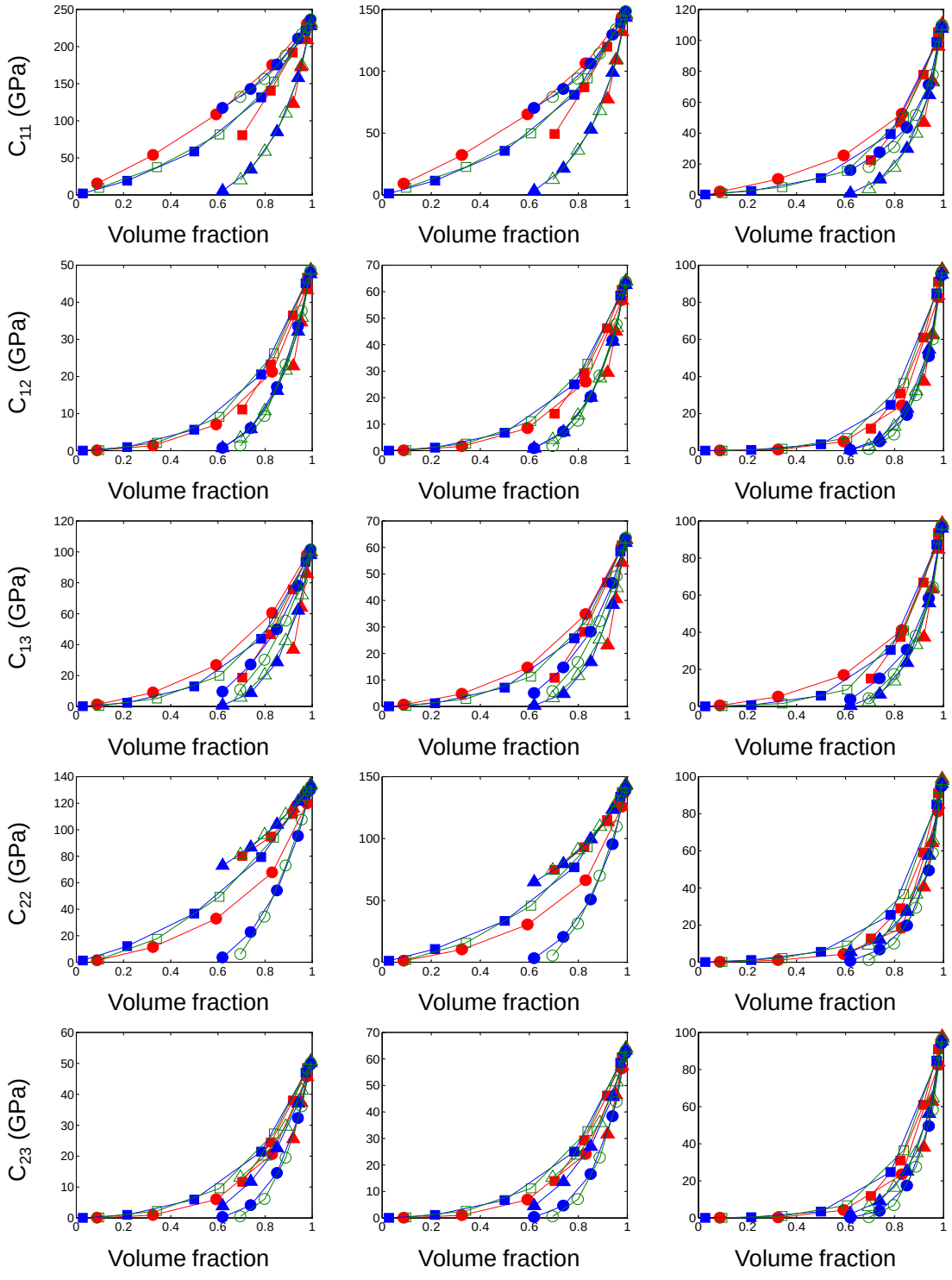

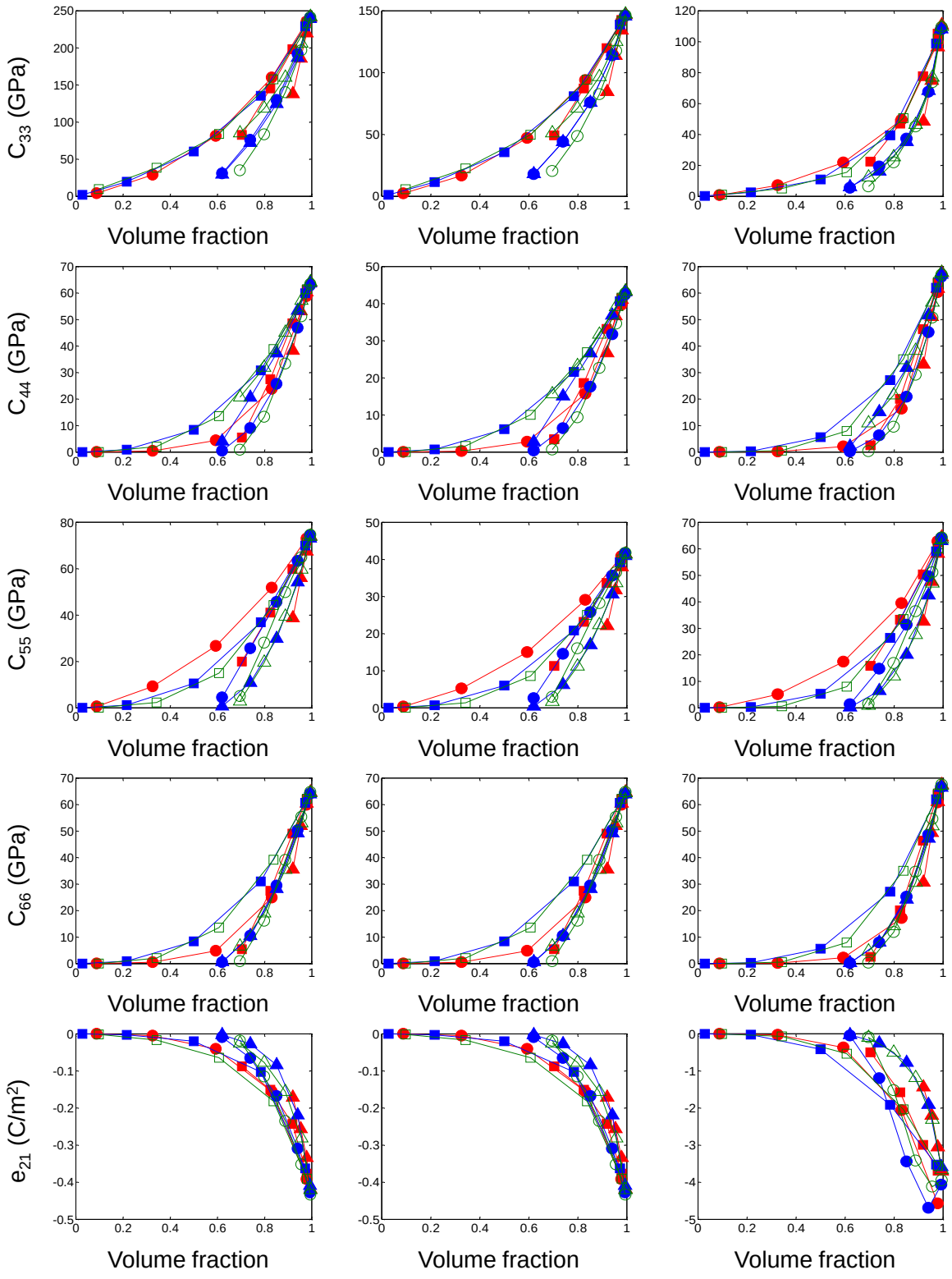
C33 (GPa)
C44 (GPa)
C55 (GPa)
C66 (GPa)
e21 (C/m2)
Volume fraction

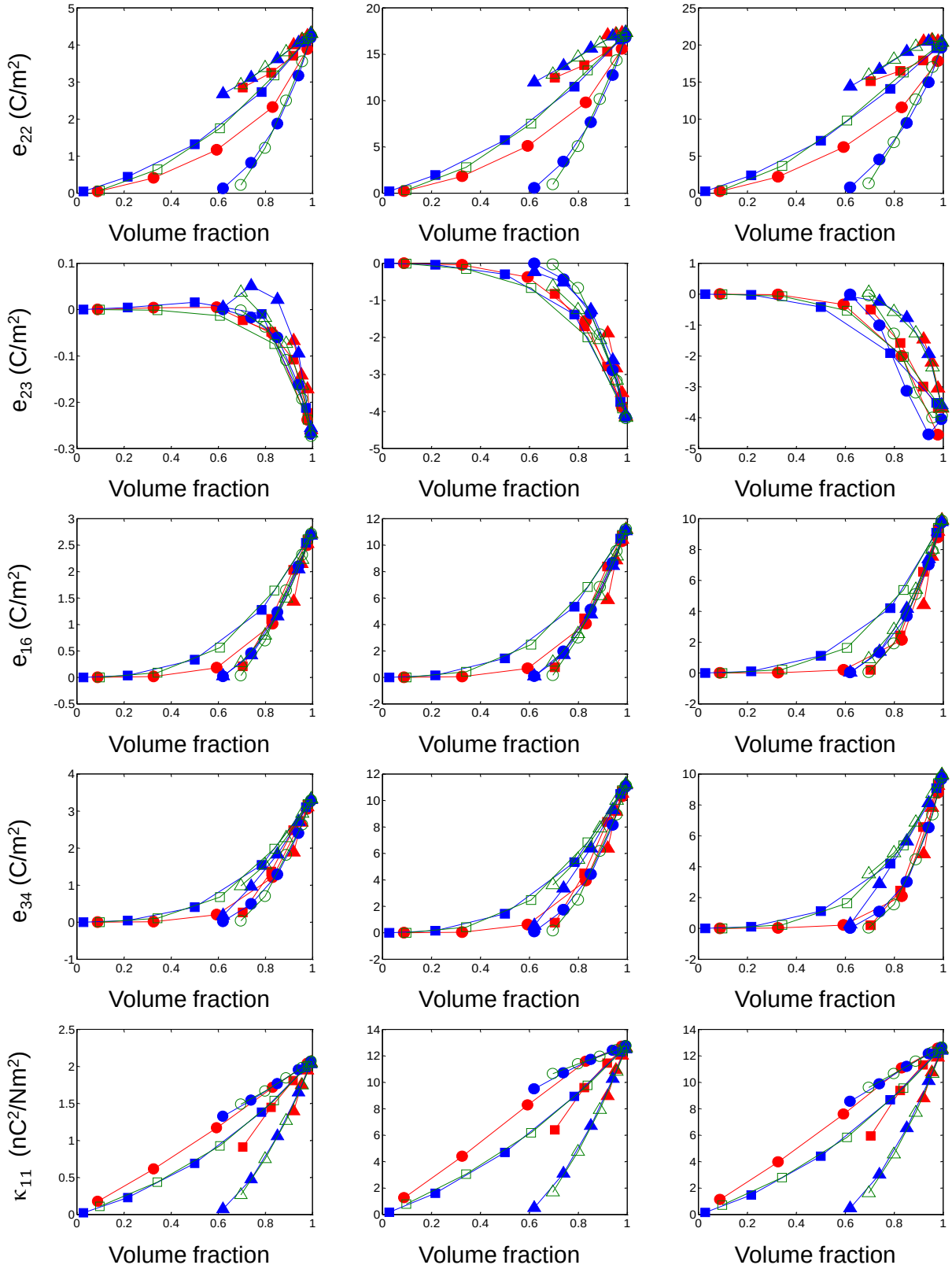
e22 (C/m2)
e23 (C/m2)
e16 (C/m2)
e34 (C/m2)
κ11 (nC2/Nm2)
Volume fraction

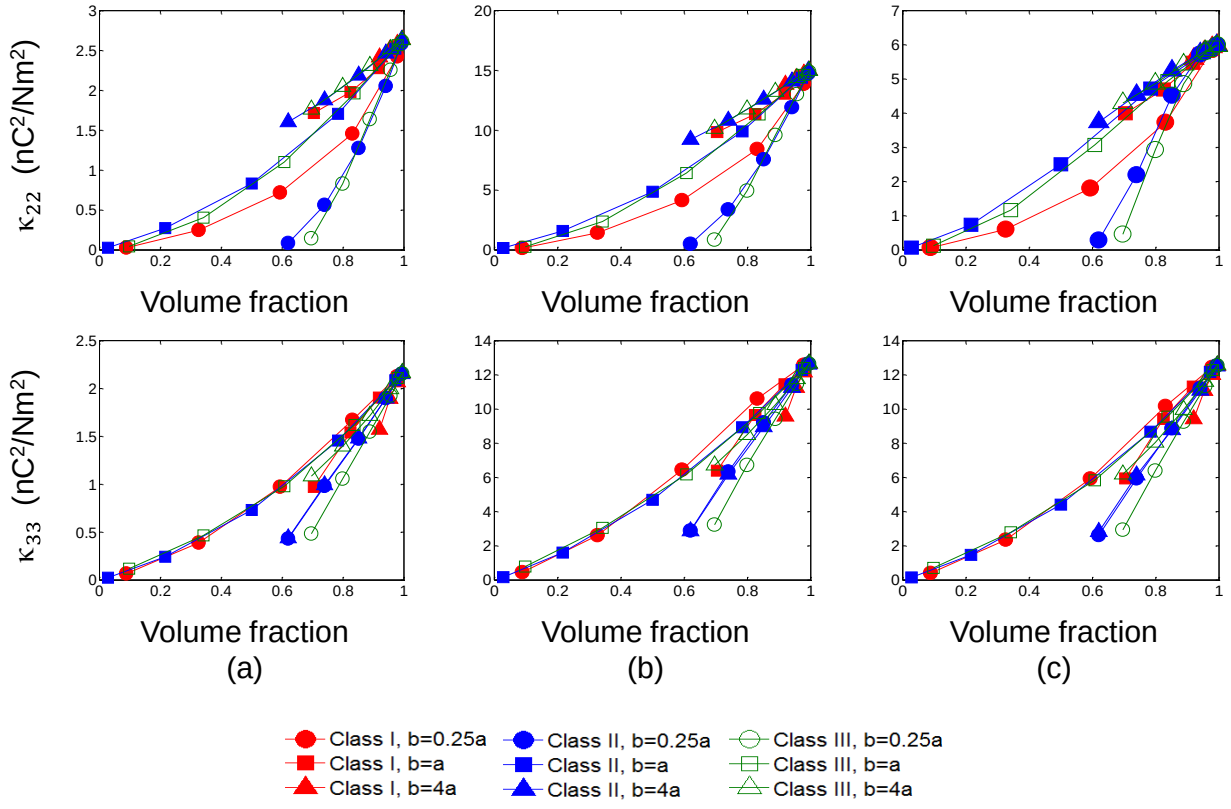

Figure 5.3: Variation of the fundamental elastic, dielectric and piezoelectric properties of three different classes (Class I, Class II and Class III), each with three porosity shapes (b=0.25a, b=a and b=4a) of piezoelectric foam structures with respect to material volume fraction for three novel materials; (a) barium sodium niobate (BNN); (b) barium titanate ($BaTiO_3$); and (c) relaxor ferroelectrics (RL)

(iii) As expected, the piezoelectric foam structures that belong to Class I, II and III with porosity aspect ratio of b=a made of materials such as barium titanate and relaxor ferroelectrics have shown to exhibit high transverse crystal symmetry of 4mm (i.e. $C_{11} = C_{33}$) whereas, barium sodium niobate foam exhibit lower crystal symmetry of mm2 (i.e. $C_{11} \neq C_{33}$) (Table 5.2). The piezoelectric foam structures that belong to Class I, II and III with flat-cuboidal and elongated-

cuboidal foam structures (i.e. *b=0.25a* and *b=4a*), for all three materials have shown to exhibit reduced crystal symmetry of mm2 (orthorhombic crystal system).

Table 5.2: Variation of crystal symmetry of three different classes (Class I, Class II and Class III), each with three porosity shapes (b=0.25a, b=a and b=4a) of piezoelectric foam structures for three novel materials (barium sodium niobate (BNN), barium titanate ($BaTiO_3$) and relaxor ferroelectrics (RL))

	Barium sodium niobate (BNN) (mm2)	Barium titanate ($BaTiO_3$) (4mm)	Relaxor ferroelectrics (RL) (4mm)
	(b=0.25a) (b=a) (b=4a)	(b=0.25a) (b=a) (b=4a)	(b=0.25a) (b=a) (b=4a)
(Class I)	mm2 mm2 mm2	mm2 4mm mm2	mm2 4mm mm2
(Class II)	mm2 mm2 mm2	mm2 4mm mm2	mm2 4mm mm2
(Class III)	mm2 mm2 mm2	mm2 4mm mm2	mm2 4mm mm2

The Scherrer Equation can be utilized in order to calculate the crystal size, which is given as;

$$\tau = \frac{K\lambda}{\beta \cos\theta} \qquad [5.1]$$

Where τ= mean size of the crystal,

K= shape factor, with a value close to unity (its typical value is about 0.94),

λ= X-ray wavelength (assumed as 1 Angstroms),

β= Line broadening at half the maximum intensity (FWHM),

θ= Bragg angle.

According to the XRD patterns analyzed in [108], the crystal size for 0% MnO_2 can be calculated using equation 5.1 as follows;

$$\tau = \frac{0.94*1}{1* cos15.5} = 0.9754 \text{ nm}$$

Furthermore, for a unit cell of 1mm × 1mm ×1mm made up of relaxor ferroelectrics (PMN-0.33 PT) must have approximately 1.077*e^{18} crystals in it to be continuous with no micro/macro porosity in it.

(iv) In general, modifying the microstructural features such as structural aspect ratio and porosity aspect ratio significantly enhances the figures of merit for foam structures made of different piezoelectric materials. For example, at 30% porosity volume fraction, d_h, g_h and $d_h g_h$ are, respectively, increased by 21%, 360%, 457% for barium sodium niobate foams, 75%, 548%, 1037% for barium titanate and 12%, 221% and 259% for relaxor ferroelectrics foams by changing shape of the porosity for equiaxed foam (L1=L2=L3) structure (Class II) from a cuboidal shape (i.e. $b=a$) to a flat-cuboidal (i.e. $b=0.25a$).

Furthermore, among all materials analyzed, relaxor ferroelectrics foams have shown to exhibit higher figures of merit (i.e., K_t, d_h, g_h, $d_h gh$ *and* M) for all the foam structures. For example, at 91.1 % porosity volume fraction (i.e. 8.9% material volume fraction), longitudinally short (i.e. Class I with L2=0.25L1) foam structure with flat-cuboidal shape (i.e. $b=0.25a$) porosity, the K_t, d_h, g_h, $d_h g_h$ and M are, respectively 0.9524, 2.55 nm/V, 40.1 Vm/N, 100 nm^2/N and 100.31Vpa^{-1}.

Piezoelectric coupling constant (K_t) for the foam structures have shown increase with increase in porosity volume fractions. At about 97 % porosity volume fraction (i.e. about 3% material volume fraction) for equiaxed (L1=L2=L3) foam structure (Class II) with cuboidal porosity shape (i.e. $b=a$), relaxor ferroelectrics foams exhibit higher piezoelectric coupling constant (K_t ~0.954), barium sodium niobate foams exhibits lowest piezoelectric constant (K_t ~0.240) and barium titanate foams showed intermediate behaviour (K_t ~0.442).

As expected, for 3-3 type piezoelectric foam structures, receiving sensitivity (M) has shown to increase with increase in porosity volume fractions for all of the materials (Fig. 5.4) and thus making them suitable for applications such as hydrophones.

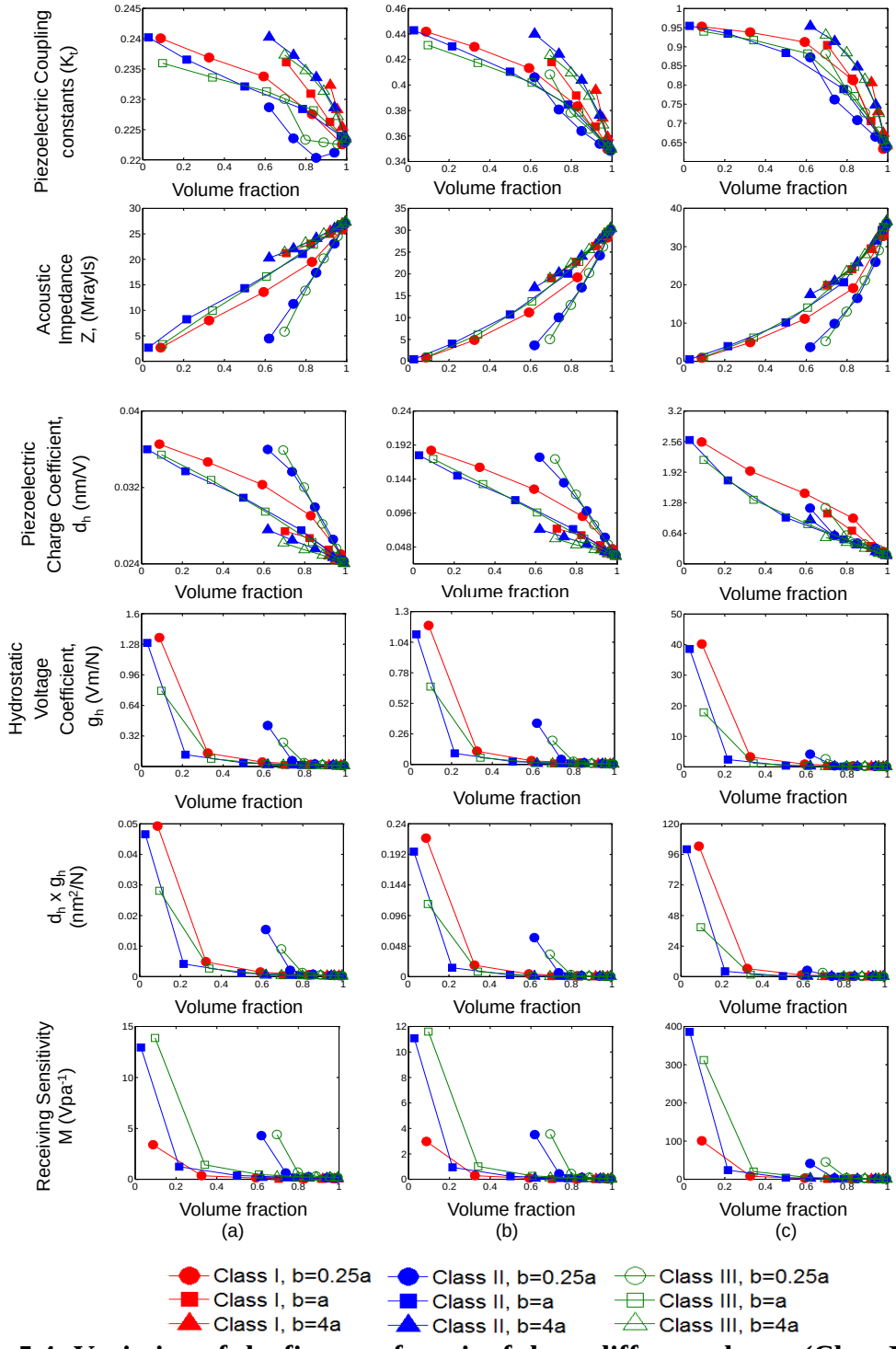

Figure 5.4: Variation of the figures of merit of three different classes (Class I, Class II and Class III), each with three porosity shapes (b=0.25a, b=a and b=4a) of piezoelectric foam structures with respect to material volume fraction for three novel materials; (a) barium sodium niobate; (b) barium titanate ($BaTiO_3$); and (c) relaxor ferroelectrics (RL)

Due to structural limitations, the maximum porosity volume fractions (> 40%) are achieved for longitudinally short foam structure (Class I) with flat-cuboidal porosity (i.e. $b=0.25a$), equiaxed foam structure (Class II) with cuboidal porosity (i.e. $b=a$) and longitudinally tall foam structures (Class III) with cuboidal porosity (i.e. $b=a$) and hence these foam structures in general exhibit higher receiving sensitivity. However, equiaxed foam structure (Class II) and longitudinally tall foam structure (Class III) with flat-cuboidal porosity (i.e. $b=0.25a$) have shown significant increase in receiving sensitivity even at lower porosity volume fractions (between 20-40%) for all the materials analyzed.

(v) Tables 5.3, 5.4 and 5.5 shows the normalized values of the various effective electromechanical coefficients and selected figures of merit for all of the materials analysed, with respect to their single cell properties. The porosity volume fraction of 30% (material volume fraction of 70%), with an exception of Class I with a porosity aspect ratio of 4 (due to structural limitations maximum induced porosity volume fraction is only about 8%), has been used to analyse the normalised values.

The fundamental electromechanical coefficient values for various porosity aspect ratios, when normalized to the reference structure values, found to decrease for a particular selected material. For example, elastic constant in the 1-direction i.e. C_{11} for Class I foam structure with porosity aspect ratio of 1 and is made up of barium sodium niobate (Table 5.3), barium titanate (Table 5.4) and relaxor ferroelectric (Table 5.5) respectively, values are 67%, 56%, and 56% less than C_{11} of the reference structure values.

However, at the selected porosity volume fraction of 30%, basic figures of merit such as d_h, g_h, $d_h g_h$ have higher normalising values as shown in Tables 5.3, 5.4 and 5.5. For example, piezoelectric foam structure with porosity aspect ratio of 0.25 and made up of barium sodium niobate (Table 5.3), d_h, g_h, $d_h g_h$ normalised values respectively are, 29%, 245% and 346% for

Table 5.3: The variation of the fundamental elecromechanical properties and selected figures of merit with change in the foam shape and the porosity aspect ratio by normalizing to the properties of the reference foam structure i.e. Class II with porosity aspect ratio of 1, for the barium sodium niobate (BNN)

V.f= 0.70	Class I				Class II				Class III		
	Porosity Aspect Ratio				*Porosity Aspect Ratio*				*Porosity Aspect Ratio*		
	0.25	**1**	**4**		**0.25**	**1**	**4**		**0.25**	**1**	**4**
C_{11}	0.57	0.33	0.51		0.56	0.44	0.09		0.55	0.44	0.09
C_{12}	0.23	0.21	0.46		0.07	0.28	0.07		0.03	0.28	0.07
C_{13}	0.37	0.17	0.35		0.20	0.30	0.05		0.11	0.29	0.06
C_{22}	0.34	0.59	0.86		0.11	0.47	0.60		0.05	0.48	0.60
C_{23}	0.20	0.22	0.49		0.04	0.29	0.17		0.01	0.28	0.26
C_{33}	0.45	0.33	0.56		0.24	0.43	0.23		0.15	0.43	0.35
C_{44}	0.15	0.08	0.59		0.08	0.34	0.23		0.02	0.33	0.32
C_{55}	0.48	0.26	0.51		0.25	0.35	0.08		0.08	0.32	0.04
C_{66}	0.16	0.08	0.54		0.09	0.33	0.09		0.02	0.33	0.11
e_{16}	0.15	0.07	0.52		0.09	0.32	0.09		0.02	0.32	0.11
e_{21}	0.16	0.19	0.39		0.09	0.14	0.03		0.05	0.22	0.06
e_{22}	0.37	0.65	0.92		0.12	0.52	0.68		0.06	0.52	0.68
e_{23}	0.04	0.08	0.24		0.03	-0.04	-0.04		0.01	0.09	-0.12
e_{34}	0.14	0.07	0.56		0.08	0.32	0.20		0.01	0.31	0.30
κ_{11}	0.68	0.43	0.67		0.71	0.55	0.15		0.72	0.55	0.14
κ_{22}	0.37	0.64	0.91		0.14	0.53	0.67		0.06	0.53	0.67
κ_{33}	0.58	0.43	0.72		0.37	0.56	0.37		0.23	0.55	0.50
K_t	1.04	1.06	1.04		1.01	1.03	1.07		1.03	1.03	1.06
Z	0.49	0.64	0.89		0.28	0.58	0.65		0.19	0.58	0.65
d_h	1.29	1.14	1.03		1.45	1.19	1.11		1.49	1.18	1.09
g_h	3.45	1.78	1.14		10.37	2.25	1.65		24.44	2.21	1.63
d_h*g_h	4.46	2.03	1.18		14.99	2.69	1.82		36.42	2.60	1.78
M	0.86	0.44	0.28		10.37	2.25	1.65		42.77	3.86	2.86

Table 5.4: The variation of the fundamental elecromechanical properties and selected figures of merit with change in the foam shape and the porosity aspect ratio by normalizing to the properties of the reference foam structure i.e. Class II with porosity aspect ratio of 1, for the barium titanate ($BaTiO_3$)

V.f= 0.70	Class I				Class II				Class III		
	Porosity Aspect Ratio				*Porosity Aspect Ratio*				*Porosity Aspect Ratio*		
	0.25	**1**	**4**		**0.25**	**1**	**4**		**0.25**	**1**	**4**
C_{11}	0.54	0.32	0.51		0.53	0.43	0.09		0.53	0.42	0.09
C_{12}	0.21	0.20	0.45		0.07	0.26	0.07		0.03	0.26	0.07
C_{13}	0.33	0.16	0.35		0.17	0.27	0.04		0.09	0.26	0.05
C_{22}	0.30	0.51	0.78		0.09	0.41	0.51		0.04	0.42	0.51
C_{23}	0.19	0.20	0.48		0.04	0.26	0.15		0.01	0.26	0.23
C_{33}	0.43	0.32	0.56		0.23	0.43	0.23		0.14	0.42	0.34
C_{44}	0.14	0.07	0.61		0.09	0.36	0.25		0.02	0.35	0.36
C_{55}	0.48	0.26	0.52		0.25	0.36	0.09		0.08	0.32	0.05
C_{66}	0.15	0.07	0.56		0.10	0.36	0.10		0.02	0.35	0.11
e_{16}	0.14	0.06	0.51		0.10	0.33	0.08		0.02	0.33	0.11
e_{21}	0.20	0.19	0.41		0.09	0.21	0.05		0.04	0.24	0.06
e_{22}	0.40	0.72	0.98		0.13	0.55	0.75		0.06	0.55	0.74
e_{23}	0.17	0.19	0.44		0.06	0.21	0.11		0.01	0.24	0.15
e_{34}	0.13	0.06	0.56		0.09	0.33	0.21		0.02	0.33	0.32
κ_{11}	0.77	0.49	0.70		0.81	0.59	0.16		0.84	0.59	0.14
κ_{22}	0.38	0.65	0.92		0.15	0.54	0.68		0.06	0.55	0.68
κ_{33}	0.65	0.49	0.75		0.41	0.59	0.40		0.27	0.59	0.53
K_t	0.31	0.54	0.81		0.09	0.43	0.55		0.04	0.44	0.55
Z	0.47	0.62	0.75		0.26	0.55	0.62		0.17	0.55	0.62
d_h	3.35	2.17	1.28		4.46	2.54	1.84		5.00	2.41	1.73
g_h	8.82	3.35	1.39		30.38	4.68	2.71		78.68	4.43	2.56
d_h*g_h	29.59	7.28	1.78		135.42	11.90	4.99		393.58	10.69	4.42
M	2.21	0.84	0.35		30.38	4.68	2.71		137.70	7.75	4.47

Table 5.5: The variation of the fundamental elecromechanical properties and selected figures of merit with change in the foam shape and the porosity aspect ratio by normalizing to the properties of the reference foam structure i.e. Class II with porosity aspect ratio of 1, for the relaxor ferroelectrics (RL)

V.f= 0.70	Class I				Class II				Class III		
	Porosity Aspect Ratio				*Porosity Aspect Ratio*				*Porosity Aspect Ratio*		
	0.25	**1**	**4**		**0.25**	**1**	**4**		**0.25**	**1**	**4**
C_{11}	0.30	0.19	0.41		0.20	0.24	0.05		0.16	0.22	0.04
C_{12}	0.10	0.11	0.37		0.03	0.14	0.03		0.01	0.13	0.03
C_{13}	0.24	0.14	0.36		0.11	0.19	0.03		0.05	0.17	0.03
C_{22}	0.08	0.12	0.39		0.04	0.16	0.09		0.01	0.15	0.09
C_{23}	0.09	0.11	0.37		0.02	0.14	0.06		0.00	0.13	0.06
C_{33}	0.27	0.19	0.42		0.12	0.24	0.10		0.06	0.22	0.11
C_{44}	0.07	0.03	0.48		0.05	0.26	0.15		0.01	0.22	0.16
C_{55}	0.39	0.23	0.49		0.15	0.27	0.05		0.03	0.24	0.02
C_{66}	0.08	0.03	0.44		0.06	0.26	0.06		0.01	0.22	0.07
e_{16}	0.06	0.02	0.44		0.08	0.29	0.07		0.01	0.26	0.10
e_{21}	0.22	0.12	0.37		0.16	0.36	0.03		0.03	0.26	0.03
e_{22}	0.41	0.74	1.01		0.15	0.58	0.78		0.07	0.61	0.79
e_{23}	0.21	0.12	0.38		0.13	0.36	0.05		0.02	0.26	-0.01
e_{34}	0.06	0.02	0.48		0.06	0.29	0.19		0.00	0.26	0.36
κ_{11}	0.72	0.46	0.69		0.74	0.57	0.16		0.76	0.57	0.14
κ_{22}	0.42	0.66	0.93		0.24	0.68	0.71		0.09	0.64	0.72
κ_{33}	0.61	0.46	0.74		0.39	0.57	0.41		0.24	0.57	0.49
K_t	1.40	1.43	1.28		1.25	1.31	1.47		1.39	1.35	1.47
Z	0.38	0.53	0.79		0.21	0.45	0.53		0.15	0.47	0.53
d_h	7.54	6.34	1.89		4.15	3.70	4.02		6.70	4.00	3.25
g_h	17.98	9.59	2.04		17.54	5.46	5.66		77.06	6.28	4.55
d_h*g_h	135.64	60.83	3.86		72.70	20.20	22.79		516.43	25.13	14.79
M	4.50	2.40	0.51		17.54	5.46	5.66		134.86	10.99	7.95

class I, 45%, 937% and 1399% for class II, and 49%, 2344%, and 3542% for class III more than the reference structure values. Whereas, piezoelectric foam structure with porosity aspect ratio of 0.25 and made up of barium titanate (Table 5.4), d_h, $g_{h,}$ $d_h g_h$ normalised values respectively are, 235%, 782% and 2859% for class I, 346%, 2938%, and 13442% for class II, and 400%, 7768% and 39258% for class III, and for relaxor ferroelectric (Table 5.5), d_h, $g_{h,}$ $d_h g_h$ normalised values respectively are, 654%%, 1698% and 13464% for class I, 315%, 1654% and 7170% for class II and 570%, 7606% and 51543% for class III, more than the reference structure values.

5.6 Conclusions

Several analytical, numerical and experimental studies have demonstrated that porous piezoelectric materials, especially 3-3 type porous piezoelectric materials exhibit a combination of properties that are desirable for certain practical applications such as hydrophones. However, a comprehensive study of the effect of foam microstructural features and simultaneously piezoelectric material properties on the overall response of 3-3 type piezoelectric foam structures has not yet been investigated in details. Hence, this chapter also focused on developing a comprehensive understanding of the effect of foam shape, porosity aspect ratio, porosity volume fraction and simultaneously the fundamental piezoelectric material properties in a range of piezoelectric material systems such as barium sodium niobate, barium titanate and relaxor ferroelectric material on the effective electromechanical response of 3-3 type piezoelectric foams. The following principal conclusions were obtained:

(i) For all the foam structures analyzed, the fundamental elastic, dielectric, and piezoelectric properties increase nonlinearly with increasing material volume fraction.

(ii) Comparative studies of electromechanical properties along the longitudinal direction (parallel to poling direction) have shown that barium titanate foams exhibit highest dielectric constant (κ_{22}) as compared to barium sodium niobate and relaxor ferroelectrics foams whereas, relaxor ferroelectric foams exhibits higher piezoelectric coefficient (e_{22}).

(iii) In transverse direction (i.e. perpendicular to poling direction), barium sodium niobate foam exhibits higher elastic constant in the 1-direction (C_{11}) as compared to barium titanate and relaxor ferroelectrics foams whereas, barium titanate foam exhibit higher dielectric constant (κ_{11}).

(iv) For foam structures with a particular shape and made of barium sodium niobate and barium titanate, the principal electromechanical properties in transverse direction such as C_{11} and κ_{11} are higher for piezoelectric foam structure with flat-cuboidal porosity (i.e. $b=0.25a$) as compared to foam structures with cuboidal and elongated-cuboidal porosity (i.e. $b=a$ and $b=4a$) whereas, in longitudinal direction, C_{22}, κ_{22} and e_{22} are equal or higher for piezoelectric foam structures with elongated porosity (i.e. $b=4a$) as compared to lower porosity aspect ratios i.e. b=0.25a (flat-cuboidal) and b=a (cuboidal).

(v) For relaxor ferroelectrics foams, elastic constant in transverse and longitudinal direction i.e. C_{11} and C_{22} respectively, are higher for foam structures with cuboidal porosity (i.e. $b=a$) than for foam structures with flat-cuboidal (i.e. $b=0.25a$) and elongated-cuboidal (i.e. $b=4a$) porosity aspect ratios for all classes except Class I, C_{11} are higher for foam structures with flat-cuboidal porosity aspect ratio (i.e. $b=0.25a$) as compared to other porosity aspect ratios. The piezoelectric coefficient (e_{22}) and dielectric constant (κ_{22}) are higher for foam structures with elongated porosity aspect ratio structure (i.e. $b=4a$) as compared to lower porosity aspect ratios (i.e. $b=0.25a$ or $b=a$) for the foam structures with a particular shape.

(vi) Piezoelectric foam structures that belong to Class I, II and III with cuboidal porosity (i.e. $b=a$), barium titanate and relaxor ferroelectrics foams have shown to exhibit high transverse crystal symmetry of 4mm ($C_{11}=C_{33}$) whereas, barium sodium niobate foams exhibits lower crystal symmetry of mm2. However, piezoelectric foam structures that belong to Class I, II and III with flat-cuboidal and elongated-cuboidal foam structures (i.e. $b=0.25a$ and $b=4a$), for all materials have shown to exhibit reduced crystal symmetry of mm2.

(vii) Modifying the microstructural features such as structural aspect ratio and porosity aspect ratio significantly enhances the figures of merit (hydrostatic strain coefficient (d_h), the hydrostatic voltage coefficient (g_h), the hydrostatic figure of merit ($d_h g_h$) and receiving sensitivity (M)) for foam structures made of different piezoelectric materials.

(viii) In general, among all materials analyzed, relaxor ferroelectrics foams have shown to exhibit higher figures of merit (i.e., K_t, d_h, g_h, $d_h gh$ and M). By inducing porosity (~97%), relaxor ferroelectric foams observed maximum increase of 50.72% for piezoelectric coupling constant (K_t) whereas barium sodium niobate (BNN) observed lowest increase of 7.6%.

(ix) As expected, for 3-3 type piezoelectric foam structures, receiving sensitivity (M) has shown to increase with increase in porosity volume fractions for all of the materials. Equiaxed foam structure (Class II) and longitudinally tall foam structure (Class III) with flat-cuboidal porosity (i.e. $b=0.25a$) have shown significant increase in receiving sensitivity even at lower porosity volume fractions (between 20-40%) for all the materials analyzed.

CHAPTER 6

6 Conclusions

Piezoelectric materials are important members of the smart materials family as explained in Chapter 1. Various smart materials such as magnetostrictive and electrostrictive materials, shape memory alloys, electro-rheological and magnetorheological fluids etc., have their broad applications in various fields. In this thesis, piezoelectric materials have been chosen in order to characterize their electromechanical properties and figures of merit to utilize them for various underwater applications such as hydrophones. Considering the importance of porosity (high figures of merit) among piezoelectric materials, numerous literatures have been studied in Chapter 2, to understand the phenomenon behind capturing the full electromechanical response of porous piezoelectric materials numerically.

Chapter 3 details finite element modelling used to model porous (3-0, 3-1 and 3-3 type) piezoelectric structures, using unit-cell approach. ABAQUS has been extensively used to construct unit-cell, which represents porous (3-0, 3-1 and 3-3 type) piezoelectric structures. Appropriate boundary conditions are invoked for various porous piezoelectric structures (i.e. 3-0, 3-1 and 3-3 type) to ensure that the electromechanical deformation response of the unit-cell, under conditions of electrical and mechanical loading, are representative of the deformation of the macroscopic piezoelectric structures. With the implementation of various boundary conditions, elastic, piezoelectric and dielectric coefficients have been evaluated (Chapter 4 and 5) using constitutive linear relationship for piezoelectric materials. Piezoelectric figures of merit such as piezoelectric coupling constant (K_t), acoustic impedance (Z), hydrostatic strain coefficient (d_h), hydrostatic voltage coefficient (g_h), hydrostatic figures of merit ($d_h g_h$) and receiving sensitivity (M) have been evaluated (Chapters 4 and 5).

Finite element modelling (Chapter 3) is utilized for the modelling of 3-0, 3-1 and 3-3 type porous piezoelectric structures made of Lead Zirconium Titanate (PZT-7A) and relaxor (PMN-PT based) ferroelectrics (RL), and is explained in Chapter 4. Chapter 4 also details the various comparisons of elastic, dielectric and piezoelectric properties between various porous (3-0, 3-1 and 3-3 type) piezoelectric structures made up of lead zirconium titanate (PZT-7A) and relaxor (PMN-PT based) ferroelectrics (RL). Furthermore, piezoelectric figures of merit such as the coupling constant (K_t), the hydrostatic strain coefficient (d_h), and the hydrostatic figure of merit ($d_h g_h$) of (PMN-PT based) relaxor foams are significantly higher (by 40%, 900%, and 3000%, respectively, for 3-3 type foams with 50% porosity) than those observed in equivalent (PZT-7A based) traditional piezoelectric foams.

In Chapter 5, a three-dimensional finite element model is developed to accurately predict the electromechanical response of 3-3 type piezoelectric foam structures made of several classes of piezoelectric materials such as barium sodium niobate (BNN), barium titanate ($BaTiO_3$) and relaxor (PMN-PT based) ferroelectrics (RL). Nine different types of foam structures are identified based on the microstructural features and there electromechanical response is characterized as a function of foam shape, porosity aspect ratio, porosity volume fraction and simultaneously material properties. Based on the three-dimensional finite element simulations, the following principal conclusions are obtained: (i) Microstructural features and material properties were found to have a significant effect on various elastic, dielectric and piezoelectric constants of the foam structures and their corresponding figures of merit; (ii) At about 97 % porosity volume fraction for equiaxed (L1=L2=L3) foam structure (Class II) with cuboidal porosity shape (i.e. $b=a$), relaxor ferroelectrics foams exhibit highest piezoelectric coupling constant (K_t~0.954), barium sodium niobate foam exhibit lowest piezoelectric constant (K_t~0.240) and barium titanate foams showed intermediate behaviour with K_t~0.442; (iii) All

piezoelectric materials showed enhanced piezoelectric figures of merit by modifying the shape of the porosity. For example, at 30% porosity volume fraction, d_h, g_h and $d_h g_h$ are, respectively, increased by 21%, 360%, and 457% for barium sodium niobate foams, 75%, 548%, and 1037% for barium titanate foams and 12%, 221% and 259% for relaxor ferroelectrics foams by changing shape of the porosity for equiaxed foam (L1=L2=L3) structure (Class II) from a cuboidal shape (with $b=a$) to a flat-cuboidal (with $b=0.25a$).

In a nutshell, porous piezoelectric materials have been found to be having the improved figure of merits such as piezoelectric coupling constant (K_t), acoustic impedance (Z), hydrostatic strain coefficient (d_h), hydrostatic voltage coefficient (g_h), hydrostatic figures of merit ($d_h g_h$) and receiving sensitivity (M), as compared to single crystal piezoelectric materials, hence make them suitable to use as sensors and actuators in various underwater applications. The 3-3 porosity type piezoelectric foam structures found to have the promising elastic, dielectric and piezoelectric properties and higher figure of merits, that's why they can be used as various sensors and actuators.

As, receiving sensitivity of 3-3 porosity type piezoelectric foam structures had been found to be relatively higher as compared to 3-0 and 3-1 type porous piezoelectric foam structures, the hydrophone transducer's sensitivity can also be improved by implementing 3-3 type porous piezoelectric materials. Relaxor ferroelectrics (RL) with 3-3 type porosity had been found to be having extremely high figures of merit as compared to the other piezoelectric materials studied in this thesis, hence should be preferred over other available piezoelectric materials to be used as hydrophone transducers, sensors and actuators.

Furthermore, in order to select appropriate piezoelectric structures among various other structures studied in this thesis and in order to use them in underwater acoustics applications i.e. hydrophones, various piezoelectric structures (consists of different material volume fractions)

because of their higher figure of merits are selected as shown in Table 6.1 and considered as better candidates for fabrication of hydrophones.

Table 6.1: Description of the selected piezoelectric material out of various other materials studied in this thesis in order to choose the best suitable piezoeelctric structure to be used for the fabrication of underwater acoustics device i.e. hydrophones

Material Volume Fraction (v.f)	Piezoelectric Material	Structure
2.8%	Relaxor ferroelectrics(RL)	L1=L2=L3 (Class II, b=a)
8.8%	Relaxor ferroelectrics(RL)	L1=L3, L2=0.25L1 (Class I, b=0.25a)
9.7%	Relaxor ferroelectrics(RL)	L1=L3, L2=1.75L1 (Class III, b=a)
62%	Relaxor ferroelectrics(RL)	L1=L2=L3 (Class II, b=0.25a)
69.6%	Relaxor ferroelectrics(RL)	L1=L3, L2=1.75L1 (Class III, b=0.25a)

There are number of limitations involved while performing finite element analysis to capture the elecromechanical response of various porous piezoelectric structures. First of all, the porous piezoelectric structures studied in this thesis has been assumed to be perfectly poled along the poling direction i.e. 2-direction. However, it's impossible to get material perfectly poled experimentally. Secondly, elecromechanical behaviour could be different for porous piezoelectric materials: if there are multiple porosities and have different porosity shapes instead of the uniform rectangular porosity (which is considered in this thesis). Furthermore, to achieve higher volume fraction of porosity is impractical due to certain limitations of manufacturing

techniques as well as the brittle nature of piezoelectric ceramics i.e. chances of breakage while poling for the porous piezoelectric materials. Also, experimentally, it's difficult to induce the perfectly aligned uniform porosity in all three directions. However, considering various available computer operated machines, which can reliably create the porosity in the piezoelectric structures, limitations mentioned above can be reduced.

Considering the advantages of the piezo-composites such as, improving the brittle nature of piezoelectric ceramics, finite element modelling of the piezo-composites has to be considered in the future work. Also, different types of piezo-composites such as, 3-0, 3-1 and 3-3 type should also be considered, while performing finite element analysis, to get various results to predict the most suitable electromechanical response of piezo-composites for various applications. Also, study of various novel materials such as lead zirconium titanate (PZT-7A), barium sodium niobate (BNN), barium titanate ($BaTiO_3$), and relaxor (PMN-PT based) ferroelectrics (RL), effecting the elecromechanical properties of piezo-composites should be studied in detail. Furthermore, experimental technique which utilizes the fabrication processes for piezoelectric materials such as sintering has to be developed, in order to get complete elecromechanical response for both piezoelectric ceramics and composites.

References

1. "Canadian Military Journal", *Autumn*, **2000**, 25-32.
2. Hurlebaus S., and Gaul L. "Smart Structure Dynamics," *Mechanical Systems and Signal Processing*, **20,** 255-281 (2006).
3. Tzou H.S., Lee H-J., and Arnold S.M., "Smart Materials, Precision Sensors/Actuators, Smart Structures, and Structonic Systems," *Mechanics of Advanced Materials and Structures*, **11**, 367-393 (2004).
4. W. G. Cady, Piezoelectricity *Volume-I* (McGraw-Hill, New York, 1946).
5. W. G. Cady, Piezoelectricity *Volume-II* (McGraw-Hill, New York, 1946).
6. PZT manual "The Piezoelectric effect" online at: http://www.aurelienr.com/electronique/piezo/piezo.pdf
7. R. Kar-Gupta and T.A. Venkatesh, "Electromechanical Response of Porous Piezoelectric Materials," *Acta. Mater.*, **54,** 4063-78 (2006).
8. H. Kara, R. Ramesh, R. Stevens, and C.R. Bowen, "Porous PZT Ceramics for Receiving Transducers," *IEEE Trans. Ultrason. Ferroelectr. Freq. Control*, **50**, 289-296 (2003).
9. Z li, A Huang, G Luan, and J Zhang, "Finite Element Analyzing of Underwater Receiving Sensitivity of PMN-0.33PT Single Crystal Cymbal Hydrophone," *Ultrasonics.*, **44**, e759-e762 (2006).
10. S.H Choy, X.X. Wang, H.L.W. Chan, and C.L. Choy, "Electromechanical and Ferroelectric Properties of $(Bi_{1/2}Na_{1/2})TiO_3$-$(Bi_{1/2}K_{1/2})TiO_3$- $(Bi_{1/2}Li_{1/2})TiO_3$-$BaTiO_3$ lead-free piezoelectric ceramics for accelerometer application," *Appl. Phys.*, **A89**, 775-781 (2007).

11. W.H. Duan, Q. Wang, and S.T. Quek, "Applications of Piezoelectric Materials in Structural Health Monitoring and Repair: Selected Research Examples," *Materials,* **3**, 5169-5194 (2010).

12. P. Muralt, R.G. polcawich, and S. Trolier-Mckinstry, "Piezoelectric Thin Films for Sensors, Actuators, and Energy Harvesting," *MRS Bulletin*, **34**, 658-664 (2009).

13. S.R. Anton, and H.A. Sodano, "A Review of Power Harvesting Using Piezoelectric Materials (2003–2006)," *Smart Mater. Struct*, **16**, R1-R21 (2007).

14. J. Qiu, and H. Ji, "The Application of Piezoelectric Materials in Smart Structures in China," *Int'l J. of Aeronautical & Space Sci.* **11(4)**, 266–284 (2010).

15. J. Nuffer, and T. Bein, " Application of piezoelectric materials in transportation industry," *Global Symposium on Innovative Solutions for the Advancement of the Transport Industry* 4-6 October 2006.

16. H. Janocha, " Adaptronics and Smart Structures: Basics, Materials, Design and Applications" *Second, revised edition*.

17. C. Shakeri, M.N. Noori, and Z. Hou, "Smart Materials and Structures: a review," *Proceeding of the 4th Materials Engineering Conference*, **2**, 863-876 (1996).

18. F.V. Hunt, "Electroacoustics: The analysis of Transduction, and its Historical Background," *Acoustical Society of America*, 1982.

19. A.E. Clark, "Magnetostrictive rare earth-Fe2 compounds," *ferromagnetic materials.* **1**, 531-589 (1980).

20. J.D. Marcelo, C.S. Ralph, and B.F. Alison, "Structural Magnetic Strain Model for Magnetostrictive Transducers, " *IEEE transactions on magnetics*, **36,** 545-556 (2006).

21. K.S. Challagulla, "Modelling of Smart Composite Structures," *Thesis, Doctor of Philosophy, Dalhousie University* (2006).

22. K.S. Challagulla, and A.V. Georgiades, "Micromechanical Analysis of Magneto-electro-thermo-elastic Composite Materials with Applications to Multilayered Structures" *Int. J. Eng. Sc.*, **49**, 85-104 (2011).

23. Technical Insights, "Smart materials: Emerging Markets for Intelligent Gels, Ceramics, Alloys, and Polymer, " *John Wiley & Sons Inc*, 1999.

24. Wikipedia online at: http://en.wikipedia.org/wiki/Shape-memory_alloy.

25. Y. Adachi, S. Unjob, and M. Kondoh "Develepoment of shape memory alloy damper for intelligent bridge systems," *Proceeding of the International symposium on shape memory materials, Japan*, 31-34 (1999).

26. S. Saadat, H. Davoodi, Z. Hou, Y. Suzuki, and A. Masouda, "Using NiTi SMA tendons for vibrational control of coastal structures," *Smart Mater. Struc.*, **10**, 697-704 (2001).

27. J.V. Humbeeck, and S. Kustov, "Active and Passive Damping of noise and vibrations through shape memory alloys: applications and mechanisms," *Smart Mater. Struc*, **14**, S171-S185 (2005).

28. A.V. Aganov, and A.G. Zakharov, "Electrorheological Fluids," *Russian Journal of General Chemistry*, **80**, 567-575 (2010).

29. K. Bohon, and S. Krause, "An Electrorheological Fluid and Silioxane Gel Based Electromechanical Actuator: Working toward an Artificial Muscle," *Journal of polymer science*, **36**, 1091-1094 (1998).

30. Y. Ribakov, and J. Gluck, "Active Control of Mdof Structures with Supplemental Electrorheological Fluid Dampers," *Earthquake Engineering and Structural Dynamics*, **28**, 143-156 (1999).

31. P. Sheng, and W. Wen, "Electrorheological Fluids: Mechanisms, Dynamics, and Microfluidics Applications" *Annual review of fluid mechanics*, **44**, 143-174 (2012).

32. O. Ashour, and C.A. Rogers, "Magnetorheological Fluids: Materials, Characterization, and Devices," *Journal of intelligent material systems and structures*, **7**, 123-130 (1996).

33. P. Holister, T.R. Harper, and C.M.P. Cientifica, "Nanotubes," *CMP Cientifica*, (Jan 2003).

34. K. Balasubramanian, and M. Burghard, "Chemically Functionalized Carbon Nanotubes," *reviews small*, **2**, 180-192 (2005).

35. B. Chandra, "Synthesis and Electronic Transport in Known Chirality Single Wall Carbon Nanotubes," *Thesis, Doctor of Philosophy, Columbia University* (2009).

36. Wikipedia online at: http://en.wikipedia.org/wiki/Carbon_nanotube

37. Z. Li, J. Xu, J.P. O`Byrne, L. Chen, K. Wang, M.A. Morris, and J.D. Holmes, "Freestanding Bucky Paper with High Strength from Multi-Wall Carbon Nanotubes," *Mater. Chem. Phys.*, **135**, 921-927 (2012).

38. B.B Parekh, G. fanchini, G. Eda, and M. Chhowalla, "Improved Conductivity of Transparent Single-Wall Carbon Nanotube Thin Films Via Stable Postdeposition Functionalization," *App. Phys. Lett.*, 90, 121913-1-3 (2007).

39. J. Gou, "Single-Walled Nanotube Bucky Paper and Nanocomposite," *Polymer Int., **55**,* 1283-1288 (2006).

40. K. Tanaka, H. Aoki, H. Ago, T. Yamabe, and K. Okahara, "Interlayer Interaction of Two Graphene Sheets as a Model of Double-layer Carbon Nanotubes," *Pergamon,* **35**, 121-125 (1997).

41. Wikipedia online at: http://en.wikipedia.org/wiki/Graphene

42. R. Kar-Gupta and T.A. Venkatesh, "Electromechanical Response of Piezoelectric Composites: Effect of Geometric Connectivity and Grain Size," *Acta. Mater.,* **56,** 3810-3823 (2008).

43. R.E. Newnhamm, D.P. Skinner, and L.E Cross, "Connectivity and Piezoelectric-Pyroelectric Composites," *Mater Res Bull.,* **13**, 525-536 (1978).

44. J. F. Tressler, S. Alkoy, A. Dogan, and R. E. Newnham, "Functional Composites for sensors, actuators and transducers," *Composites, Part A,* **30**, 477-482 (1999).

45. K. Nagata, H. Igarashi, K. Okazaki, and R.C. Bradt, "Properties of an Interconnected Porous Pb(Zr, Ti)O_3 Ceramic," *Jpn. J. Appl. Phys.,* **19,** L37-L40 (1980).

46. K. Hikita, K. Yamada, M. Nishioka, and M. Ono, "Piezoelectric Properties of the porous PZT and the porous PZT composite with silicone rubber," *Ferroelectrics,* **49**, 265-272 (1983).

47. S. Kumamoto, K. Mizumura, Y. Kurihara, H. Ohhashi, and K. Okuno, "Experimental Evaluation Cylindrical Ceramic Tubes Composed of Porous Pb(ZrTi)O_3 Ceramics," *Jpn. J. Appl. Phys., Part ,* **30**, 2292-2294 (1991).

48. Y. Mikata, "Explicit Determination of Piezoelectric Eshelby tensors for a spheroidal inclusion," *Int J. Solids Struc.,* **38**, 7045-7063 (2001).

49. M.L. Dunn and M.J. Taya, "Electromechanical Properties of Porous Piezoelectric Ceramics," *J. Am. Ceram. Soc.,* **76,** 1697-706 (1993).

50. C. R. Bowen and V. Y. Topolov, "Piezoelectric Sensitivity of $PbTiO_3$-based Ceramic/Polymer Composites with 0-3 and 3-3 Connectivity," *Acta Mater.,* **51**, 4965-4976 (2003).

51. H. Banno, "Effects of Shape and Volume Fraction of Closed Pores on Dielectric, Elastic, and Electromechanical Properties of Dielectric and Piezoelectric Ceramics - A Theoretical Approach," *Ceram. Bull.,* **66**, 1332-1337 (1987).

52. C.N. Della and D. Shu, "The Performance of 1-3 piezoelectric composites with a Porous Non-Piezoelectric matrix," *Acta Materialia.,* **56,** 754-761 (2008).

53. G. Altay and M. C. Dokmeci, "Variational Principles for the Equations of Porous Piezoelectric Ceramics," *IEEE Trans. Ultrason., Ferroelect., Freq. Contr.*, **52**, 2112-2119 (2005).

54. T.E.G. Alvarez-Arenas and F.M.E Freijo, "New Constitutive Relations for Piezoelectric Composites and Porous Piezoelectric Ceramics" *J. Acoust. Soc. Am.*, **100**, 3104-3114 (1996).

55. J. Bravo-Castillero, R. Rodriguez-Ramos, R. Guinovart-Diaz, F.J. Sabina, A.R. Aguiar, U.P. Silva, and J.L. Gomez-Munoz, "Analytical Formulae for Electromechanical Effective Properties of 3–1 Longitudinally Porous Piezoelectric Materials," *Acta. Mater.*, **57,** 795-803 (2009).

56. C.R. Bowen and H. Kara, "Pore Anisotropy in 3–3 Piezoelectric Composites," *Mater. Chem. Phys.,* **75,** 45-9 (2002).

57. S. Iyer and T.A. Venkatesh, "Electromechanical Response of Porous Piezoelectric Materials: Effects of Porosity Connectivity," *Appl. Phys. Lett.*, **97,** 072904 (2010).

58. S. Iyer and T.A. Venkatesh, "Electromechanical Response of (3-0) Porous Piezoelectric Materials: Effects of Porosity Shape," *J. Appl. Phys.*, **110,** 034109 (2011).

59. R. Kar-Gupta and T.A. Venkatesh, "Electromechanical Response of Porous Piezoelectric Materials: Effects of Porosity Distribution," *Appl. Phys. Lett*., **91,** 062904 (2007).

60. K.S. Challagulla and T.A. Venkatesh, "Computational Modelling of Piezoelectric Foams," *JOM.*, **65,** 256-266 (2013).

61. P.W. Bosse, K.S. Challagulla, and T.A. Venkatesh, "Effects of Foam Shape and Porosity Aspect Ratio on the Electromechanical Properties of 3-3 Piezoelectric Foams," *Acta Mater.*, **60,** 6464-6475 (2012).

62. K.S. Challagulla and T.A. Venkatesh, "Electromechanical Response of Piezoelectric Foams," *Acta Mater.,* **60,** 2111-27 (2012).

63. R. Guo, C-A. Wang, and A. Yang, "Effects of Pore Size and Orientation on Dielectric and Piezoelectric Properties of 1–3 Type Porous PZT Ceramics," *J. Eur. Ceram. Soc.,* **31,** 605-609 (2011).

64. K. Boumchedda, M. Hamadi, and G. Fantozzi, "Properties of a Hydrophone Produced with Porous PZT Ceramic," *J. Eur. Ceram. Soc.,* **27,** 4169-4171 (2007).

65. C.R. Bowen, A. Perry, A.C.F. Lewis, and H. Kara, "Processing and Properties of Porous Piezoelectric Materials with High Hydrostatic Figures of Merit," *J. Eur. Ceram. Soc.,* **24,** 541-545 (2004).

66. A. Nasedkin, A. Rybjanets, L. Kushkuley, Y. Eshel and R. Tasker, "Different Approaches to Finite Element Modeling of Effective Moduli of Porous Piezoceramics with 3-3 (3-0) connectivity," *Proc. IEEE Ultrason. Symp.,* **3**, 1648-1651 (2005).

67. U. Bast and W. Wersing, *Ferroelectrics,* **65**, 11 (1985).

68. C-B. Yoon, S-M. Lee, S-H. Lee, H-E. Kim, and K-W. Lee, "Transverse 1-3 Piezoelectric Ceramic/Polymer Composite with Mult-Layered PZT Ceramic Blocks," *Sensors and Actuators.,* **134**, 480-485 (2007).

69. A. Safari, A. Halliyal, L.J. Bowen and R.E. Newnham, "Flexible Composite Transducers," *J. Am. Ceram. Soc.,* **65**, 207-209 (1982).

70. S. Schwarzer, and A. Roosen, "Tape Casting of Piezo Ceramic/Polymer Composites," *J. Eur. Ceram. Soc.,* **19**, 1007-1010 (1999).

71. R. Steinhausen, T. Hauke, W. Seifert, H. Beige, W. Watzka, S. Seifert, D. Sporn, S. Starke, and A. Schonecker, "Finescaled Piezoelectric 1-3 Composites: Properties and Modelling," *J. Eur. Ceram. Soc.,* **19**, 1289-1293 (1999).

72. T.R Gururaja, W.A. Schulze, L.E. Cross, R.E. Newnham, B.A. Auld, and Y.J. Wang, "Piezoelectric Composite Materials for Ultrasonic Transducer Applications. Part I: Resonant Modes of Vibration of PZT Rod-Polymer Composites," *IEEE Trans. Sonics and Ultrasonics.,* **Su-32**, 481-498 (1985).

73. K. Rittenmyer, T. Shrout, W.A. Schulze and R.E. Newnham, "Piezoelectric 3-3 composites," *Ferroelectrics,* **4**, 189-195 (1982).

74. Y-C. Chen and S. Wu, "Piezoelectric Composites with 3-3 Connectivity by Injecting Polymer for Hydrostatic Sensors," *Ceram. Int.,* **30**, 69-74 (2004).

75. X. Lin, K. Zhou, T.W. Button, and D. Zhang, "Fabrication, Characterization and Modelling of Piezoelectric Fiber Composites," *J. Appl. Phys.,* **114,** 027015 (2013).

76. X-J. Lin, K-C. Zhou, X-Y. Zhang, and D. Zhang, "Development, Modelling and Application of Piezoelectric Fiber Composites," *Trans. Nonferrous Met. Soc. China.,* **23**, 98-107 (2013).

77. K.S. Challagulla, and T.A. Venkatesh, "Electromechanical Response of 2-2 Layered Piezoelectric Composites: A Micromechanical Model Based on the Asymptotic Homogenization Method," *Philosophical Magazine,* **89**, 1197-1222 (2009).

78. R. Kar-Gupta and T.A. Venkatesh, "Electromechanical Response of 1-3 Piezoelectric Composites: An Analytical Model," *Acta. Mater.* **55,** 1093-1108 (2007).

79. R. Guinovart-Diaz, J. Bravo-Castillero, R. Rodrigues-Ramos, F.J. Sabina and R. Martinez-Rosado, "Overall Properties of Piezoelectric materials 1-3," *Mater. Lett*. **48** 93- 98 (2001).

80. C.N. Della and D. Shu, "Performance of 1-3 piezoelectric composites with Porous Piezoelectric matrix," *Appl. Phys. Lett.,* **103,** 132905 (2013).

81. H. Ren and H. Fan, "The role of Piezoelectric Rods in 1-3 Composite for the Hydrostatic Response Applications," *Sensors and Actuators.,* **128**, 132-139 (2006).

82. L. Guang, W. Li-Kun, L. Gui-Dong, Z. Jin-Duo, and L. Shu-Xiang, "A Study of a 1-3-2 type Piezoelectric composite," *Ultrasonics.*, **44**, e639-e642 (2006).

83. C.R. Bowen, A. Perry, H. Kara, and S.W. Mahon, " Analytical Modelling of 3-3 Piezoelectric Composites," *J. Eur. Ceram. Soc.*, **21**, 1463-1467 (2001).

84. K.S. Challagulla, A.V. Georgiades, G.C. Saha, and A.L. Kalamkarov, "Micromechanical Analysis of Grid-reinforced Thin Composite Generally Orthotropic Shells," *Composites*, **39,** 627-644 (2008).

85. K.S. Challagulla, A.V. Georgiades, and A.L. Kalamkarov, "Asymptotic Homogenization Modelling of Smart Composite Generally Orthotropic Grid-reinforced Shells: Part I-thoery," *Eur J. Mech. Sol.*, **29**, 530-540 (2010).

86. A.V. Georgiades, K.S. Challagulla, and A.L. Kalamkarov, "Asymptotic Homogenization Modelling of Smart Composite Generally Orthotropic Grid-reinforced Shells: Part II-Applications," *Eur J. Mech. Sol.*, **29**, 541-556 (2010).

87. K.S. Challagulla, A.V. Georgiades, and A.L. Kalamkarov, "Asymptotic Homogenization Modelling of Thin Composite Network Structures," *Composite struc..*, **79**, 432-444 (2007).

88. A.L. Kalamkarov and A.V. Georgiades, "Micromechanical Modelling of Smart Composite Structures," *Smart Mater. Struct*. **11**, 423-434 (2002).

89. A.V. Georgiades, A.L. Kalamkarov, and K.S. Challagulla, "Asymptotic Homogenization Model for Generally Orthotropic Reinforcing networks in Smart Composite plates," *Smart Mater. Struc.*, **15**, 1197-1210 (2006).

90. A.L. Kalamkarov and A.G. Kolpakov, "Analysis, Design and Optimization of Composite Structures," *Wiley, New York*, 1997.

91. R. Rodrigues-Ramos, F.J. Sabina, R. Guinovart-Diaz and J. Bravo-Castillero, "Closed-Form Expressions for the Effective Coefficients of a Fiber-reinforced Composite with Transversely Isotropic Constituents- I. Elastic and Square Symmetry," *Mech.Mater*. **33** 223-235 (2001).

92. J. Bravo-Castillero, R. Guinovart-Diaz, F.J. Sabina and R. Rodrigues-Ramos, "Closed-Form Expressions for the Effecive Coefficients of a Fiber-reinforced Composite with Transversely Isotropic Constituents- II. Piezoelectric and Square Symmetry," *Mech.Mater*. **33** 237-248 (2001).

93. G. Zhang, and M.S Wu, "Connectivity and Shape Effects on the Effective Properties of Piezoelectric-Polymeric Composites," *Int. J. Eng. Sc.,* **48**, 37-51 (2010).

94. R. Kar-Gupta and T.A. Venkatesh, "Electromechanical Response of (2-2) layered Piezoelectric Composites," *Smart Mater. Struct.*, 22**,** 025035 (2013).

95. R. Kar-Gupta and T.A. Venkatesh, "Electromechanical Response of 1-3 Porous Piezoelectric Composites: Effect of Poling Characteristics," *J. Appl. Phys.,* **98,** 054102 (2005).

96. H. E-Pettermann, and S. Suresh, "A Comprehensive Unit Cell Model: A Study of Coupled Effects in Piezoelectric 1-3 Composites," *Int. J. Sol. St.,* **37**, 5447-5464 (2000).

97. H. Berger, S. Kari, U. Gabbart, R. Rodriguez-Ramos, J Bravo-Castillero, and R. Guinovat-Diaz, "Calculation of Effective Coefficients for Piezoelectric Fiber Composites Based on a General Numerical Homogenization Technique," *J. Compstruct.,* **71**, 397-400 (2005).

98. E. Lopez-Lopez, F.J. Sabina, R. Guinovart-Diaz, J. Bravo-Castillero, and R. Rodriguez-Ramos, "Overall Longitudinal Shear Elastic Modulus of a 1–3 Composite with Anisotropic Constituents," *Int. J. Sol. St.,* **50**, 2573-2583 (2013).

99. Y. Li, H. Zheng, S. Long, and L. Wu, “Effects of the Piezoelectric Phase’s Geometric Properties on Effective Coefficients of 1-3 Piezoelectric Composites,” *Comp. Mater. sci.*, **50**, 2135-2141 (2011).

100. C. Poizat and M. Sester, “Effective Properties of Composites with embedded Piezoelectric Fibres,” *Comp. Mater. Sc.*, **16**, 89-97 (1999).

101. R.W.C Lewis, A.C Dent, and C.R. Bowen, “Network Modelling of 3-3 piezocomposite materials,” *Ferroelectrics*, **351**, 216-224 (2007).

102. Z. Hongyan, L. Luxian, and S. Yapeng, “Finite Element Model and Effect of Material Parameters on Properties of 3-3 Piezocomposites,” *Acta Mater. Compositae. Sinica*, **22**, 160-165 (2005).

103. Q-X. Bao, L-H. Zhu, Q-W. Huang, and J. Xv, “Preparation of Textured $Ba_2Nb_5O_{15}$ Ceramics by Templated Grain Growth,” *Ceram. Int.*, **32,** 745-749 (2006).

104. P. Kumar, S. Singh, M. Spah, J.K. Juneja, C. Prakash, and K.K. Raina, “Synthesis and Dielectric Properties of Substituted Barium Titanate Ceramics,” *J. alloy and compound*, **489,** 59-63 (2010).

105. L.A. Reznitchenko, I.A. Verbenko, O.N. Razumovskaya, L.A. Shilkina, A.A. Bokov, A.I. Miller, and M.V. Talanov, “Preparation, Structure and Piezoelectric Properties of PZN-PMN-PT Ceramics in the Composition Range of Large PZN Concentrations,” *Ceram. Int.*, **38,** 3835-3839 (2012).

106. X. Zhao, J. Wang, K-H. Chew, H.L-W. Chan, C-L. Choy, Z. Yin, and H. Luo, “Composition Dependence of Piezoelectric Constant and Dielectric Constant Tunability in the (001)-Oriented $Pb(Mg_{1/3}Nb_{2/3})O_3$-$PbTiO_3$ Single Crystals,” *Mater. Lett.*, **58,** 2053-2056 (2004).

107. J.H. Lee, Y.J. Oh, T.Y. Kim, M.R. Choi, and W. Jo, "Piezoelectric and Electromechanical Properties of Relaxor Ferroelectric $Pb(Mg_{1/3}Nb_{2/3})O_3$(65%)-$PbTiO_3$(35%) Thin Films Observed by Scanning Microscopy," *Ultramicroscopy,* **107,** 954-957 (2007).

108. J-H. Park, J. Park, J-G. Park, B-K. Kim, and Y. Kim, "Piezoelectric Properties in PMN-PT Relaxor Ferroelectrics with MnO_2 Addition," *J. Eur. Ceram. Soc.,* **21,** 1383-1386 (2001).

109. V. Y. Topolov, C. R. Bowen, and P. Bisegna, "Electromechanical Coupling Factors of Novel 0-3-0 Composites Based on PMN-xPT Single Crystals," *Ferroelectrics,* **422**, 40-43 (2011).

110. V. Y. Topolov, P. Bisegna, S. V. Glushanin, and A. A. Panich, "Analysis of the Piezoelectric Performance of Modern 0-3-Type Composites Based on Relaxor-Ferroelectric Single Crystals," *Ferroelectrics,* **413**, 11 (2011).

111. J. Singh, T.A. Venkatesh, and, K.S. Challagulla. "Electromechanical properties of relaxor ferroelectric foams," *Appl. Phys. Lett.*, **103**, 172901 (2013).

112. X. Z. Liu, S. J. Zhang, J. Luo, T. R. Shrout, and W. W. Cao, "A Complete Set of Material Properties of Single Domain 0.26Pb(In1/2Nb1/2)O_3-0.46Pb(Mg1/3Nb2/3)O_3-0.28$PbTiO_3$ single crystals," *Appl. Phys.Lett.*, **96**, 012907-1-3 (2010).

113. R. Shukla, K. K. Rajan, P. Gandhi, and L. C. Lim, "Complete Sets of Elastic, Dielectric, and Piezoelectric Properties of [001]-Poled Pb(Zn1/3Nb2/3)O_3-(6-7)%$PbTiO_3$ Single Crystals of [110]-Length Cut," *Appl. Phys. Lett.*, **92**, 212907-1-3 (2008).

114. G. Y. Xu, Z. Zhong, Y. Bing, Z. G. Ye, and G. Shirane, "Electric-field-induced Redistribution of Polar Nano-Regions in a Relaxor Ferroelectric," *Nature Mater.,* **5**,134-140 (2006).

115. C. J. He, D. Zhou, F. F. Wang, H. Q. Xu, D. Lin, and H. S. Luo, "Elastic, Piezoelectric, and Dielectric Properties of Tetragonal Pb(Mg1/3Nb2/3)O_3-$PbTiO_3$ Single Crystals," J. *Appl.Phys.*, **100**, 086107 (2006).

116. E. A. McLaughlin, T. Q. Liu, and C. S. Lynch, "Relaxor Ferroelectric PMN-32%PT Crystals under Stress, Electric Field and Temperature Loading: II-33-mode measurements," *Acta Mater.*, **53**, 4001(2005).

117. D. Y. Zhou, M. Kamlah, and D. Munz, "Uniaxial Compressive Stress Dependence of the High-Field Dielectric and Piezoelectric Performance of Soft PZT Piezoceramics," *J. Mater. Res.*, **19**, 834 (2004).

118. H. Cao, V. H. Schmidt, R. Zhang, W. W. Cao, and H. S. Luo, "Elastic, Piezoelectric, and Dielectric Properties of 0.58Pb(Mg 1/3Nb2/3)O_3-0.42$PbTiO_3$ Single Crystal," *J. Appl.Phys.*, **96**, 549 (2004).

119. S. E. Park and T. R. Shrout, "Ultrahigh Strain and Piezoelectric Behavior in Relaxor Based Ferroelectric Single Crystals," *J. Appl. Phys.* **82**, 1804-1811 (1997).

120. R. Kar-Gupta and T.A. Venkatesh, "Electromechanical Response of 1-3 Piezoelectric Composites: A Numerical Model to assess the effects of fiber distribution," *Acta. Mater.*, **55, 1275-1292** (2007).

121. C.N. Della, and D. Shu, "On the Performance of 1-3 Piezoelectric Composites with a Passive and Active Matrix," *Sensors and Actuators*, **140**, 200-206 (2007).

122. F. Moleiro, C.M.M. Soares, C.A.M Sores, and J.N Reddy, "Benchmark Exact Solutions for the Static Analysis Of Multilayered Piezoelectric Composite Plates using PVDF," *Comp. Str.*, **107**, 389-395 (2014).

123. G.M. Odegard, "Constitutive Modelling of Piezoelectric Polymer Composites," *Acta. Mater.*, **52**, 5315-5330 (2004).

124. J-H. Seol, J.S. Lee, H-N. Ji, Y-P Ok, G.P. Kong, K-S Kim, C.Y. Kim, and W-P. Tai, "Piezoelectric and dielectric properties of $(K_{0.44}Na_{0.52}Li_{0.04})(Nb_{0.86}Ta_{0.10}Sb_{0.04})O_3$–PVDF composites" *Ceram. Int.,* **38S**, S263-S266 (2012).

125. L. Wang, J. Zhu, X. Zou, and F. Zhang, "$PbTiO_3$ –P(VDF/TeFE/ Composites for Piezoelectric Sensors," *Sensors and Actuators.,* **B66**, 266-268 (2000).

126. P. Han, S. Pang, J. Fan, X. Shen, and T. Pan, "Highly Enhanced Piezoelectric Properties of PLZT/PVDF Composite by Tailoring the Ceramic Curie Temperature, Particle Size and Volume Fraction," *Sensors and Actuators.,* **A204**, 74-78 (2013).

127. X-D. Chen, D-B. Yang, Y-D. Jiang, Z-M. Wu, D. Li, F-J Gou, and J-D. Yang, "0-3 Piezoelectric Composite Film with high d_{33} coefficient," *Sensors and Actuators.,* **A65**, 194-196 (1998).

128. X. Guan, Y. Zhang, H. Li, and J. Ou, "PZT/PVDF Composites Doped with Carbon Nanotubes," *Sensors and Actuators.,* **A194**, 228-231 (2013).

129. Z. Ahmad, A. Prasad, and K.Prasad, "A Comparative Approach to predicting Effective Dielectric, Piezoelectric and Elastic Properties of PZT/PVDF Composites," *Physica B.,* **404**, 3637-3644 (2009).

130. F. Wang, C. He, Y. Tang, X. Zhao, and H. Luo, "Single-Crystal $0.7Pb(Mg_{1/3}Nb_{2/3})O_3$–$0.3PbTiO_3$/epoxy 1–3 Piezoelectric Composites Prepared by the Lamination Technique," *Mater. Chem. Phys.,* **105**, 273-277 (2007).

131. J-H. Park, J. Park, J-G. Park, B-K. Kim, and Y. Kim, "Piezoelectric Properties in PMN-PT Relaxor Ferroelectrics with MnO_2 Addition," *J. Eur. Ceram. Soc.,* **21**, 1383-1386 (2001).

132. K.C. Kim, Y.S. Kim, H.J. Kim, and S.H. Kim, "Finite Element Analysis of Piezoelectric Actuator with PMN-PT Single Crystals for Nanopositioning," *Curr. Appl. Phys.,* **6**, 1064-1067 (2006).

133. K.H. Lam, and H.L.W. Chan, "Piezoelectric and Pyroelectric Properties of 65PMN-35PT/P(VDF-TrFE) 0-3 Composites," *Comp. Sci. Tech.,* **65**, 1107-1111 (2005).

134. K.K. Rajan, M. Shanthi, W.S. Chang, J. Jin, and L.C. Lim, "Dielectric and Piezoelectric Properties of [0 0 1] and [0 1 1]-Poled Relaxor Ferroelectric PZN-PT and PMN-PT single Crystals," *Sensors and Actuators.,* **A133**, 110-116 (2007).

135. Q. Li, Y. Zhang, Z. Xia, and X. Chu, "MPB design and Crystal Growth of PMN-PT-PZ Relaxor Ferroelectrics," *J. Cryst. Gro.,* **318**, 851-855 (2011).

136. W. Wu, D. Xiao, J. Wu, J. Li, J. Zhu, and B. Zhang, "Microstructure and Electrical Properties of Relaxor (1-x)[$(K_{0.5}Na_{0.5})_{0.95}Li_{0.05}$]($Nb_{0.95}Sb_{0.05}$)$O_3$-x$BaTiO_3$ Piezoelectric Ceramics," *Ceram. Int.,* **38**, 2277-2282 (2012).

137. Z. Yao, Z. Song, H. Liu, H. Huo, M. Cao, and Z. Yu, "Relaxor and Ferro/Piezoelectric Behaviour in BiScO3-(Na0.5Bi0.5)TiO3-PbTiO3 Piezoelectric Ceramics," *J. alloy and compound., In Press.*

138. L. Li, Z. Xu, S. Xia, Z. Li, X. Ji, and S. Long, " PIN-PMN-PT Single-Crystal-Based 1-3 Piezoelectric Composites for Ultrasonic Transducer Applications," *J. Elec. Mater.,* **42**, 2564-2569 (2013).

139. R. Zhang, B. Jiang, and W.W. Cao, "Elastic, Piezoelectric, and Dielectric Properties of Multidomain 0.67Pb(Mg1/3Nb2/3)O3–0.33PbTiO3 Single Crystals," *J. Appl. Phys.,* **90,** 3471-3475 (2001).

140. A.W. Warner, G.A. Coquin, and J.L. Fink, "Elastic and Piezoelectric Constants of $Ba_2NaNb_5O_{15,}$" *J. Appl. Phys.,* **40,** 4353-4356 (1969).